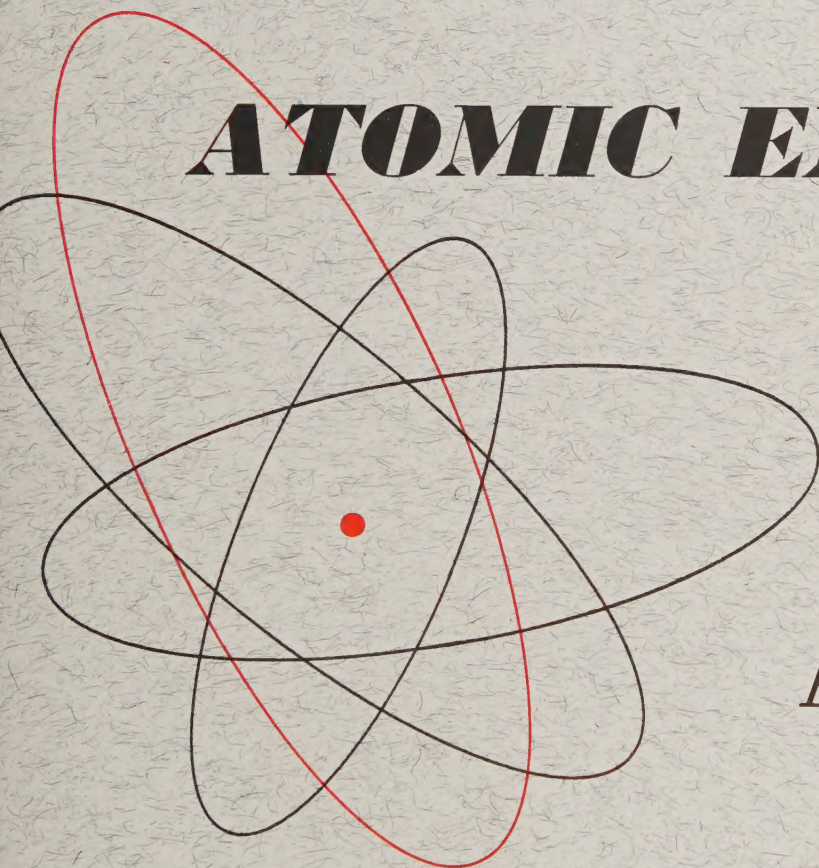


Volume 8, No. 5

June, 1961

THE SOVIET JOURNAL OF

# **ATOMIC ENERGY**



Атомная  
энергия

TRANSLATED FROM RUSSIAN

CONSULTANTS BUREAU

# Research by Soviet Experts Translated by Western Scientists

## Soviet Research on the LANTHANIDE AND ACTINIDE ELEMENTS, 1949-1957

An important contribution to the literature of nuclear chemistry, this collection of papers is a comprehensive presentation of Soviet research on the chemistry of lanthanides and actinides. The 106 reports included in this collection appeared in the major Soviet chemical journals translated by Consultants Bureau, as well as in the Soviet Journal of Atomic Energy, 1949-1957.

The five sections, totalling 657 pages, provide broad representation of contemporary Soviet research in this important aspect of nuclear science. This collection should be accessible to all nuclear researchers, whether theoretical or applied.

Each part may be purchased as follows:

<b>Basic Chemistry</b> (25 papers) .....	<b>\$15.00</b>
<b>Analytical and Separation Chemistry</b> (30 papers) .....	<b>\$20.00</b>
<b>Nuclear Chemistry (and Nuclear Properties)</b> (32 papers) ...	<b>\$22.50</b>
<b>Geology</b> (10 papers) .....	<b>\$7.50</b>
<b>Nuclear Fuel Technology</b> (9 papers) .....	<b>\$7.50</b>
<b>Complete collection</b> .....	<b>\$65.00</b>

## RADIATION CHEMISTRY, PROCEEDINGS OF THE FIRST ALL-UNION CONFERENCE MOSCOW, 1957

More than 700 of the Soviet Union's outstanding research scientists participated in this conference sponsored by the Academy of Sciences and the Ministry of the Chemical Industry. Each of the 56 reports read in the various sessions covers either the theoretical or practical aspects of radiation chemistry, and special attention is given to radiation sources used in radiation-chemical investigations. The general discussions which followed each report and reflected various points of view on the problem under analysis are also included.

### **Primary Acts in Radiation Chemical Processes**

heavy paper covers 5 reports, plus discussion ..... illustrated ..... **\$25.00**

### **Radiation Chemistry of Aqueous Solutions (Inorganic and Organic Systems)**

heavy paper covers 15 reports, plus discussion ..... illustrated ..... **\$50.00**

### **Radiation Electrochemical Processes**

heavy paper covers 9 reports, plus discussion ..... illustrated ..... **\$15.00**

### **The Effect of Radiation on Materials Involved in Biochemical Processes**

heavy paper covers 6 reports, plus discussion ..... illustrated ..... **\$12.00**

### **Radiation Chemistry of Simple Organic Systems**

heavy paper covers 9 reports, plus discussion ..... illustrated ..... **\$30.00**

### **The Effect of Radiation on Polymers**

heavy paper covers 9 reports, plus discussion ..... illustrated ..... **\$25.00**

### **Radiation Sources**

heavy paper covers 3 reports ..... illustrated ..... **\$10.00**

*Individual volumes may be purchased separately.*

*NOTE: Individual reports from each volume are available  
at \$12.50 each. Tables of contents sent upon request.*

**special price for the 7-volume set ..... \$125.00**

Payment in sterling may be made to Barclay's Bank in London, England.

## CONSULTANTS BUREAU

227 West 17th Street • New York, N.Y., U.S.A.

# THE SOVIET JOURNAL OF **ATOMIC ENERGY**

*A translation of ATOMNAYA ÉNERGIYA,  
a publication of the Academy of Sciences of the USSR*

(Russian Original Dated May, 1960)

Vol. 8, No. 5

June, 1961

## CONTENTS

	PAGE	RUSS. PAGE
Winners of Lenin Prizes . . . . .	341	I
Determination of the Mean Number of Secondary Fission Neutrons from the Fragment Mass Distribution. Yu. A. Zysin, A. A. Lbov, and L. I. Sel'chenkov. . . . .	343	409
An Investigation of the Properties of Metals and Some Steels after Irradiation by Fast Neutrons. Sh. Sh. Ibragimov, V. S. Lyashenko, and A. I. Zav'yalov . . . . .	347	413
Vapor Pressure of T <sub>2</sub> O. M. M. Popov and F. I. Tazetdinov . . . . .	353	420
Radiometric Analysis of Ores on Conveyers. L. N. Posik, S. I. Babichenko, and R. A. Grodko . . . . .	358	425
Angle-Energy Distribution of $\gamma$ -Radiation Scattered in Water and Iron. Yu. A. Kazanskii	364	432
Universal Apparatus with a Co <sup>60</sup> $\gamma$ -Ray Source with an Activity of 60,000 g-eq of Ra for Simulating Radiation-Chemical Apparatuses, and Investigations (The "K-60,000"). A. Kh. Breger, V. B. Osipov, and V. A. Gol'din . . . . .	371	441
LETTERS TO THE EDITOR		
Investigation of the Spent Fuel Element of the First Atomic Power Station. A. P. Smirnov- Averin, V. I. Galkov, Yu. G. Sevast'yanov, N. N. Krot, V. I. Ivanov, I. G. Sheinker, L. A. Stabenova, B. S. Kir'yanov, and A. G. Kozlov . . . . .	375	446
On Improving the Efficiency of Power Station Reactors with Gaseous Coolants. T. Kh. Margulova and L. S. Sterman . . . . .	377	448
Measurement of the Fast Neutron Flux Distribution in the Core of the VVR-S Reactor with Respect to Changes in the Electrical Conductivity of Germanium Specimens. E. Aleksandrovich and M. Bartenbakh . . . . .	381	451
Calculation of Thermal Shocks in Reactor Structural Parts. Yu. E. Bagdasarov . . . . .	383	452
600-kev Proton Injector for a Linear Accelerator. Yu. N. Antonov, L. P. Zinov'ev, and V. P. Rashevskii . . . . .	386	454
Mean Number of Prompt Neutrons Emitted in Photofission of Th <sup>232</sup> and U <sup>238</sup> by $\gamma$ -rays Produced in the F <sup>19</sup> (p, $\alpha$ )O <sup>16</sup> Reaction. L. I. Prokhorova and G. N. Smirenkin . . . . .	390	457
Electron Acceleration in a Traveling-Wave Cyclical Waveguide Accelerator. A. A. Vorob'ev, A. N. Didenko, and E. S. Kovalenko . . . . .	392	459
Use of Scintillation Counters in Gammascopy. V. E. Nesterov . . . . .	394	461
NEWS OF SCIENCE AND TECHNOLOGY		
Atomic Energy at the Soviet Exposition in Havana. L. Kimel', and V. Tsurkov . . . . .	397	464
Atomic Energy of the All-China Exposition on Industry and Means of Communication. Shen Chung-po . . . . .	399	464

# CONTENTS (continued)

	PAGE	RUSS. PAGE
[Washington Conference of the American Nuclear Physics Society and Atomic Industrial Forum. Sources: Nucleonics <u>17</u> , No. 12, 17-23 (1959); Nuclear Power <u>5</u> , No. 45, 111-116 (1960) . . . . .		467]
[Development of Nuclear Power in the Countries of South and Central America . . . . .		467]
[Organic Moderated Reactors for Land-Based and Seagoing Facilities. . . . .		470]
[Reactor as a Neutron Source . . . . .		472]
Measurement of Magnetic Moment of $Li^8$ . . . . .	400	473
[New Foreign Articles on Rolling of Uranium . . . . .		474]
[On the Use of Statistical Analysis Techniques in Explorations for Uranium Deposits. Source: R. Bates, Econ. Geol. <u>54</u> , No. 3, 449 (1959) . . . . .		476]
BIBLIOGRAPHY		
New Literature . . . . .	401	480

## NOTE

The Table of Contents lists all material that appears in Atomnaya Energiya. Those items that originated in the English language are not included in the translation and are shown enclosed in brackets. Whenever possible, the English-language source containing the omitted reports will be given.

Consultants Bureau Enterprises, Inc.

## WINNERS OF LENIN PRIZES

Translated from Atomnaya Énergiya, Vol. 8, No. 5, pp. I-II,  
May, 1960

The Committee of the Council of Ministers of the USSR for the Lenin prizes in the field of Science and Technology has assigned the prizes for 1960 to the following scientists for their scientific research on the physics of fast-neutron nuclear reactors: Academician (Academy of Sciences of the UkrSSR) A. I. Leipunskii, Drs. of Phys. and Math. Sci., O. D. Kazachkovskii and I. I. Bondarenko, and Cand. of Phys. Math. Sci., L. N. Usachev.

Nuclear reactors working with fast neutrons occupy a special place in nuclear energetics. Back in 1949, A. I. Leipunskii calculated that in such reactors one could realize an extensive production of nuclear fuel. Consequently, the use of energy reactors working with fast neutrons, together with the use of energy reactors working with thermal neutrons, would allow complete use of extracted uranium, which is equivalent to increasing by a factor 100 the fuel resources of nuclear power engineering.

The main difficulty in the practical realization of a chain reaction in a reactor consisted in the fact that many problems of the physics of such reactors were still unsolved. There appeared no publication concerning fast reactors in the foreign literature until 1955. Therefore, a school of specialists was formed and developed independently in the Soviet Union in the physics of fast-neutron reactors. This school was headed by A. I. Leipunskii, O. D. Kazachkovskii, I. I. Bondarenko, and L. N. Usachev.

Under their guidance the problems of the physics of fast-neutron reactors were studied on a theoretical basis, experiments for establishing the constants necessary for calculation were carried out, the foundations of the theory were elaborated, and practical work for building fast-neutron reactors was started.

Subsequently, critical assemblies and fast-neutron reactors were constructed (BR-1, BR-2, BR-3, BR-4, and BR-5). The construction of each new apparatus was a logical continuation and generalization of experience accumulated, and a development of the theory and practice of reactors working with fast neutrons.

The last apparatus of this series—BR-5, started in the summer of 1958—has all the main characteristics of an atomic electric power plant, and is a prototype of the future powerful atomic plants with fast-neutron reactors.

The Lenin prize for the construction of the complex of research water-water reactors VVR-2, VVR-S, and ITR was assigned to the scientists S. M. Feinberg, V. V. Goncharov, G. A. Stolyarov, T. N. Zubarev, P. I. Khris-tenko, V. F. Kozlov, and O. I. Lyubimtsev.

The construction of research reactors is the basis for the use of atomic energy. Perhaps there has been no development of its use that has not taken place as a direct or indirect result of work on research reactors. The obtainment of radioactive isotopes, the radiation treatment and testing of materials, the study of the physical problems of high-power reactors, the testing of thermoemitting elements for nuclear power plants and transport atomic equipment under construction or in project, the testing of components, joints and materials for high power reactors,



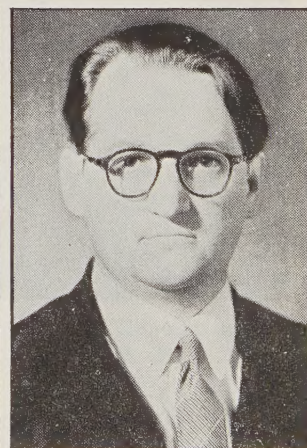
A. I. Leipunskii



O. L. Kazachkovskii



I. I. Bondarenko



L. N. Usachev

investigations in neutron physics, biology and medicine investigations concerning the radiation of supply products, radiation polymerization, and many other problems are solved with the help of research reactors.

Our industry produces at present in mass research water-water reactors of the types VVR-2, VVR-S, and ITR. Some scientific research institutes of the Soviet Union and of foreign countries are equipped with them.

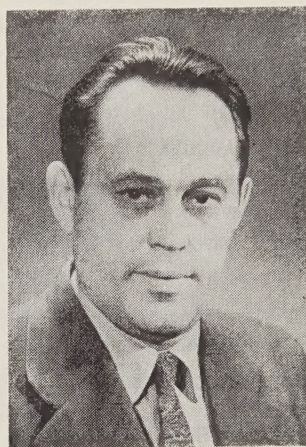
The compactness, the low cost, the reliability of operation, and the wide possibilities for experimental research are the main advantages of the water-water reactors whose construction is recognized by the Lenin prize.

The first of these reactors—VVR-2—was constructed when the world literature included no publication concerning such reactors. Nevertheless, the group of specialists solved successfully all the problems concerning the construction and the physics of the reactor, its regulation, its operational stability, etc.

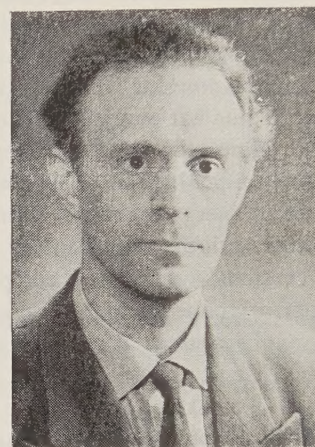
The construction of the complex of research water-water reactors is a great achievement in the field of the use of atomic energy for peaceful purposes. The vast development of experimental work on such reactors that exists at present permits a wider use of atomic energy in the national economies of the USSR and other countries.



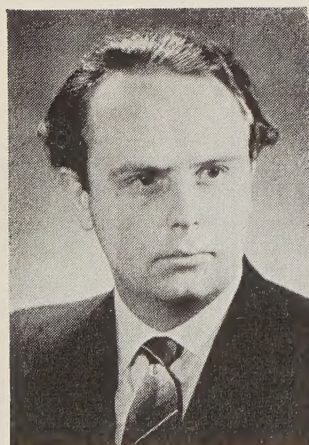
S. M. Feinberg



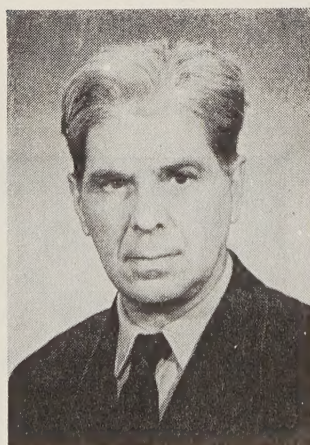
V. V. Goncharov



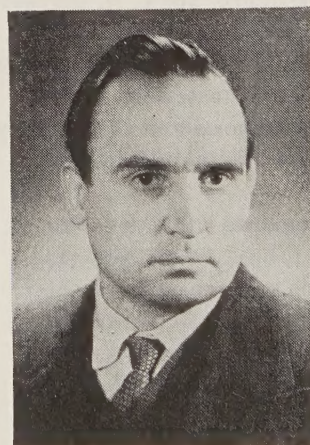
G. A. Stolyarov



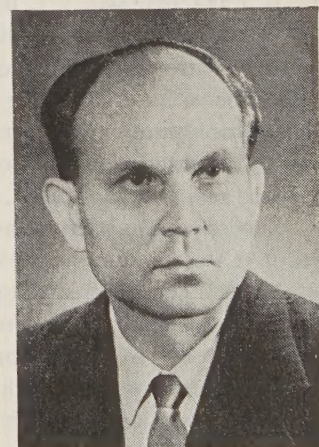
T. N. Zubarev



P. I. Khristenko



V. F. Kozlov



O. I. Lyubimtsev

# DETERMINATION OF THE MEAN NUMBER OF SECONDARY FISSION NEUTRONS FROM THE FRAGMENT MASS DISTRIBUTION

Yu. A. Zysin, A. A. Lbov, and L. I. Sel'chenkov

Translated from Atomnaya Énergiya, Vol. 8, No. 5, pp. 409-412,  
May, 1960

Original article submitted September 3, 1959

A method is presented for computing the mean number of secondary fission neutrons  $\bar{\nu}$  from the fission-fragment mass distribution curves. The error of the method is estimated. It is shown that in those cases in which the fragment mass distribution curves are carefully studied,  $\bar{\nu}$  can be determined with satisfactory accuracy by this method. The value of  $\bar{\nu}$  is computed for fission in  $\text{Th}^{232}$ ,  $\text{U}^{233}$ ,  $\text{U}^{235}$ ,  $\text{U}^{238}$ ,  $\text{Pu}^{239}$ ,  $\text{Am}^{241}$ , and  $\text{Cf}^{252}$ . The results are discussed and compared with results obtained by other methods. The partial values  $\bar{\nu}_m$  are computed for thermal-neutron fission of  $\text{U}^{233}$  and  $\text{U}^{235}$ .

At the present time the mass distribution of fission fragments has been studied in many cases of fission in heavy nuclei [1-11]. In some cases the accuracy and completeness of the experimental data are adequate for computing the mean number of secondary fission neutrons  $\bar{\nu}$  with satisfactory results. Although the quantity  $\bar{\nu}$  has been measured very precisely by indirect methods [12-14], this calculation is of great interest since it allows us to determine the values of  $\bar{\nu}$  by an independent method. Furthermore, this technique allows us to obtain the value of  $\bar{\nu}$  for those cases in which it has not been determined by other methods. Finally, in principle, using the fission-fragment mass distribution curves it should be possible to compute the partial values of  $\bar{\nu}_m$ , i.e. the mean number of fission neutrons corresponding to a given ratio for the mass numbers of the heavy and light fragments  $(A_H/A_L)_m$ .

Attempts to estimate  $\bar{\nu}$  from the fission-fragment mass distribution curves have been carried out earlier [8-10, 15]; however, these estimates were extremely approximate. In the present paper, for the first time, the possibilities of this method are investigated in detail, the errors involved are studied, and calculations of  $\bar{\nu}$  are carried out for cases in which the error is shown to be small.

In the general case

$$\bar{\nu} = A_0 - 2\bar{A}, \quad (1)$$

where  $A_0$  is the mass number of the fissioning nucleus and  $\bar{A}$  is the mean mass number of all fragments, where  $\bar{A} = \sum_l \alpha_l A_l / \sum_l \alpha_l$  ( $A_l$  is the mass number of the fragment and  $\alpha_l$  is the fragment yield). It is well known that  $\sum_l \alpha_l = 2$ . In practice, however, it is not convenient to

use Eq. (1) to determine  $\bar{\nu}$  because of the appreciable errors involved. The error in the determination of  $\bar{\nu}$  is found to be much smaller if another expression is used:

$$\bar{\nu} = A_0 - (\bar{A}_H + \bar{A}_L), \quad (2)$$

which takes account of the fact that two fragments are formed as a result of fission — the light and heavy fragments, which are characterized by the mass numbers  $\bar{A}_L$  and  $\bar{A}_H$ , respectively. This formulation of the problem is valid in all cases of fission in which the original nucleus is not highly excited since ternary fission and cases in which protons and alpha particles are emitted can obviously be neglected.

The quantities  $\bar{A}_L$  and  $\bar{A}_H$  can be determined by averaging the masses of the light and heavy fragments, respectively, using the expressions

$$\bar{A}_L = \frac{\sum_i A_i \alpha_i}{\sum_i \alpha_i} \quad \text{and} \quad \bar{A}_H = \frac{\sum_k A_k \alpha_k}{\sum_k \alpha_k}.$$

From the definition of yields it is obvious that  $\alpha_i$  and  $\alpha_k$  summed separately over the light and heavy fragments should be equal to unity. Because of the inaccuracy in the experimental determination of the individual yields, however, these quantities are found to be only approximately equal to unity; hence, in computing  $\bar{\nu}$  from Eq. (2) it is important to introduce two normalization conditions:  $\sum_i \alpha_i = 1$  and  $\sum_k \alpha_k = 1$ .

We now consider the mean-square-error  $\Delta \bar{\nu}$  and its dependence on the uncertainty in the experimentally determined quantities  $\alpha$ . From the expression for the determination of the error in  $\bar{\nu}$  due to the  $l$ th term and

Fissioning nucleus	emission which accompanies fission	Energy	Determination of $\bar{\nu}$ by the present method				Determination of $\bar{\nu}$ by other methods	
			$A_0$	$\bar{A}_L$	$\bar{A}_H$	$\bar{\nu}^*$	$\bar{\nu}^{**}$	reference
$U^{233}$	Neutrons	Thermal	234	$93,3 \pm 0,1$	$138,2 \pm 0,1$	$2,5 \pm 0,2$	$2,52 \pm 0,03$	[12, 13]
$U^{235}$	"	"	236	$94,8 \pm 0,1$	$138,8 \pm 0,1$	$2,4 \pm 0,2$	$2,47 \pm 0,03$	[12, 13]
$Pu^{239}$	"	"	240	$98,5 \pm 0,2$	$139,0 \pm 0,1$	$2,5 \pm 0,3$	$2,92 \pm 0,04$	[12, 13]
$Am^{241}$	"	Reactor spectrum	242	$101 \pm 0,3$	$138,3 \pm 0,3$	$2,7 \pm 0,6$	$3,14 \pm 0,05$	[14]
$Th^{232}$	"	Fission spectrum	233	$91,4 \pm 0,1$	$139,8 \pm 0,3$	$1,8 \pm 0,4$	1,8***	[12]
$U^{235}$	"	The same	236	$95,6 \pm 0,2$	$138,4 \pm 0,3$	$2,0 \pm 0,5$	$2,50 \pm 0,06^{****}$	[12, 13]
$U^{238}$	"	"	239	$97,3 \pm 0,1$	$138,9 \pm 0,1$	$2,8 \pm 0,2$	$2,65 \pm 0,07^{*****}$	[12, 13]
$U^{235}$	"	14 Mev	236	$96,3 \pm 0,2$	$135,5 \pm 0,2$	$4,2 \pm 0,4$	$4,13 \pm 0,24$	[12, 13]
$U^{238}$	"	14 Mev	239	$97,0 \pm 0,3$	$137,0 \pm 0,4$	$5,0 \pm 0,6$	$4,50 \pm 0,32$	[12, 13]
$U^{238}$	$\gamma$ rays	8-10 Mev	238	$96,6 \pm 0,1$	$138,7 \pm 0,3$	$2,7 \pm 0,4$	—	—
$U^{238}$	"	16 Mev	238	$97,4 \pm 0,1$	$137,5 \pm 0,3$	$3,1 \pm 0,4$	—	—
$U^{238}$	"	48 Mev	238	$96,5 \pm 0,2$	$137,2 \pm 0,3$	$4,3 \pm 0,5$	—	—
$Cf^{252}$	Spontaneous fission	—	252	$106,3 \pm 0,3$	$140,9 \pm 0,3$	$4,8 \pm 0,6$	$3,84 \pm 0,12$	[13]

\*The uncertainty in  $\bar{\nu}$  is determined by the sum of the uncertainties for  $\bar{A}_L$  and  $\bar{A}_H$ . The actual uncertainty in  $\bar{\nu}$  is smaller.

\*\*We give the experimental values of  $\bar{\nu}$  obtained by other methods, which are averaged over many measurements. Hence, the uncertainty is appreciably smaller than the experimental uncertainties in the individual methods.

\*\*\*This is obtained by direct extrapolation by the values of  $\bar{\nu}_1 = 2.35 \pm 0.07$  for  $E_n = 3.5$  Mev and  $\bar{\nu}_2 = 4.64 \pm 0.20$  for  $E_n = 14.2$  Mev.

\*\*\*\*For an effective energy of 0.7-0.74 Mev.

\*\*\*\*\*For an energy of 1.5 Mev.

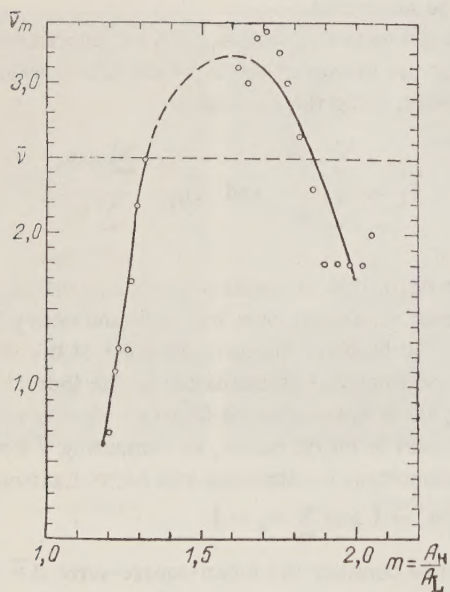


Fig. 1. Partial values  $\bar{\nu}_m$  for thermal-neutron fission of  $U^{233}$ .

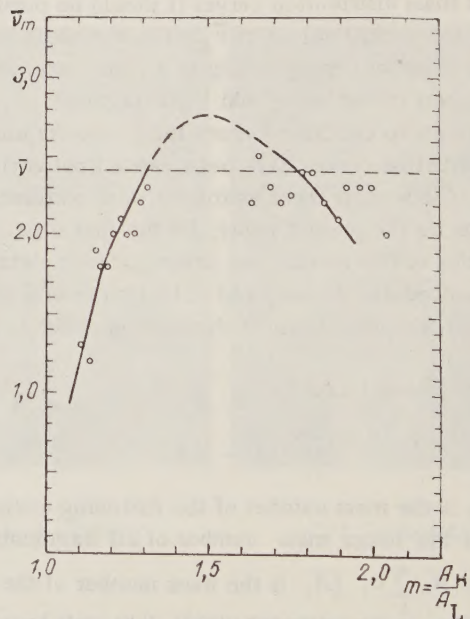


Fig. 2. Partial values  $\bar{\nu}_m$  for thermal-neutron fission of  $U^{235}$ .

from the corresponding normalization conditions, it can be shown that when Eq. (1) is used

$$\Delta \bar{v} = \pm \epsilon \sqrt{\sum_i \alpha_i^2 (\bar{A}_L - A_i)^2}; \quad (3)$$

while when Eq. (2) is used

$$\Delta \bar{v} = \pm \epsilon \sqrt{\sum_i \alpha_i^2 (\bar{A}_L - A_i)^2 + \sum_k \alpha_k^2 (\bar{A}_H - A_k)^2}, \quad (4)$$

where  $\epsilon = \Delta \alpha / \alpha$  is the relative uncertainty in the determination of  $\alpha$  (for simplicity we assume that  $\epsilon$  is the same in all cases).

In the case of thermal-neutron fission of  $U^{235}$ , computing  $\bar{v}$  from Eq. (1) we find  $\Delta \bar{v} \approx \pm 1.3$ ; computing this same quantity from (2) we find  $\Delta \bar{v} \approx \pm 0.15$  (in both cases we assume that  $|\epsilon| \approx 0.05$ ). Thus, when Eq. (2) is used the accuracy of the calculation is an order of magnitude better than the accuracy attained with Eq. (1).

The accuracy depends strongly on the asymmetry in the fission-fragment mass distribution curve, which is determined by the depth of the valley. If the mass number  $A_L$  (characterized by the yield  $\alpha_L$ ), intermediate between the numbers of light and heavy fragments, refers to the heavy fragment rather than the light fragment, or vice versa, an additional error  $\Delta \bar{v}_I = |(\bar{A}_H - \bar{A}_L) \alpha_L|$  (with an accuracy to second order) occurs. As an example we estimate  $\Delta \bar{v}_I$  for fission of  $U^{235}$  by thermal neutrons (the asymmetry is well defined,  $\alpha_L \approx 10^{-4}$ ) and for fission by neutrons with energies of 14 Mev (in which case the asymmetry is weaker,  $\alpha_L \approx 10^{-2}$ ). Taking  $(\bar{A}_H - \bar{A}_L) \approx 40$ , in the first case we have  $\Delta \bar{v}_I \approx 0.004$ ; in the second case  $\Delta \bar{v}_I \approx 0.4$ . Thus for fission by 14-Mev neutrons the quantity  $\Delta \bar{v}_I$  can make a sizeable contribution in the final uncertainty.

Since the error in the determination of  $\bar{v}$  by the method described here depends on the uncertainty in the yield determination, it is extremely important that the yields (absolute or relative)  $\alpha_i$  and  $\alpha_k$  be known for the greatest possible number of mass numbers  $A_i$  and  $A_k$ . Interpolation of the fragment mass distribution curve for  $A$  with unknown values of  $\alpha$  increases the error. For this reason the calculations reported here were limited to those cases in which the fragment mass distribution curves were known rather completely and characterized by well-defined asymmetries. In this work we have used data published up to January, 1959 [1-11]. It should be noted that experimental refinement of the fission-fragment mass distribution curves will make it possible to compute  $\bar{v}$  for many other cases of interest in the future. For the cases which have been studied, refinement of the distribution curves will make it possible to increase the accuracy in the determination of  $\bar{v}$ . In certain cases (for example, for  $U^{238}(\gamma, f)$ , [2]) appropriate distributions have not been studied with the necessary detail; however, by using "reflected" points and a successive approximation

technique it is possible to carry out the necessary calculations. It should be noted, however, that in this case it is necessary to take account of the variation of the partial value values  $\bar{v}_m$  as a function of the type of fission which is involved.

The results of the calculations of  $\bar{v}$  by the method reported here are given in the Table. For comparison purposes, we also show values of  $\bar{v}$  determined experimentally by indirect methods. As is apparent from the Table, in the majority of cases the values of  $\bar{v}$  computed by the present method are in satisfactory agreement with the values determined by other methods.

It may be indicated that the data for  $\bar{v}$  for fission of  $U^{238}$  by  $\gamma$  rays with energies of 8-10, 16, and 48 Mev are new. In all cases the uncertainty in the determination of  $\bar{A}_L$  and  $\bar{A}_H$  are obtained from the spread in the results of the calculations by different versions of the mass distribution curves; these curves in turn are obtained by different methods and are affected by the spread in the experimental points and the individual uncertainties.

The fission-fragment mass distribution curves also allow us to compute the partial values  $\bar{v}_m = A_0 - (A_H + A_L)_m$ ; the mass numbers  $A_H$  and  $A_L$  are coupled, i. e. characterized by the same yield  $\alpha_m (A_H/A_L = m)$ . Relation between  $\bar{v}$  and  $\bar{v}_m$  is expressed by the formula

$$\bar{v} = \frac{\sum_m \alpha_m \bar{v}_m}{\sum_m \alpha_m}. \quad (5)$$

The difference  $A_0 - (A_H + A_L)_m$  will determine the partial numbers of secondary neutrons for a given pair of mass numbers  $A_H$  and  $A_L$  under the following conditions: 1) the mass distribution curve is measured very carefully, 2)  $\alpha_m$  is a sensitive function of  $A$ , 3) there is no fine structure in the mass distribution curve, 4) the curve itself is monotonic in the region considered, and 5)  $\bar{v}_m$  and the distribution of probability for emission of one, two, three, etc. neutrons are weak functions of  $A$ .

The calculation of  $\bar{v}_m$  was carried out only for fission of  $U^{233}$  and  $U^{235}$  by thermal neutrons, for which there are experimental yield values for almost all the mass numbers. It will be apparent that this method of determining  $\bar{v}_m$  is not accurate in the region  $1.3 < m < 1.7$ . The curves that have been obtained (Figs. 1 and 2) are similar in shape to the analogous curves obtained for  $U^{233}$  by another method [16]. The maximum value of  $\bar{v}_m$  is obtained for values  $m \approx 1.5$ . In both cases there is a characteristic sharp reduction in  $\bar{v}_m$  for fission into fragments of approximately equal mass. If we consider the emission of secondary neutrons to be the result of excitation of fragments, which are not spherical in shape [17], it may be assumed that the fragments in symmetric fission are more spherical than the fragments due to asymmetric fission.

# LITERATURE CITED

1. S. Katcoff, *Nucleonics* 16, 4, 78 (1958).
2. R. Duffield, R. Schmitt, R. Sharp, Report No. 678 (USA) Second Int'l. Conf. on the Peaceful Uses of Atomic Energy (Geneva, 1958).
3. A. N. Protopopov et al., *Atomnaya Energiya* 5, 2, 130 (1958)\*.
4. M. P. Anikina et al., Second Int'l. Conf. on the Peaceful Uses of Atomic Energy (Geneva, 1958); Reports by Soviet Scientists, Nuclear Physics [in Russian] (Atomizdat, Moscow, 1959) Vol. I, p. 396.
5. L. Bunney et al., Report No. 643 (USA) Second Int'l. Conf. on the Peaceful Uses of Atomic Energy (Geneva, 1958).
6. K. Fritze, G. McMullen, and H. Thode, Report No. 187 (Canada) Second Int'l. Conf. on the Peaceful Uses of Atomic Energy (Geneva, 1958).
7. L. Bunney et al., Report No. 644 (USA) Second Int'l. Conf. on the Peaceful Uses of Atomic Energy (Geneva, 1958).
8. J. Cuninghame, *J. Inorg. and Nucl. Chem.* 4, 1 (1957).
9. J. Cuninghame, *J. Inorg. and Nucl. Chem.* 5, 1 (1957).
10. L. Glendenin and E. Steinberg, *J. Inorg. and Nucl. Chem.* 1, 45 (1955).
11. J. Cuninghame, *J. Inorg. and Nucl. Chem.* 6, 181 (1958).
12. R. Leachman, Second Int'l. Conf. on the Peaceful Uses of Atomic Energy (Geneva, 1958) Selected Reports of Foreign Scientists, Neutron Physics (Atomizdat, Moscow, 1959) Vol. II, p. 342; *Atomic Engineering Abroad*, 1, 11 (1959).
13. I. I. Bondarenko et al., Second Int'l. Conf. on the Peaceful Uses of Atomic Energy (Geneva, 1958) Report of Soviet Scientists, Nuclear Physics [in Russian] (Atomizdat, Moscow, 1959) Vol. I, p. 438.
14. V. I. Lebedev and V. I. Kalashnikova, *Atomnaya Energiya* 5, 2, 176 (1958)\*.
15. R. Jensen and A. Fairhall, *Phys. Rev.* 109, 942 (1958).
16. J. Fraser and C. Milton, *Phys. Rev.* 93, 818 (1954).
17. Ya. B. Zel'dovich and Yu. A. Zysin, *Zhur. Éksp. i Teoret. Fiz.* 10, 8, 851 (1940).

\*Original Russian pagination. See C. B. translation.

# AN INVESTIGATION OF THE PROPERTIES OF METALS AND SOME STEELS AFTER IRRADIATION BY FAST NEUTRONS

Sh. Sh. Ibragimov, V. S. Lyashenko, and A. I. Zav'yalov

Translated from *Atomnaya Énergiya*, Vol. 8, No. 5, pp. 413-419,  
May, 1960

Original article submitted May 28, 1959

The article considers the effect of the irradiation by fast neutrons and of a subsequent heat-treatment on the properties of some metallic materials. The change of the properties of materials upon irradiation is explained in terms of the formation of various types of defects on the crystal lattice, which are annealed at appropriate temperatures. The kinetics of the defect elimination processes leading to a strengthening of the material is studied, and their activation energy is determined.

It is well known that under the action of nuclear particles, especially of fast neutrons, significant changes take place in the physical and mechanical properties of various materials. The extent of these changes depends principally upon the particle energy, the integral dose, and the temperature of irradiation.

The change of mechanical properties of metallic materials under the action of heavy nuclear particles has some similarity with the strengthening produced by cold deformations. The cause of the property change in both cases could be looked for in the appearance of disturbances of the regularity of the crystal structure of the materials and defects of the lattice. On the other hand, some experimental data show an essential difference between the changes produced in a material by nuclear particles and those produced by a cold plastic deformations [1-3]. One can suppose that the disturbances arising under the action of nuclear particles are a complicated phenomenon; additional experimental and theoretical investigations are required before they can be explained.

The present paper reports an investigation of the effect of fast neutrons on the structure and properties of iron, nickel, molybdenum, and some steels, whose chemical composition is given by Table 1.

Samples of the materials mentioned above were irradiated in the active zone of an experimental BR-2 reactor [4] after an appropriate heat-treatment in special hermetically welded tubes of 1Kh18N9T steel. The average integral dose was  $1.8 \cdot 10^{20}$  fast neutrons per  $1 \text{ cm}^2$ , and the irradiation temperature was 40-70°C.

The properties of the materials studied, before and after irradiation, are presented in Table 2. The data of the table show that as a result of irradiation by fast neutrons, the strength, hardness, and electric resistance increased, and the relative lengthening decreased. The degree of property change depended upon the nature of

TABLE 1. Chemical composition of some steels

Steel type	Contents of principal elements, %				
	C	Cr	Ni	Mo	Ti
1Kh18N9	0,14	16,0	9,5	—	—
1Kh18N9T	0,11	16,7	9,2	—	0,6
1Kh18N12	0,09	16,6	12,0	—	—
1Kh18N12M2T	0,10	17,2	12,4	2,1	0,5
1Kh18N17	1,12	16,1	16,9	—	—

the irradiated material: a more or less complex composition of a steel due to alloying with various elements did not seem to have any important effect on the magnitude of the change in question. The greatest change was observed for molybdenum (its relative lengthening decreased by a factor more than 10, its electric resistivity had a 33% increase); this may have depended upon the high annealing temperature and upon the high elastic constants of molybdenum.

With the purpose of studying the temperature stability of radiation defects and establishing the temperature of complete regression of the properties, the irradiated samples were subjected to annealing at various temperatures for 30 min. After each treatment the microhardness and (in some instances) the electric resistance of the samples were determined. The results of the microhardness measurements are given in Figs. 1 and 2.

The data presented in Figs. 1 and 2 show that: 1) as a result of heating at appropriate temperatures a complete elimination of the increase in microhardness took place; 2) the increase in microhardness upon heat-treatment took place in a temperature range higher for materials with body-centered cubic lattices (iron, molybdenum) than for materials with face-centered cubic

TABLE 2. Properties of metals and of some steels before and after irradiation

Material	Heat-Treatment	Strength limit, kg/mm <sup>2</sup>		Relative lengthening, %		Microhardness, kg/mm <sup>2</sup>				Specific electric resistance, μ ohm· cm			
		before ir- radiation	after ir- radiation	variation	before ir- radiation	after ir- radiation	variation	before ir- radiation	after ir- radiation	variation	before ir- radiation	after ir- radiation	variation
Iron, 99.84 % pure	Annealing at 760°C for 1 hr.	39,5	59,5	20,0	36,5	45,0	-21,5	117,0	185,0	68,0	15,2	16,4	1,2
Nickel, 99.97 % pure	Annealing at 760°C for 1 hr	43,0	59,0	16,0	49,5	26,0	-23,5	115,0	199,0	84,0	7,8	8,2	0,4
Molybdenum, 99.9 % pure	Annealing at 1100°C for 1 hr	69,0	—	—	27,0	2,0	-25,0	215,0	303,0	88,0	5,5	7,3	1,8
Steel	Tempering from 1100°C in water	62,0	74,0	9,0	69,0	47,0	-22,0	157,0	252,0	95,0	—	—	—
1Kh18N9T		63,5	75,0	11,5	77,0	49,0	-28,0	150,0	260,0	110,0	—	—	—
1Kh18N12		54,5	66,5	12,0	65,0	41,0	-24,0	135,0	235,0	100,0	—	—	—
1Kh18N12M2T		60,0	70,5	10,5	71,5	43,5	-28,0	143,0	241,0	98,0	77,0	77,6	0,6
1Kh18N17		51,5	63,0	11,5	58,0	36,0	-22,0	131,0	232,0	101,0	76,9	77,6	0,7

lattices (nickel, austenite steels); 3) the temperature of complete annealing depended upon the melting temperature of a material: *ceteris paribus* (e. g. for identical crystal lattices) this temperature was higher for a higher melting temperature; 4) alloying with various elements, and changes in composition of austenite steels almost did not affect the behavior of the curve of microhardness increase. When iron was alloyed with chromium and nickel, the tempering temperature shifted toward higher temperatures, and became the same as in nickel: this is evidently related to the change of the crystal structure of the material as a result of alloying.

Figure 3 shows the specific electric resistance change in irradiated and nonirradiated samples of molybdenum in relation to the annealing temperature. It is clear that

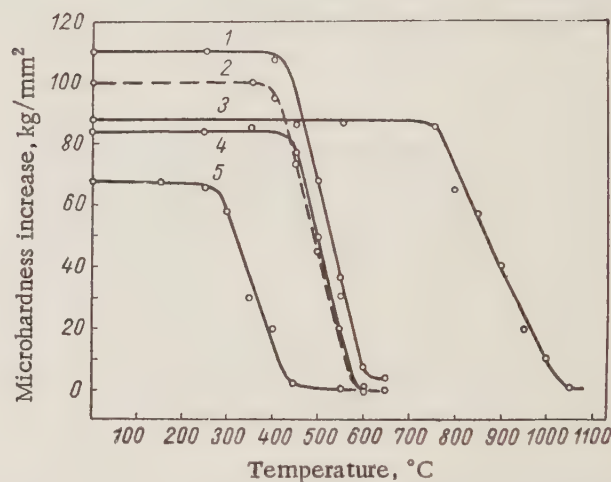


Fig. 1. Increase in microhardness of irradiated metals and steels vs. annealing temperature: 1, steel 1Kh18N9T; 2, steel 1Kh18N17; 3, molybdenum; 4, nickel; 5, iron.

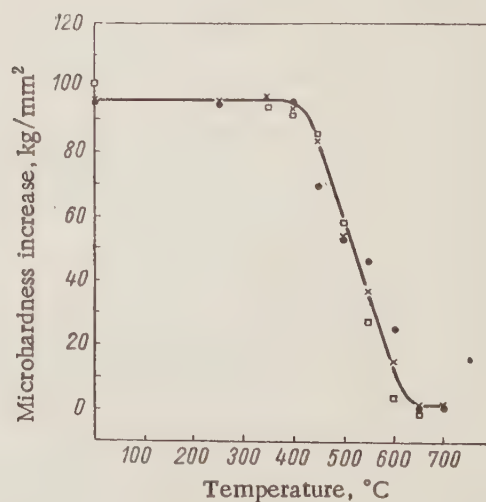


Fig. 2. Increase in microhardness of irradiated steels vs. annealing temperature: ●, steel 1Kh18N9; □, steel 1Kh18N12; x, steel 1Kh18N12M2T.

the regression of electric resistance of irradiated molybdenum took place continuously in a wide temperature range, and was complete at a temperature of 700°C; the behavior of the curve representing the changes in electric resistance vs. annealing temperature is sharply different from that of the analogous curve for microhardness. This suggests that the radiation defects leading to a change in the electric resistance were of a nature much different from that of defects leading to a strengthening of the metal.

On the basis of the data reported in Fig. 1 we chose some temperatures at which the kinetics of the microhardness restoration process in iron were studied; the kinetic data served also for the determination of the activation energy.

The curves representing the microhardness decrease for irradiated iron in relation to the duration of perma-

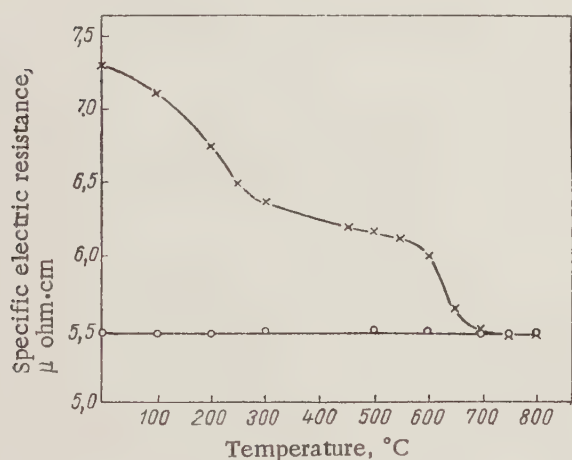


Fig. 3. Change of specific electric resistance of irradiated (x) and nonirradiated samples (O) of molybdenum vs. annealing temperature.

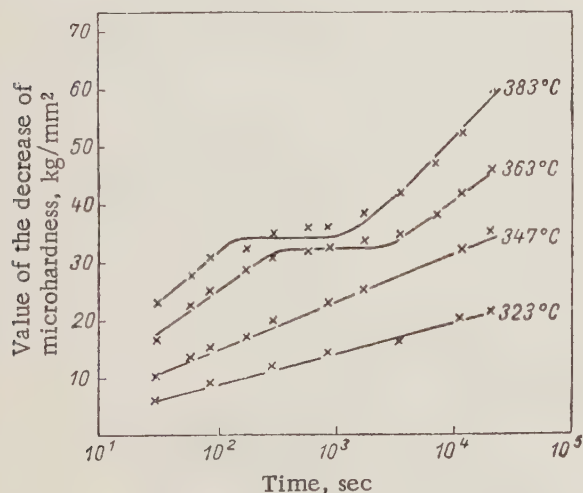


Fig. 4. Decrease of the microhardness of an irradiated sample vs. time of permanence at various annealing temperatures.

ence at various temperatures are reported in Fig. 4. The figure shows that an increase in the isothermal annealing temperature changed the character of the kinetic curves. Consequently, the defects due to irradiation and leading to a strengthening of the metal were apparently of different types and had different degrees of stability.

Thus, the curves for temperatures of 363 and 383°C have horizontal parts: this is evidently a result of the fact that two different processes with different activation energies took place. Therefore, one can suppose that at the beginning of heating, defects of two types, having activation energies  $Q_1$  and  $Q_2$ , respectively, were present in an irradiated sample.

If such was the case, the microhardness of an irradiated sample could be described by means of the following equation:

$$H_{\text{irr}}(\tau=0) = H_0 + H' = H_0 + A_1 C_1^0 + A_2 C_2^0, \quad (1)$$

where  $H_0$  is the microhardness of the sample before irradiation;  $C_1^0$  and  $C_2^0$  are the concentrations of first and second type defects before and after irradiation ( $\tau=0$ );  $A_1$  and  $A_2$  are proportionality factors.

As a result of annealing at a temperature  $T$  during a time  $\tau$ , the microhardness of a sample would be

$$H_{\text{irr}}(\tau) = H_0 + A_1 C_1(\tau) + A_2 C_2(\tau), \quad (2)$$

where  $C_1$  and  $C_2$  are the concentrations of first and second type defects at the time  $\tau$ .

On the basis of the data relating to the study of the annealing of irradiated molybdenum, we think that the defects observed in the crystal lattice were not Frenkel type defects, but defects of another type. Therefore, we shall suppose that the change of the number of defects with time upon annealing obey the following equations:

$$\frac{dC_1}{d\tau} = -\frac{C_1}{\gamma_1(T)}; \quad (3)$$

$$\frac{dC_2}{d\tau} = -\frac{C_2}{\gamma_2(T)}, \quad (4)$$

where  $\gamma_1(T)$  and  $\gamma_2(T)$  are the average times in which the disappearance of first and second type defects took place, respectively, at a temperature  $T$ .

The solutions of these equations are

$$C_1 = C_1^0 e^{-\frac{\tau}{\gamma_1(T)}}; \quad (5)$$

$$C_2 = C_2^0 e^{-\frac{\tau}{\gamma_2(T)}} \quad (6)$$

The magnitude of the microhardness decrease of an irradiated sample subjected to annealing for a time  $\tau$  is

$$\Delta H = H_{\text{irr}}(\tau=0) - H_{\text{irr}}(\tau) = A_1 (C_1^0 - C_1) + A_2 (C_2^0 - C_2).$$

Using formulas (5) and (6), we find that

$$\Delta H = A_1 C_1^0 (1 - e^{-\frac{\tau}{\gamma_1(T)}}) + A_2 C_2^0 (1 - e^{-\frac{\tau}{\gamma_2(T)}}). \quad (7)$$

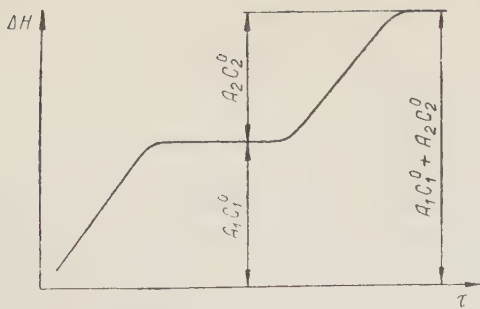


Fig. 5. Schematic dependence of the change of microhardness of an irradiated metal from the duration of heating at a temperature  $T$ .

If the activation energy  $Q_1$  is appreciably different from the energy  $Q_2$ , and e. g.,  $Q_2 > Q_1$ , then the dependence of the microhardness upon the time of annealing will have the form shown in Fig. 5.

A comparison of the theoretical curve (Fig. 5) with the experimental curve (Fig. 4) shows that for temperatures of 323 and 347°C and heatings of 6 hr, only first type defects were annealed. These defects were eliminated partially after heating for 6 hr at 323°C, and disappeared almost completely at 347°C (the value of the decrease in microhardness reached the level of the horizontal part of the curve). At 363 and 383°C both types of defects were annealed (the curves have a horizontal part); those of the second type were annealed only in part. Heating for 6 hr at 383°C was still insufficient to cause the appearance of the second horizontal part of the curve  $\Delta H = f(\tau)$  and, consequently, to eliminate completely the defects of the second type.

Let us consider short times, when  $\tau \ll \gamma_1(T)$ . Since  $Q_2 > Q_1$ , in this case we find, approximately,

$$(\Delta H)_T = A_1 C_1^0 \frac{\tau}{\gamma_1(T)}. \quad (8)$$

Using this equation, and assuming that  $\gamma_1(T) \approx e^{Q_1/RT}$ , we get for these times

$$\frac{(\Delta H)_{T_1}}{(\Delta H)_{T_2}} = \frac{e^{Q_1/RT_2}}{e^{Q_1/RT_1}}. \quad (9)$$

From (9) we can conclude that the logarithm of the microhardness decrease  $\Delta H$  is a linear function of  $1/T$  for the times under consideration.

Figure 6 shows the dependence of the decrease in microhardness of irradiated iron for  $\tau = 1.5$  min upon the reciprocal of the temperature (semilogarithmic scale). It can be seen from it that the experimental points lie well on the straight line. From the angle of the straight line with the axis of the abscissa we find the activation energy, which is 16,500 cal/mole.

The quantity  $Q_1$  is close to the activation energy for the elimination of second order deformations in an iron wire (15,000 cal/mole) deformed by 95% [5]. In

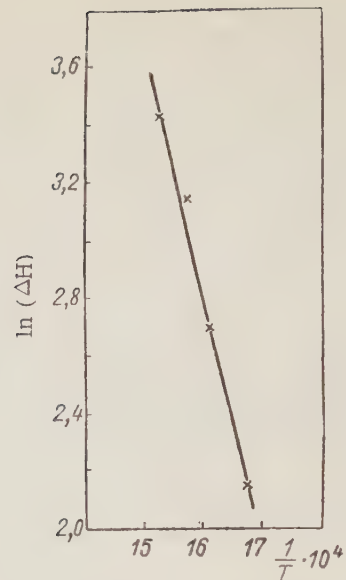


Fig. 6. Temperature of the microhardness decrease of irradiated iron.

addition, the process of first-type-defect annealing (beginning of the decrease of microhardness of irradiated iron, see Fig. 1) begins at the same temperature as the elimination of second order deformations upon annealing of cold deformed iron [6]. Therefore, we can suppose that this process is related to the elimination of defects of the type of second order deformations, and, therefore, hasn't the character of a diffusion process. Were it a diffusion process, it would begin at a temperature markedly dependent upon the degree of alloying of the material. Experiment shows that, on the contrary, this temperature remains almost the same when the alloying is changed, and depends principally upon the crystal structure and the melting temperature of the material. Thus, iron and nickel have very similar properties, and differ only by their crystal structure. Iron has a body-centered cubic lattice, and the temperature at which it starts annealing is  $\sim 270^\circ\text{C}$ . Nickel has a face-centered cubic lattice, and the temperature at which annealing begins is  $\sim 430^\circ\text{C}$ . It must be noted that a significant decrease of second order deformations in cold deformed nickel also starts at  $\sim 430^\circ\text{C}$  [6]. The steels we investigated had a face-centered cubic lattice, roughly the same melting temperature, and, notwithstanding the difference in composition, also an identical temperature of beginning of annealing ( $\sim 430^\circ$ ).

Let us now consider times when  $\gamma_1(T) \ll \tau \ll \gamma_2(T)$ . In this case Eq. (7) gives

$$(\Delta H)_T = A_1 C_1^0 + A_2 C_2^0 \frac{\tau}{\gamma_2(T)}. \quad (10)$$

Therefore, the decrease in microhardness of an irradiated sample upon annealing at the expense of the elimination of only second type defects (all first type defects

having already been suppressed for the times under consideration) is equal to

$$(\Delta H^*)_T = (\Delta H)_T - A_1 C_1^0 = A_2 C_2^0 \frac{\tau}{\gamma_2(T)}. \quad (11)$$

Assuming that  $\gamma_2(T) \approx e^{Q_2/RT_2}$ , we find

$$\frac{(\Delta H^*)_{T_1}}{(\Delta H^*)_{T_2}} = \frac{e^{Q_2/RT_2}}{e^{Q_2/RT_1}}. \quad (12)$$

This relation allows us to determine the activation energy of second type defects. Using the data for temperature  $T_1=636^\circ\text{K}$  and  $T_2=656^\circ\text{K}$  with  $\tau=360$  min, reported in Fig. 4, we find for  $Q_2$  the value 28,700 cal/mole.

Thus, the activation energy of the process of annealing of second type defects is appreciably higher than  $Q_1$ , and roughly two times lower than the activation energy of spontaneous diffusion in iron.

Consequently, we must conclude that the elimination of second type defects proceeds without diffusion. This is proved also by the fact that the temperature of the process is practically independent of the degree of alloying.

An x-ray investigation shows the presence, in irradiated iron, of defects in the form of third order deformations. It has been suggested [6] that the value of the activation energy for the elimination of third order defects must have a value intermediate between the value of the activation energy for the elimination of second order deformations and the value of the recrystallization activation energy (the latter is 45,000-55,000 cal/mole in iron). Therefore, we think that the process observed by us with an activation energy of 28,700 cal/mole is related to the elimination of defects of the type of third order deformations.

At present there are contradictory data [2,7] concerning the effect of a neutron field on the microstructure of some pure metals, in particular nickel and copper. We have carried out an investigation of iron (Fig. 7), nickel, and molybdenum microstructures, before and after

irradiation, and after annealing of the irradiated samples. The investigation shows that under the influence of a neutron field (at 40-70°C) and as a result of a subsequent heat-treatment, no significant changes took place in the microstructures of the metals.

The results and the discussion given above permit us to draw the following conclusions:

1. As a result of irradiation of metallic materials by fast neutrons at 40-70°C, their mechanical properties and their electric resistances change due to the formation of various types of defects in the crystal lattice.

2. The radiation defects leading to a strengthening of the materials have a nature essentially different from that of the defects producing an increase in the electric resistances of the materials; the former undergo annealing at much higher temperatures than the latter. The temperature of annealing of these defects is independent of the degree of alloying.

3. The strengthening of an irradiated sample of a metallic material is due to defects of the type of second order and third order deformations, which are annealed without the intervention of diffusion and have activation energies of 16,500 and 28,700 cal/mole, respectively.

4. The strengthening upon irradiation and annealing of irradiated metals is not accompanied by a change of their microstructures.

5. Irradiation by fast neutrons of austenite steels produces a change of the strength characteristics (limits of strength and hardness) remarkably independent of the degree of alloying.

The authors express their gratitude to V. M. Agranovich for his useful participation in the discussion of the results of this work.

#### LITERATURE CITED

1. F. Kunz and A. Holden, *Acta Metallurgica* 2, 6, 816 (1954); see also the collection: *Effect of Nuclear Radiations on the Structure and Properties of Metals and Alloys* [in Russian] (Metallurgizdat, Moscow, 1957) p. 63.



Fig. 7. Microstructure of iron ( $\times 400$ ): a) before irradiation; b) after irradiation.

2. S. T. Konobeevskii, N. F. Pravdyuk, and V. I. Kutaitsev, Reports of the International Conference on the Peaceful Uses of Atomic Energy (Geneva, 1955) [in Russian] (Goskhimizdat, Moscow, 1958) Vol. 7, p. 526.
3. V. S. Lyashenko and Sh. Sh. Ibragimov, Atomnaya Energiya 6, 3, 277 (1959).\*
4. A. I. Leipunskii et al., Atomnaya Energiya 2, 6, 497 (1957).\*
5. V. A. Il'ina et al., Problems of Metallurgy and Physics of Metals. Third Collection of Papers of the Institute of Metallurgy and Physics of Metals [in Russian] (Metallurgizdat, Moscow, 1952) p. 178.
6. Ya. S. Umanskii et al., Physical Foundations of Metallurgy [in Russian] (Metallurgizdat, Moscow, 1955) pp. 465, 471.
7. C. Bruch, W. Mc Hugh, and L. Doig, Atomic Technology Abroad No. 1, 40 (1958).

\*Original Russian pagination. See C. B. translation.

# VAPOR PRESSURE OF T<sub>2</sub>O

M. M. Popov and F. I. Tazetdinov

Translated from Atomnaya Energiya, Vol. 8, No. 5, pp. 420-424,

May, 1960

Original article submitted November 3, 1959

The procedure is described and the results of the determination of the vapor pressure of samples of high-percent-age tritium water (containing 83.4 and 98.1 mole % T<sub>2</sub>O) in the 12-95°C temperature range are given. To calculate the pressure of the gaseous products of the radiolysis of water and nuclear transformations the measurements were carried out by the static method at two different volumes of the apparatus. It was found that the boiling points of HTO and T<sub>2</sub>O are 100.8 and 101.6°C, the heats of vaporization at these temperatures are 9.9 and 10.0 kcal/mole, and the standard entropies are 19.3 and 19.0 units, respectively.

In the literature there are two brief reports on measurements of the vapor pressure of tritium water with a low T<sub>2</sub>O content. The results of the measurements are contradictory: in one case the boiling point of HTO was less than H<sub>2</sub>O [1], and in the other it was higher [2]. This article describes the procedure and results of measurements of the vapor pressure of two samples of high-percentage T<sub>2</sub>O in the 12-95°C temperature range.

## Measurement Method and Equipment

The vapor pressure of T<sub>2</sub>O can be measured by the static method if the measurements are carried out at several (not less than two) different volumes of the apparatus, in spite of the fact that gaseous products, formed as a result of the radioactivity of tritium, are inevitably present above the T<sub>2</sub>O. Since a variation in the volume does not influence the pressure of the saturated vapor, the

total pressure of the mixture of vapor and gases can be subdivided into the individual components. In all probability the concentration of hydrogen peroxide formed by the radiolysis of the sample is very low [3] and therefore has little influence on the measured vapor pressure. This measurement method was selected because it can be easily carried out for microamounts of the sample (not more than one drop) and does not require special safety measures.

The measurements were carried out in a glass (ZS5K) apparatus that differed from ordinary apparatus for static measurements by the fact that its working volume could be modified (see fig. ). The null instrument was a differential mercury manometer 3. The volume was changed by altering the mercury level in the manometer 3. By bringing the mercury meniscus into contact with the ends of glass needles sealed inside the manometer tube it was possible to reproduce two known volumes with an error of  $\pm 0.005 \text{ cm}^3$ . Manometers 3 and 4 were made from tubes with an internal diameter of  $\sim 15 \text{ mm}$ .

The pressure was measured by cathetometers. The measurement errors of pressures up to 200 mm Hg were 0.03 mm, above 200 mm Hg they were 0.06 mm.

Manometer 3 was thermostatically controlled separately from the liquid sample at a temperature 5-10°C above the temperature of the sample, to avoid condensation of vapor on the walls of the manometer during variations in the volume. The temperature variations of the thermostat 7 (see fig. ) were not more than  $+0.003^\circ\text{C}$ . The temperature was measured by mercury thermometers, graduated in  $0.1^\circ$ , with an accuracy of up to  $0.01^\circ$ . The thermometers were checked against standard platinum resistance thermometers under the experimental conditions.

The liquid samples (about 4 mM) were obtained by reacting cupric oxide, heated to  $350^\circ\text{C}$ , with tritium purified by uranium. The reaction product was condensed directly in the measuring apparatus. The isotopic composition of the initial tritium was determined by means of a

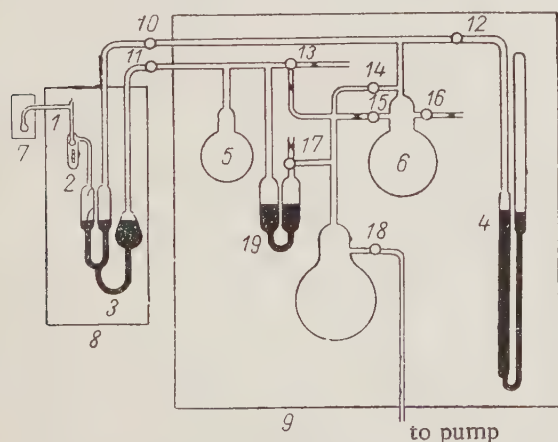


Diagram of the apparatus for measuring the vapor pressure: 1) ampoule with sample; 2) opening device; 3) zero reading manometer; 4) manometer; 5,6) buffer volumes; 7,9) thermostats; 10-18) taps; 19) compressor.

quartz gas balance.\* The working principle of the balance and the method for the determinations are described in [4]. The use of mercury traps and electromagnetic valves instead of traps in the apparatus made it possible to avoid contact of the purified tritium and the sample (obtained) with organic grease.

To determine the vapor pressure at a given temperature, three pressure readings were taken: the first and last readings were taken at the volume of the gaseous phase  $V_1$ , and the second at the volume  $V_2$ . The pressure  $P_1$  at the volume  $V_1$ , corresponding to the moment of the second reading, was found from the results of the first and last readings, taking the rate of accumulation of the gases between these readings as constant. This value of  $P_1$  and the result of the second reading  $P_2$  correspond to the same amount of gas in the apparatus, but to the two values of the volume  $V_1$  and  $V_2$ . By employing the law of partial pressures  $P_1 = P_v + \bar{p}_1$  and  $P_2 = P_v + \bar{p}_2$  and the Mendeleev-Clapeyron law

$$\begin{aligned} \bar{p}_1(V_1 - V_3) &= (n - x)RT_2; & \bar{p}_1V_3 &= xRT_1; \\ \bar{p}_2(V_2 - V_3) &= (n - y)RT_2; & \bar{p}_2V_3 &= yRT_1, \end{aligned}$$

the vapor pressure of the sample was found by the following equation:

$$P_v = \frac{1}{V_2 - V_1} \left( P_2V_2 - P_1V_1 - \Delta PV_3 \frac{T_2 - T_1}{T_1} \right), \quad (1)$$

where  $P_v$  is the pressure of the saturated vapor of the sample;  $\bar{p}_1$  and  $\bar{p}_2$  are the partial pressures of the gases in the mixture at  $V_1$  and  $V_2$ ;  $V_3$  is the part of the volume of the gaseous phase present in the thermostat 7;  $x$  and  $y$  are the amounts of gas in this volume;  $T_1$  and  $T_2$  are the temperatures of thermostats 7 and 8, respectively ( $^{\circ}\text{K}$ ) (see fig. );  $\Delta P = P_1 - P_2$ , and  $n$  is the number of moles of gas in the apparatus. The absolute values of  $V_1$ ,  $V_2$ , and  $V_3$  were determined with an error of  $\sim 10\%$ .

The following equations for the vapor pressure of  $\text{H}_2\text{O}$  (mm Hg):

$$\lg P = 8,0344 - \frac{1711,0}{t + 232}; \quad (2)$$

$$\lg P = 8,0632 - \frac{1725,5}{t + 233}, \quad (3)$$

where  $t$  is the temperature of the water ( $^{\circ}\text{C}$ ), were obtained by preliminary measurements of the vapor pressure of two samples of water prepared from cylinder hydrogen purified by uranium.

The measurements were carried out in the presence of 3 and 13  $\mu\text{M}$  of hydrogen. In four cases out of 30, the deviations of the experimental points from those calculated by the corresponding equation exceeded the maximum experimental error. Equations (2) and (3) give values of the vapor pressure of  $\text{H}_2\text{O}$ , which differ from the data of [5] at  $20^{\circ}\text{C}$  by +0.02 and +0.01 mm, and at  $100^{\circ}\text{C}$  by -0.6 and +1.2 mm, and a boiling point of 100.02 and

99.95 $^{\circ}\text{C}$ . The values of the heats of vaporization of  $\text{H}_2\text{O}$  in the 0-100 $^{\circ}\text{C}$  range, calculated from equations (2) and (3), agree to 1% with the data of [5].

## Results and Their Discussion

Tables 1 and 2 give the results of measurements of the vapor pressure of two samples of tritium water with a total  $\text{T}_2\text{O}$  content of 83.4 and 98.1 mole % (remainder  $\text{H}_2\text{O}$ ).

The data obtained with the more concentrated sample were evaluated after conversion to 100%  $\text{T}_2\text{O}$ . When the results were studied the limits of indeterminacy of the experimental points were taken as equal to the maximum measurement errors indicated in Tables 1 and 2. In our opinion, the systematic errors due to the approximate nature of the laws used for the derivation of equation (1), the neglect of variations in the rate of accumulation of gases in the apparatus between the three pressure readings at a given temperature, the variation in the isotopic composition of the samples and the presence of peroxide in them (only in the most unfavorable cases) could, in all, represent only one tenth of the measurement errors and were not taken into account.

The data obtained can be represented by the equations

$$\lg P = 8,0933 - \frac{1721,2}{t + 229} \quad \text{for } 83,4\% \text{ } \text{T}_2\text{O}; \quad (4)$$

$$\lg P = 7,9957 - \frac{1654,9}{t + 222} \quad \text{for } 100\% \text{ } \text{T}_2\text{O}. \quad (5)$$

The constants of the equations were found by a graphical method [6].

In experiments with 98.1%  $\text{T}_2\text{O}$  (see Table 2), in seven cases the discrepancy between the experimental data and those calculated by means of equation (5) exceeds the limits of experimental error. Such cases also occurred during "blank" measurements. It is probable that the individual readings included in these measurements were taken under conditions differing appreciably from equilibrium conditions. In the presence of a varying amount of gases, when the volume of the apparatus must be kept constant, complete attainment of equilibrium in our apparatus is hardly possible because with a variation in the pressure the volume of the apparatus also varies; as a result of the adjustment of the volume, the processes of vaporization or condensation are accelerated, which causes concentration of gases in certain parts of the volume, i.e. to some extent a removal of the system from equilibrium. We can, therefore, speak only of approximate practical equivalence of the measured pressure to equilibrium.

To avoid the accumulation of a large amount of gas in the apparatus and an increase in the measurement errors,

\* These measurements were carried out by M. D. Senin and Yu. M. Morozov, to whom the authors wish to express their sincere thanks.

TABLE 1. Vapor Pressure of 83.4% T<sub>2</sub>O (volume of the apparatus: V<sub>1</sub>=3.886 cm<sup>3</sup>, V<sub>2</sub>=10.652 cm<sup>3</sup>, V<sub>3</sub>=0.32 cm<sup>3</sup>)

Expt. no.	T <sub>1</sub> , °C	T <sub>2</sub> , °C	P <sub>1</sub> , mm Hg	P <sub>2</sub> , mm Hg	P <sub>V</sub> , mm, Hg	maximum error, ± mm	Discrepancy from Eq. (4), mm
1	19,99	29,4	40,70	24,43	15,06	0,16	-0,10
19*	24,95	29,0	153,77	65,26	21,06	0,48	+0,38
2	30,00	40,0	57,65	38,80	27,94	0,20	-0,10
18*	34,92	40,0	161,80	78,62	37,06	0,49	-0,23
3	39,92	51,2	83,24	61,65	49,52	0,25	+0,22
4	45,01	50,3	100,84	78,03	64,90	0,28	+0,07
5	50,12	60,1	124,97	99,40	84,66	0,33	+0,18
6	50,12	60,1	126,54	100,00	84,71	0,34	+0,23
7	50,12	60,1	130,58	101,46	84,69	0,35	+0,21
8	55,02	60,2	156,50	125,60	107,81	0,42	-0,13
9	59,95	70,0	192,03	156,75	136,44	0,55	-0,51
17*	65,02	70,0	294,07	213,82	173,81	0,71	+0,32
10	70,07	79,1	274,60	238,34	217,42	0,67	-0,42
16*	75,09	80,1	309,50	283,60	270,60	0,68	+0,12
11	80,12	89,6	390,47	355,08	334,62	0,84	-0,53
15	85,22	95,8	437,52	421,65	412,39	0,89	-0,29
12	90,32	95,4	553,39	523,12	505,55	1,08	+0,77
13	90,32	95,4	525,08	512,77	505,53	1,01	+0,75
14	95,41	97,5	633,06	620,32	612,78	1,17	-0,52

\* After experiment No. 15, mercury entered the area where the head of the electromagnetic value is located (see Fig. 1); as a result, the values of V<sub>1</sub> and V<sub>2</sub> were reduced by 0.512 cm<sup>3</sup>.

TABLE 2. Vapor Pressure of 98.1% T<sub>2</sub>O (volume of the apparatus: V<sub>1</sub>=4.277 cm<sup>3</sup>, V<sub>2</sub>=11.043 cm<sup>3</sup>, V<sub>3</sub>=0.40 cm<sup>3</sup>)

Expt. no.	T <sub>1</sub> , °C	T <sub>2</sub> , °C	P <sub>1</sub> , mm Hg	P <sub>2</sub> , mm Hg	P <sub>V</sub> , mm Hg	P <sub>T<sub>2</sub>O</sub> , mm Hg	Maximum error, ±mm	Discrepancy from Eq. (5), mm
1	12,13	20,0	15,56	11,52	8,32	8,28	0,10	-0,18
3	14,69	29,9	27,86	17,03	10,15	10,10	0,13	+0,09
2	19,87	30,4	28,39	19,77	14,30	14,24	0,13	0,00
4	25,40	29,9	39,96	27,98	20,40	20,32	0,16	+0,07
5	30,09	40,0	51,63	36,44	26,81	26,71	0,18	-0,27
6	35,77	44,8	70,80	50,71	37,98	37,86	0,22	+0,22
30	40,26	45,1	139,03	83,66	48,61	48,46	0,42	-0,02
7	40,66	44,9	85,08	63,38	49,63	49,47	0,24	-0,09
29	45,40	49,9	133,20	90,90	64,11	63,93	0,41	-0,17
8	47,41	50,6	111,58	86,92	71,31	71,12	0,27	-0,17
28	50,18	59,9	146,23	107,47	82,89	82,69	0,44	+0,37
9	50,41	60,2	138,11	104,53	83,23	83,01	0,36	-0,29
27	54,94	59,9	163,99	128,05	105,28	105,02	0,46	+0,30
10	55,93	60,2	168,36	132,25	109,37	109,12	0,40	-0,86
26	59,65	65,0	174,31	148,86	132,73	132,44	0,46	+0,52
11	61,03	69,8	202,51	165,05	141,30	141,00	0,54	-0,19
25	64,70	75,7	205,66	182,63	168,00	167,67	0,54	+0,39
12	64,75	70,0	230,09	191,80	167,54	167,19	0,58	-0,45
24	69,61	75,7	246,27	224,02	209,89	209,50	0,61	-0,25
13	70,38	80,2	279,49	241,63	217,59	217,20	0,68	+0,68
23	74,98	85,1	300,49	278,98	265,28	264,82	0,71	-0,20
14	75,72	78,9	333,21	296,73	273,59	273,12	0,76	-0,48
22	79,92	85,1	361,77	340,78	327,40	326,89	0,80	+0,04
15	80,26	85,7	383,13	352,36	332,80	332,50	0,84	-0,90
21	85,26	95,0	444,31	422,32	408,27	407,69	0,94	+0,58
16	86,32	96,9	437,36	420,63	409,90	409,34	0,94	+1,25
17	86,32	96,9	437,17	420,60	409,97	409,41	0,94	+1,32
20	90,08	95,0	529,43	508,05	494,36	493,72	1,08	+0,76
18	94,87	97,6	630,66	608,44	594,18	593,47	1,24	+0,47
31	95,11	97,4	681,40	631,58	599,87	599,16	1,33	+0,73
19	95,30	98,0	644,01	619,03	603,03	602,30	1,26	-0,44

TABLE 3. Vapor Pressure of 83.4% T<sub>2</sub>O

T, °C	Calculated from Eq. (4)	Calculated from Eq. (5)
20	15,17	14,89
40	49,52	49,02
60	137,3	136,6
80	333,5	332,5
100	727,3	726,1

equilibrium was assumed to be attained if three successive observations at intervals of 5 min showed a pressure change of the same sign, not exceeding 0,01-0,02 mm Hg (which could be caused by a variation in the amount of gases). In certain cases such a change could occur under conditions insufficiently close to equilibrium conditions, for example when the vapor and gases in the apparatus diffuse in opposite directions. The actual limits of errors of our measurements may, therefore, be somewhat wider than those given in Tables 1 and 2. But check measurements with H<sub>2</sub>O showed that the accuracy of our measurements is adequate for determining the difference in the vapor pressures of T<sub>2</sub>O and other isotopic forms of water. This is corroborated by the agreement between the results of two series of experiments with two T<sub>2</sub>O samples of different degrees of enrichment. This can be seen from Table 3, which gives the values of the vapor pressure of 83.4% T<sub>2</sub>O, obtained after averaging the experimental data and those calculated according to Raoult's law from the values for pure T<sub>2</sub>O.

At low temperatures the discrepancies are somewhat greater than the assumed experimental errors, which may be partly due to deviations of the vapor pressure of mixture of H<sub>2</sub>O and T<sub>2</sub>O from Raoult's law. In the case of mixtures of H<sub>2</sub>O and D<sub>2</sub>O, positive deviations were found [7].

In Table 4 the properties of HTO and T<sub>2</sub>O, found from the results of the present work, are compared with known data for H<sub>2</sub>O and D<sub>2</sub>O [7].

The vapor pressure and heat of vaporization of HTO were found from the geometric mean and arithmetic mean of the vapor pressure and heats of vaporization of H<sub>2</sub>O and T<sub>2</sub>O, respectively. The method of calculating the heat of vaporization is described in [6]; the critical temperature and pressure of T<sub>2</sub>O were taken as 370°C and 212 atm, i.e., somewhat lower than the corresponding constants for H<sub>2</sub>O and D<sub>2</sub>O (374.2 and 370.9°C; 218.5 and 215.7 atm, respectively [7, 8]). Data in [9] were used to calculate the entropy of the liquid state.

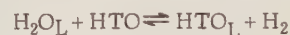
In the investigated temperature range the vapor pressure of T<sub>2</sub>O is less than the vapor pressures of H<sub>2</sub>O and D<sub>2</sub>O, but the difference between the vapor pressures of T<sub>2</sub>O and D<sub>2</sub>O is small. With an increase in temperature the  $P_{H_2O}/P_{T_2O}$  and  $P_{D_2O}/P_{T_2O}$  ratios approach unity. The vapor pressure of HTO is higher than D<sub>2</sub>O, although the

TABLE 4. Some Properties of H<sub>2</sub>O, D<sub>2</sub>O, HTO, and T<sub>2</sub>O

T, °C	H <sub>2</sub> O	D <sub>2</sub> O	HTO	T <sub>2</sub> O
Vapor pressure, mm Hg				
10	9,21	7,79	8,19	7,29
25	23,76	20,6	21,7	19,8
40	55,32	49,3	51,4	47,8
60	149,4	136,6	141,5	134,1
80	355,1	331,6	341,3	328,0
100	760,0	722,2	738,8	718,2
Boiling point, °C				
	100,0	101,4	100,8	101,6
Heat of vaporization, kcal/mole				
10	10,64	11,00	11,0	11,3
25	10,52	10,85	10,8	11,0
40	10,36	10,64	10,6	10,8
60	10,15	10,41	10,4	10,6
80	9,94	10,17	10,1	10,3
100	9,72	9,93	9,9	10,1
Entropy (S° <sub>298,16</sub> ), units				
	16,75	18,9	19,3	19,0

masses of the molecules of these compounds are the same; within the limits of accuracy of the data obtained, their heats of vaporization are also the same.

At 25°C the  $P_{H_2O}/P_{HTO}$  ratio is 1.097; at this temperature, the equilibrium constants of the reactions



and



must be 1.097-fold greater than the constants of the corresponding gaseous reactions (4.63 and 6.19 [7]), i.e. 5.08 and 6.79.

The values of the vapor pressure of HTO given in [2] are less than the values we obtained. They are less than for D<sub>2</sub>O and almost agree with our data for T<sub>2</sub>O. From [10 and 11] it follows that the vapor pressure of H-T compounds must be higher than for D-D compounds. This is confirmed experimentally for HT and D<sub>2</sub>. In contrast to our data, the data of [2] do not agree with the results of [10, 11] and, moreover, lead to such low values of the vapor pressure of T<sub>2</sub>O that the difference  $P_{H_2O} - P_{D_2O}$  is less than the difference  $P_{D_2O} - P_{T_2O}$ , which is scarcely probable.

#### LITERATURE CITED

1. W. Libby and R. Cornog, Phys. Rev., **60**, 171 (1941).
2. A. Price, Nature **181**, 268 (1958).
3. E. Hart, J. Phys. Chem. **56**, 594 (1952).
4. M. D. Senin, Yu. M. Morozov, and T. F. Karpova, Pribor. i Tekh. Eksp. **4**, 125 (1959).

5. H. Landolt and W. Börnstein, Phys. Chem. Tab. (Berlin, 1923) 5th ed., p. 1478.
6. G. Thomson, Chem. Rev., 38, 1 (1946).
7. I. Kirschenbaum, Heavy Water [Russian translation] (IL, Moscow, 1953).
8. G. Oliver and J. Grisard, J. Am. Chem. Soc., 78, 561 (1956).
9. A. Friedman and L. Haar, J. Chem. Phys. 22, 2051 (1954).
10. J. Biegeleisen, Phys. Rev. 99, 639 (1955).
11. J. Biegeleisen and E. Keer, J. Chem. Phys. 23, 2442 (1955).

# RADIOMETRIC ANALYSIS OF ORES ON CONVEYERS

L. N. Posik, S. I. Babichenko, and R. A. Grodtko

Translated from *Atomnaya Energiya*, Vol. 8, No. 5, pp. 425-431,

May, 1960

Original article submitted May 30, 1959

The physical bases, equipment, and procedure of quantitative proximate analyses of uranium ores on conveyers are briefly examined for the first time in this article. It is shown that this type of measurements may be the main method for the proximate radiometric analysis of ores in mines and factories. Data characterizing the accuracy of results obtained for ores of different material composition are given.

The method of analysis of radioactive ores on conveyers, proposed by L. N. Posik in 1952, is the further development of the widely employed method of  $\gamma$ -proximate analysis of ores in mine cars [1]. In 1956, for the analysis of ores on conveyers we used scintillation equipment, designed with the help of S. L. Yakubovich, for the first time. The use of Geiger counters for continuous control of ore during dressing was indicated in [2], but the equipment and procedure were not described.

The proximate analysis of ores on conveyers has the following physical characteristics:

- 1) the measurements are carried out in a thin ore layer;
- 2) the radiation dosage rate is proportional to the amount of uranium in the stream of ore, and not to its mean content (as in a saturated layer);
- 3) the measurement time of each finite volume of ore is limited (several seconds) and is determined by the geometry of the measuring apparatus, the distance between the transducer and the flow, and the rate of movement of the conveyor;
- 4) a higher background is present, due to radioactive contamination of the roadway and the conveyers, and the influence of the ore in the bunkers and the storage units;
- 5) in comparison with measurement in volumes, the same mass of ore gives a large number of "partial" samples, which considerably improves the statistical accuracy of the analytical results.

The total influence of the nonuniformity of distribution of the uranium, the variations in the coefficients of equilibrium and emanation, the variations in the cross section of the stream of ore, and also the density, size, and moisture content of the ore, etc. is assessed by a general criterion, that may be called the statistics of the stream. The total errors of a proximate analysis can evidently be divided into the errors due to the statistics of the stream, and the statistical errors of its  $\gamma$  count.

For a more accurate calculation of the influence of the physical characteristics on the results of the analysis of ores during movement, we will examine the analytical

equation for the radiation dosage of a stream and the formulas for assessing the statistical errors of measurements.

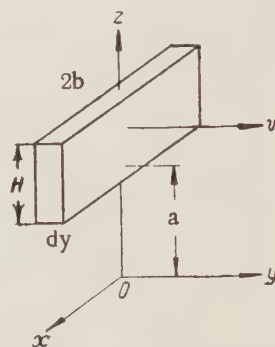


Fig. 1. Elementary vertical cross section of a planar stream of ore.

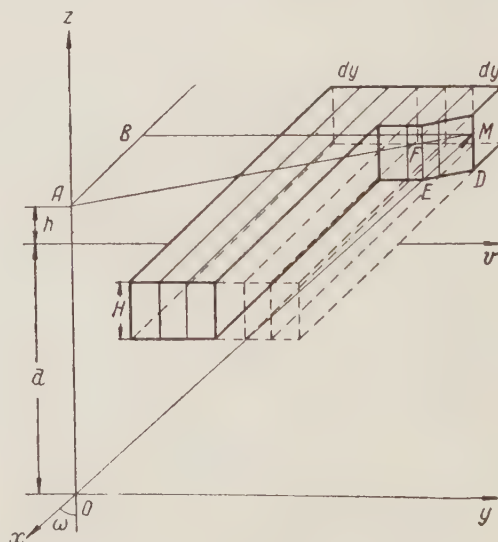


Fig. 2. Diagram of the system of coordinates for a section of a planar stream. (MD=EF=h; ME=r'; OM=r; OA=a+h; AB=x; BM=vt;  $r'/h=r/(a+h)$ ;  $r'=[h/(a+h)]r$ ).

The radiation dosage of an elementary active volume (Fig. 1) with a cross section  $S=2bH$  of infinitely small length  $dy$ , with a uranium content  $q_i$  and density  $\rho_i$ , moving at a velocity  $\underline{v}$  with respect to the point of measurement, which coincides with the origin of the coordinates, is determined by the equation

$$dD_i = K q_i \rho_i \frac{\varphi(r')}{r^2} dx dy dh dt, \quad (1)$$

where  $K$  is the  $\gamma$  constant of uranium;  $\varphi(r')$  is the absorption function of  $\gamma$  radiation in the material of the stream;  $1/r^2$  is the attenuation function;  $r^2 = (a+h)^2 + x^2 + v^2 t^2$  (Fig. 2).

As a first approximation

$$\varphi(r') = e^{-\mu_{\text{eff}} r'},$$

where  $r' = \frac{h}{a+h}$ ;  $\mu_{\text{eff}}$  is the effective absorption coefficient of a wide beam of  $\gamma$  radiation of the given stream.

We will call the period of the actual recording of the radiation of the moving volume at the point of measurement  $O$ , the exposure time. Its value is double that of the period of movement of the source with respect to the point of measurement, during the course of which the dosage rate of the radiation of the moving volume decreases from maximum (at  $t=0$  and  $y=0$ , see Fig. 2) to minimum (depending on the sensitivity of the equipment). The exposure time  $t_0 = 2t_1$  determines the length of the sensitivity zone  $2l$  of the measuring apparatus for the given analytical conditions ( $2l = v 2t_1$  and  $t_1 = l/v$ ).

The radiation dosage of a moving volume during the exposure time is evidently

$$D_i = 4K q_i \rho_i dy \underbrace{\int_0^b dx \int_0^{t_1} dt \int_0^H \frac{e^{-\mu_{\text{eff}} r'}}{r^2} dh}_{I}. \quad (2)$$

For given measurement conditions the values of  $a$ ,  $b$ ,  $H$ ,  $\underline{v}$ ,  $t_0$ , and  $\mu_{\text{eff}}$  are constant and the numerical value of the integral  $I = I(b, t_0, H, \mu_{\text{eff}}, a, v)$  is independent of  $q_i$  (within wide limits) and is also constant [3]. Assuming that this value is equal to  $I$  and  $dy = \Delta L$ , we obtain

$$D_i = 4K q_i \rho_i \Delta L I. \quad (3)$$

The amount of uranium in the volume under consideration is

$$m_i = q_i \rho_i S \Delta L.$$

Hence,

$$D_i = \frac{4KI}{S} m_i.$$

For a stream of length  $L$  consisting of  $n$  such volumes we obtain

$$D_n = \sum_{i=1}^n D_i = \frac{4KI}{S} \sum_{i=1}^n m_i = \frac{4KI}{S} M_n = \eta M_n, \quad (5)$$

where  $M_n$  is the total amount of uranium in the stream;  $\eta$  is the scaling factor of the  $\gamma$ -radiation dosage for the amount of uranium in the stream (in microrentgens per kg of uranium).

For a stream of known material composition under predetermined measurement conditions the values of  $K$ ,  $\rho$ ,  $b$ ,  $H$ ,  $v$ ,  $a$ ,  $\mu_{\text{eff}}$ , and  $t_0$  are determined empirically; the value of the integral  $I$  can, therefore, also be calculated. The dosage  $D_n$ , obtained on the basis of equation (5), therefore determines unequivocally the amount of uranium in the stream. The value of the integral  $I$  for the main types of ores and the most probable measurement conditions are tabulated on a BESM machine. Experimental measurements carried out with volume ore standards at various distances between the transducer and the standard and different velocities of the conveyer showed that the values of  $D_{\text{calc}}$  and  $D_{\text{expt}}$  differ by not more than  $\pm 10\%$ , with a mean discrepancy of  $\pm 5.6\%$ .

By means of a table for the values of  $I$  (not given here) it is easy to determine the value of the radiation dosage of active material under different measurement conditions. This makes it possible to base the selection of the optimum sensitivity of the equipment in accordance with the characteristics of the ore stream. Examples of the relation between the value of  $I$  and some of the main parameters of the stream are given in Figs. 3-6.

We must now deal with the problem of the relation between the dosage and the thickness of the ore layer. With an increase in  $H$  from 0 to 30 cm (Fig. 6) three main types of relation between  $I$  and  $H$  are distinguished: direct proportionality, nonlinear association, and a region of saturation ( $I$  is independent of  $H$ ). Maximum accuracy of the determination of the amount of uranium in the stream is ensured when the thickness of the ore layer corresponds to the region of direct proportionality. If the thickness of the ore layer corresponds to the region of nonlinear association it is necessary to ensure maximum constancy of the mean thickness of the layer.

The statistical error of the calculated value of the radiation dosage of different streams at predetermined values of the background  $D_b$  is determined by the relative root-mean-square error:

$$\begin{aligned} \sigma_n &= \pm \frac{\epsilon_{n \text{ true}}}{D_{n \text{ true}}} = \pm \frac{\sqrt{D_{n \text{ tot}} + D_{n \text{ true}}}}{D_{n \text{ tot}} - D_{n \text{ true}}} = \\ &= \pm \frac{\sqrt{2 + \frac{D_{\text{true}}}{D_b}}}{\frac{D_{n \text{ true}}}{D_b} \sqrt{D_b}}. \end{aligned} \quad (6)$$

With an increase in the value of  $D_{\text{true}}/D_b$  the value of  $\sigma_n$  decreases; to obtain small statistical errors it is, therefore, necessary to use equipment with a high  $\gamma$  radiation recording efficiency of the stream [4].

The values of  $\sigma_n$  obtained from equation (6) determine the maximum possible statistical accuracy of mea-

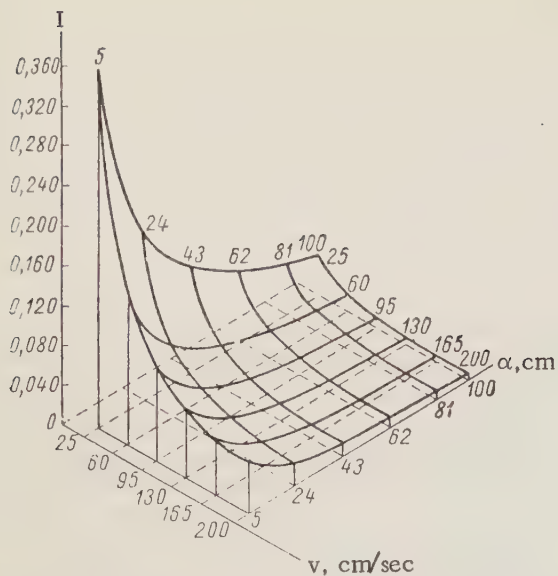


Fig. 3. Relation between the integral  $I$  and the velocity of the conveyor  $v$  and the distance between the transducer and the stream  $a$  ( $\mu=0.08 \text{ cm}^{-1}$ ;  $b=25 \text{ cm}$ ;  $H=5 \text{ cm}$ ).

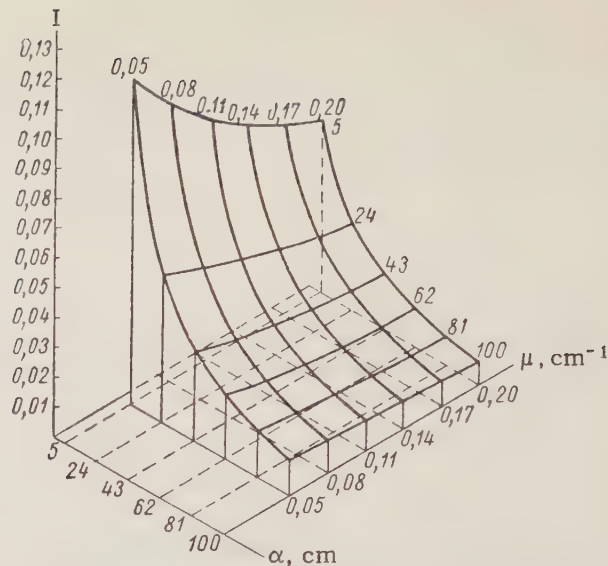


Fig. 4. Relation between the integral  $I$  and the distance between the transducer and the stream  $a$  and the absorption coefficient  $\mu$  ( $b=25 \text{ cm}$ ;  $H=5 \text{ cm}$ ;  $v=0.95 \text{ m/sec}$ ).

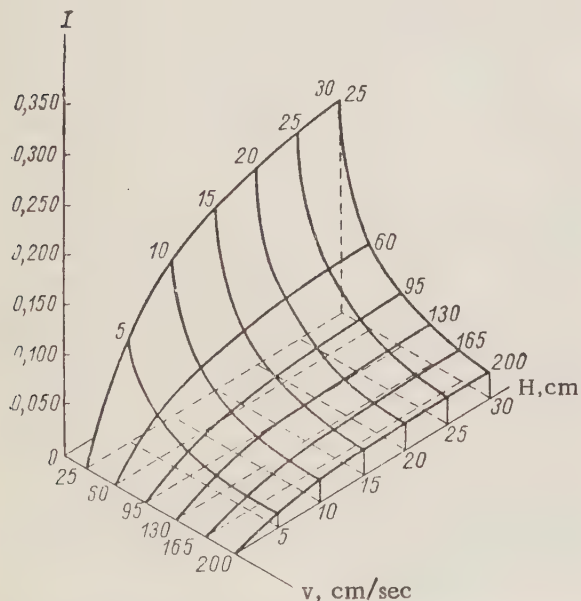


Fig. 5. Relation between the integral  $I$  and the velocity of the conveyor  $v$  and the thickness of the ore layer  $H$  ( $\mu=0.08 \text{ cm}^{-1}$ ;  $b=25 \text{ cm}$ ;  $a=43 \text{ cm}$ ).

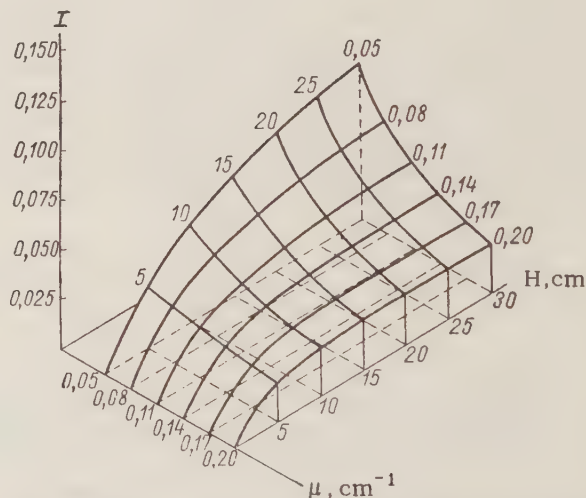


Fig. 6. Relation between the integral  $I$  and the thickness of the ore layer  $H$  and the absorption coefficient  $\mu$  ( $v=0.95 \text{ m/sec}$ ;  $b=25 \text{ cm}$ ;  $a=43 \text{ cm}$ ).

surements without taking into account the influence of the statistics of the stream. The accuracy of the final result of proximate analyses must be not less than  $\pm 5-10\%$ . Taking into account that the physical errors [1] may be considerable and are difficult to remove even by introducing the mean correction factors, it is evidently necessary to select a sensitivity of the equipment for which the value of  $\sigma_n$  is at least three-five fold less than the sum of the errors of the statistics of the stream and the counting statistics.

When the type of equipment is selected the necessity of ensuring a constant background, the maximum signal background ratio, and linearity of the counting characteristics within fairly wide limits must also be taken into account. The requirement of maximum constancy of the background has a substantial influence on the choice of the working sensitivity and the geometry of the transducer of the equipment because of the impossibility of ring screening. Moreover, since the value of the background above an empty and a loaded conveyor is different, meas-

urements of the background can be carried out only in the presence of a layer of rock on the belt. The requirement of linearity and high stability during fluctuations of the line voltage and the temperature is due to the fact that when rich, nonuniform material is measured by the absolute counting method, the interpretation of data in the case of nonlinearity of response is in practice impossible.

The RSU-T equipment used for the analysis of ores on conveyers includes the following basic elements: an external scintillation transducer, an automation unit, a counting unit (Fig. 7), and a transducer of the load. The block diagram of the unit, given in Fig. 8, shows the location of the individual components of the unit with respect to the conveyor. A functional diagram of the apparatus is given in [5].

The scintillation transducer 1 (see Fig. 7) consists of a  $\gamma$ -radiation detector—a  $40 \times 50$  mm NaI (Tl) crystal—and an FÉU-29 multiplier. The pulses from the output of

the FÉU-29 are fed to the shaping circuit kipp oscillator, which ensures discrimination of the FÉU-29 noise signals; the input sensitivity of the kipp oscillator is  $\sim 0.1$  v. The normalized signal enters the phase inverter and then passes to the cathode follower, balancing the high impedance of the circuit with the low impedance of the cable connecting the transducer with the automation unit. The length of the cable (type RK-1) is 100 m and can be increased to 120-150 m.

The automation unit 2 (see Fig. 7) has an input cascade, an intensimeter, a relay circuit for automatic remote control of the scaler and electric clock, a time relay, an electric clock, and a power supply circuit.

The transducer signal is amplified in the automation unit and is fed to the counting unit and the intensimeter. The intensimeter of the instrument has a negative feedback, which at constant time is equal to 1 sec; it improves substantially the linearity of the readings of the circuit in

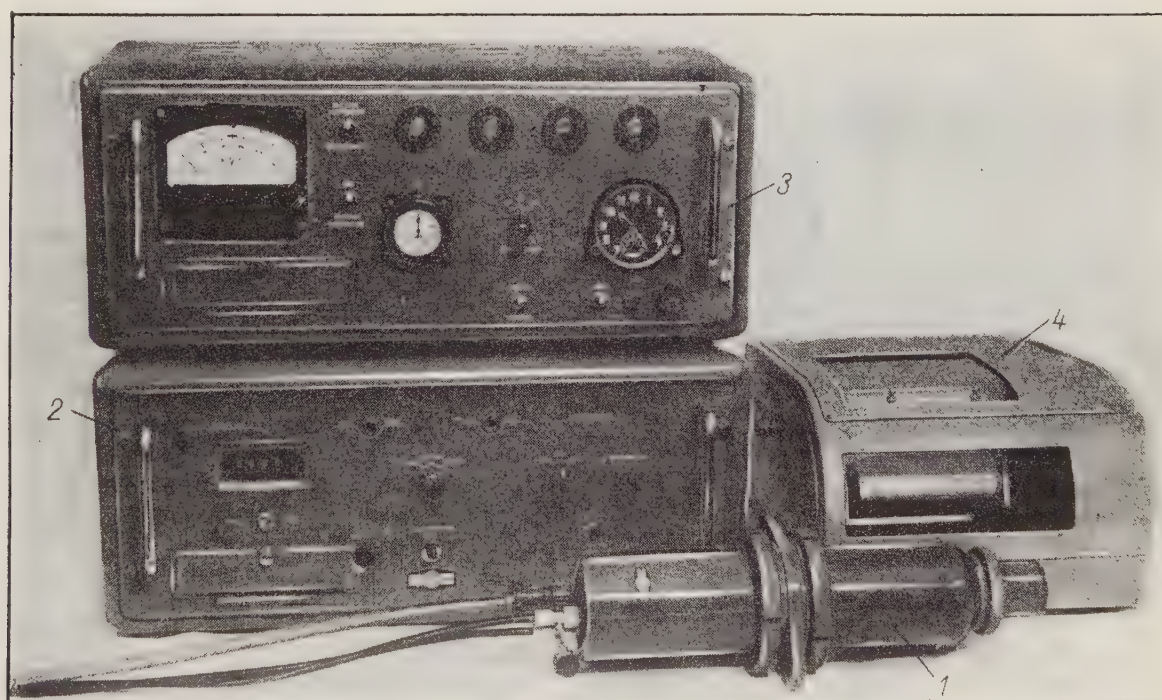


Fig. 7. General view of the RSU-T ("Volume") radiometer: 1) scintillation transducer; 2) automation unit; 3) counting unit; 4) recorder.

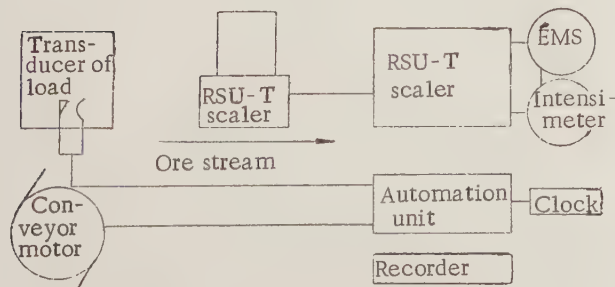


Fig. 8. Block diagram of the set of RSU-T equipment.

all three subbands:  $500 \cdot 10^3$ ,  $200 \cdot 10^3$ , and  $50 \cdot 10^3$  counts per min. The  $100 \mu\text{a}$  instrument, located in the counting unit, and the 3 ma self-recording instrument, connected to the automation unit, are the indicators for the intensimeter readings. The remote control of the scaler circuit (by signals from the conveyor motor and the transducer of the load or by means of the time relay) is effected in the grid circuit of the tube of the input amplifier.

The automatic remote control circuit consists of two MKU-48 relays, the winding of which is connected to the conveyor motor and the transducer of the load (see Fig.

Type of ore	Characteristics of the ore		Relative error, %	
	Equilibrium coefficient with respect to radiation, %	Emanation coefficient, %	type of comparisons	
			by batches	by months
Silicate	73-115	8-48	$\pm 5,7$	+0,1
"	73-115	8-48	—	+0,015
"	100	10	+3,1	+3,3
"	100	10	—	+4,5
"	100	10	—	+0,5
"	100	10	—	+3,6
Silicate-carbonate	100	10	-0,3	—
Carbonate	100	10	+2	—
Silicate-carbonate	100	1	—	+2,2
"	100	1	—	-0,05
"	100	1	—	-1,4
"	100	1	—	-1,95
Sulfide	84-117	20	$\pm 6,2$	—
Albititic	100	5	+1,7	+0,24
"	100	5	+4,7	—

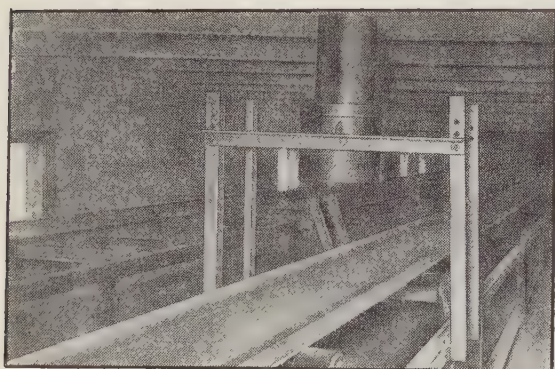


Fig. 9. General view of the transducer in a screen, installed on the conveyer.

8). The circuit causes the scaler and the intensimeter to be switched on only when ore is present on the moving conveyer. The measurement time of the radiation of the ore stream is read from the dial of the electric clock.

The electronic time switch has regular time lags of 2, 3, 4, and 5 sec; the relay is necessary for actuating the measuring apparatus at a predetermined interval during calibration, and for certain types of analysis. The relay has either remote control (for example, from the installation point of the transducer) or is controlled by the "time relay start" button on the panel of the unit (see Fig. 7).

The counting unit 3 (see Fig. 7) has an input phase inverter, from the output of which the negative pulses are fed to the shaping kipp oscillator and then pass to the decade scaling circuit, made of semiconductor elements. The resolution time of the input part of the circuit is not more than  $10 \mu$  sec. The next four scaling decades are made from dekatrons. From the output of the second, third, or fourth decade the pulse can be fed to the actuating circuit of the EMS electromechanical counter, with a dial graduated in units of  $10^3$ , and a maximum frequency of

50 counts/sec. The total recording value may, therefore, be  $10^6$ ,  $10^7$ , or  $10^8$  counts/min. Where necessary, the counting volume can be increased to  $10^9$  counts if an electro-mechanical counter with a dial graduated in  $10^4$  is connected to the outer jacks of the unit.

The counting circuit is actuated by a seconds counter or by remote control via the automation unit. To check the circuit the unit is equipped with a control generator. The counting circuit contains a high-voltage stabilized source, regulated within limits of 650-800, 800-1000, and 1000-1500 v at current loads of up to  $150 \mu$ a; a potential of 350-500 v can be used to feed the transducers on the gas-discharge counters.

A load transducer is not mass produced and it does not form part of the set of equipment. The simplest variant of the transducer is a pair of contacts, fixed to the arms of the damper or indicating system of the conveyer balance. Figure 9 shows the transducer in a screen, installed on the conveyer.

The most important type of calibration of the equipment for measurements on conveyers is the determination of the scaling factor  $\eta$ , which can be achieved by three principal methods:

1) By comparing the results of the proximate analysis with the data of the gross sampling of ore masses of different weight. The use of this method gives the most reliable value of  $\eta$ , but the necessary conditions for this are by no means always present;

2) by measuring a stationary ore standard, followed by conversion to the ore stream equivalent in measurement time. The length of such a standard must be equal to the length of the sensitivity zone of the measuring apparatus (2-3 m), which is inconvenient in practice; the cross section  $S=2bH$  and the material composition must correspond on the basis of equation (5) to the mean indices of the stream;

3) by repeated measurement of an analogous ore standard of arbitrary length on the moving conveyer, with an exposure ensuring the intersection of the whole sensitivity zone. Having determined the radiation dosage of the standard and its uranium content (by analyses of samples) it is easy to calculate the value of  $\eta$  from the ratio  $\eta = D_s/M_s$  per kg of uranium.

To increase the statistical accuracy of the value of  $D_s$  the measurements are carried out 20-25 times.

This method of calibration is somewhat less accurate than the first method, but it makes the calibration process independent of the possible errors of gross sampling and makes it possible to check the stability of the equipment and the scaling factor  $\eta$  systematically.

Table 1 gives a comparison of the results of proximate analyses of ore streams with those obtained by gross sampling.

From these data it follows that measurements on conveyers can become the principal method of proximate

analyses of commercial ores during loading and technological treatment. Favorable conditions for accurate analyses exist in factories, preparation plants and during the loading of crushed ores.

#### LITERATURE CITED

1. L. N. Posik and I. M. Tenenbaum, *Atomnaya Énergiya* 3, 7, 28 (1957).\*
2. E. Spice. *Canad. Mining and Metallurg. Bull.* (1950) No. 460, p. 446
3. V. L. Shashkin, *Atomnaya Énergiya* 2, 1, 48 (1957);\* 2, 2, 157 (1957).\*
4. V. I. Baranov, *Radiometry* [in Russian] (Izd. AN SSSR, Moscow, 1956) p. 117.
5. L. N. Posik, *Atomnaya Énergiya* 7, 6, 533 (1959).\*

---

\*Original Russian pagination. See C.B. translation.

# ANGLE-ENERGY DISTRIBUTION OF $\gamma$ RADIATION SCATTERED IN WATER AND IRON

Yu. A. Kazanskii

Translated from *Atomnaya Energiya*, Vol. 8, No. 5, pp. 454-461,

May, 1960

Original article submitted May 25, 1959

In this paper we investigate the detailed characteristics of multiple scattering of  $\gamma$  rays, in particular the angle-energy distribution, a knowledge of which allows us to calculate the attenuation of  $\gamma$  radiation in complex geometries. Measurements have been made of the angle-energy distribution of  $\gamma$  rays from a  $\text{Co}^{60}$  source in water and iron for a semiinfinite geometry and it has been established that these distributions have a maximum close to the energy corresponding to single scattering at the minimum angle. It is shown that the angular distributions are exponential and that the exponential factor is a linear function of the atomic number of the medium. The energy distributions are compared with calculations carried out by Goldstein and Wilkins [1].

The most detailed characteristic of multiple scattering of  $\gamma$  rays is the angle-energy distribution  $N(\vec{r}, \vec{\Omega}, E)$ ; a knowledge of this function is of great value in calculations of the radiation intensity in complex geometries (for example, in irradiation of a partially shielded detector or inside a scattering medium). Calculation of  $N(\vec{r}, \vec{\Omega}, E)$  involves serious difficulties and has been carried out only in a small number of cases [2, 3].

In a number of experimental papers [4-8] measurements have been made of the angle-energy distribution of scattered  $\gamma$  radiation close to a point at the boundary plane of a semiinfinite medium which contains the source of primary  $\gamma$  radiation. In the works referred to above, the geometric conditions in the experiments were such that the line connecting the center of the source and the chosen point was normal to the boundary plane; in this case the angle-energy distribution is independent of the polar angle. Hence, the function being sought depends on the distance  $r$  between the observation point and the energy of the source of scattered  $\gamma$  radiation  $E$ , and the angle  $\Theta$  between the line that joins the source and the field point and the direction of motion of the scattered  $\gamma$  photons close to this point. A  $\text{Co}^{60}$  source has been used to measure the angle-energy distributions of the scattered radiation at the boundary of a concrete medium [4] and a lead medium [5, 6]. A  $\text{Cs}^{137}$  source has been used to measure the quantity  $N(r, \Theta, E)$  for small values of the angle  $\Theta$  at the boundary of a concrete medium [8]. The function  $N(r, \Theta, E)$  has been measured with an  $\text{Au}^{198}$  source at the boundary of an iron medium [6]. In [7] the authors have communicated the results of measurements of the angle-energy distributions at the boundary of a lead barrier upon which bremsstrahlung radiation was incident; this radiation was generated by slowing down 10-Mev electrons.

In the present paper we report the results of measurements of  $N(\vec{r}, \vec{\Omega}, E)$  for  $\gamma$  radiation scattered in water and iron; a  $\text{Co}^{60}$  source has been used in this work.

## Experimental Arrangement

The measurements of the angle-energy distributions of scattered  $\gamma$  radiation in water were carried out with the apparatus shown in Fig. 1. An iron tank (dimensions  $2 \times 2 \times 1.6$  m) is filled with water; the tank has a plexiglas window opposite which there is a single-crystal scintillation spectrometer with a  $\text{CsI (Tl)}$  crystal (30 mm in diameter and 27 mm high) and an FEU-29 photomultiplier. are located inside a lead shield (100 mm thick). The directivity of the detector is provided by a collimator which is 270 mm long and has an aperture 10 mm in diameter. A pulse-height analysis is carried out by means of a 20-channel pulse-height analyzer. The distance  $a$  between the center of rotation of the spectrometer and the boundary plane of the semiinfinite medium is 10 mm.\* Hence the angle  $\Theta$  is determined from the relation

$$\Theta = \Theta' + \arctg \frac{a}{r} \operatorname{tg} \Theta', \quad (1)$$

where  $r$  is the distance along the normal from the source to the boundary plane and  $\Theta'$  is the angle of rotation of the spectrometer.

\* The fact that the axis of rotation of the spectrometer does not coincide with the boundary plane causes a variation in the distance between the field point and the source. But even when  $r=800$  mm and  $\Theta=60^\circ$  the variation in intensity is approximately 5%; when  $r>200$  mm, this variation is less than 1%. The variation in intensity is taken into account in the analysis of the experimental results.



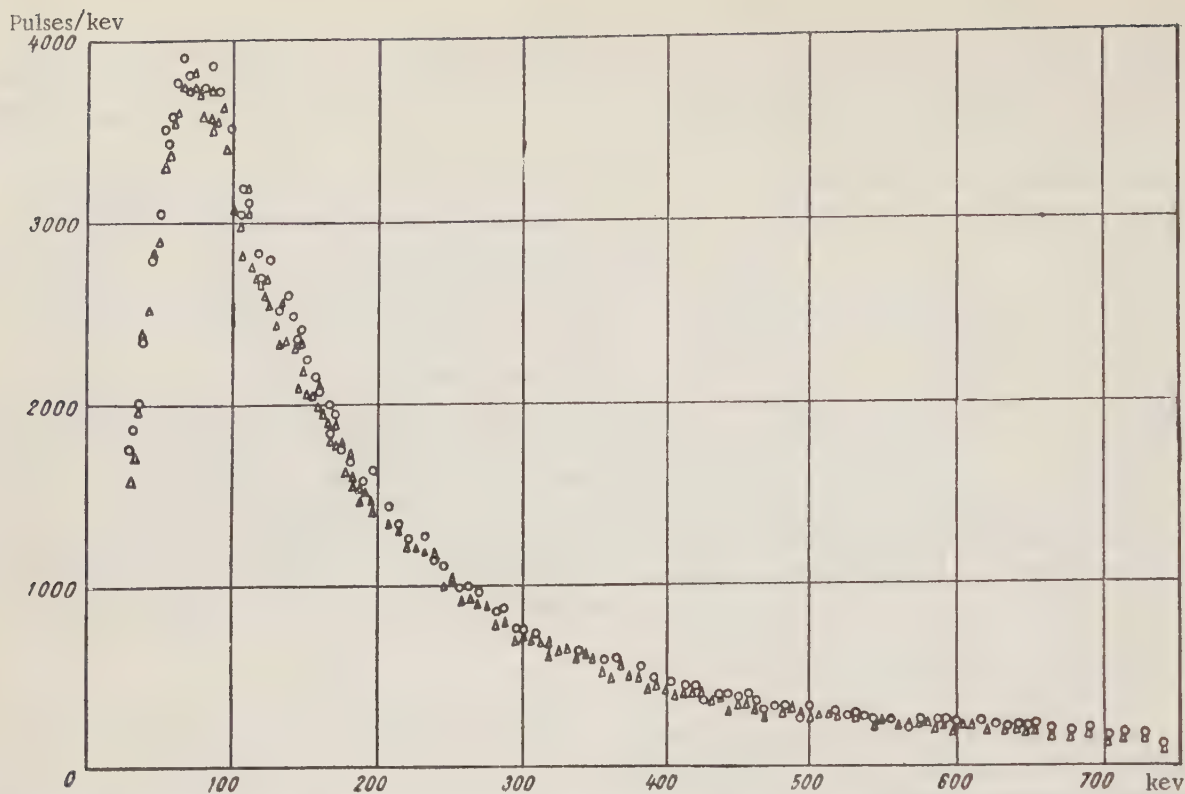


Fig. 2. Apparatus pulse-height spectrum (background subtracted) measured at  $\Theta'=30^\circ$ ,  $\alpha=0^\circ$  (triangles) and  $\Theta'=0^\circ$ ,  $\alpha=30^\circ$  (circles).

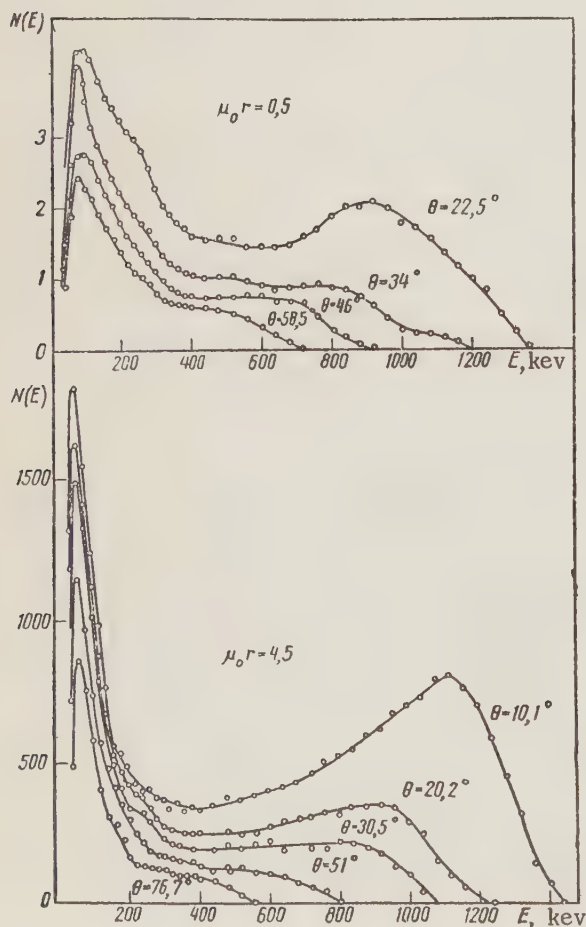


Fig. 3. Angle-energy distribution for  $\gamma$ -radiation scattered in water for a  $\text{Co}^{60}$  source with two different source-detector distances ( $\mu_0 r = 0.5$  and  $\mu_0 r = 4.5$ ).

### Results of the Measurements

In Fig. 3 we show the measured energy distributions  $N(r, \Theta, E)$  of scattered  $\gamma$  radiation from water at various angles  $\Theta$  for two source positions ( $\mu_0 r = 0.5$  and  $\mu_0 r = 4.5$ ). As the quantity  $\mu_0 r$  increases, the energy distributions show a marked variation at small energies; the scattered radiation peak in the region below 100 keV is displaced from 90 to 60 keV with an increase in this distance and becomes sharper. Similar behavior of the peak in the region of 60 keV has been observed in the integrated spectrum for scattered  $\gamma$  radiation in water [10].

The angular distribution of intensity for individual energy lines, plotted from the results of the measurements, are compared with a calculated values [2] in Fig. 4. Since the experiments were carried out for a semiinfinite geometry, while the calculations in [2] apply to a medium of infinite dimensions, one cannot expect exact agreement between the experimental and theoretical data. The greatest discrepancy is to be expected at low energies and large scattering angles  $\Theta$ . Actually, as is apparent from the comparison, the shapes of the calculated and experimental

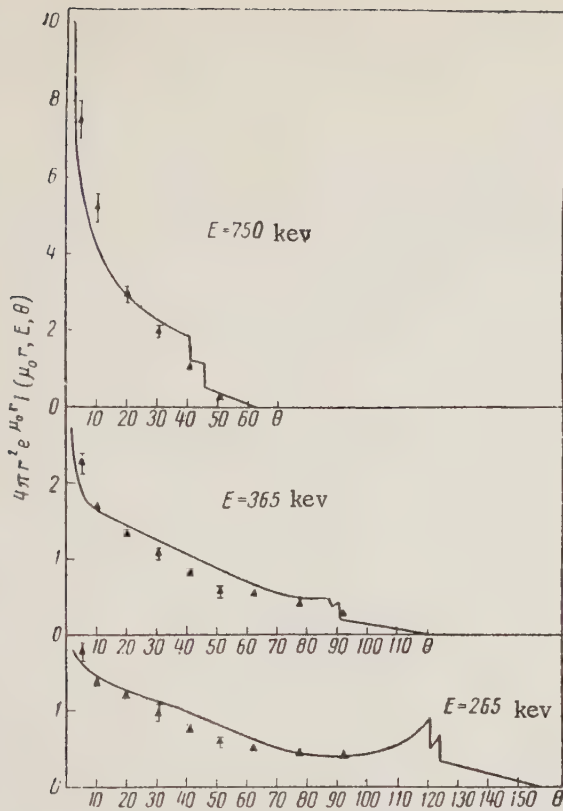


Fig. 4. A comparison of the calculated [2] (solid line) and experimental (triangles) angular distributions for a  $\text{Co}^{60}$  source ( $\mu_0 r = 3$ ).

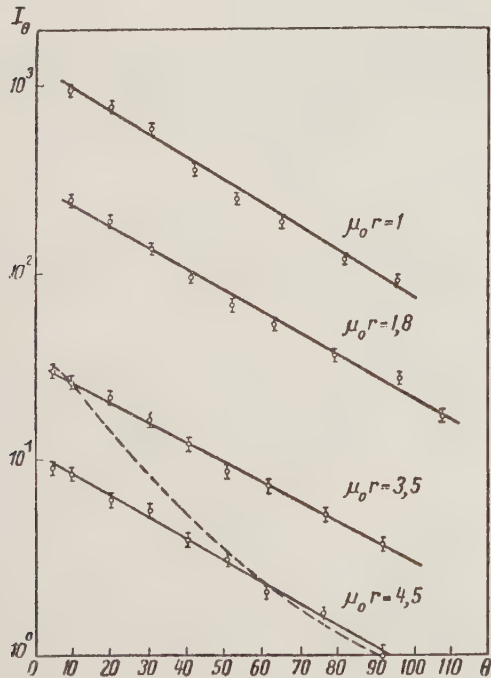


Fig. 5. Angular distribution in water for a  $\text{Co}^{60}$  source. The points show the angular distribution computed in the single-scattering approximation for  $\mu_0 r = 3.5$ , normalized to the experimental data for  $\theta = 10^\circ$ .

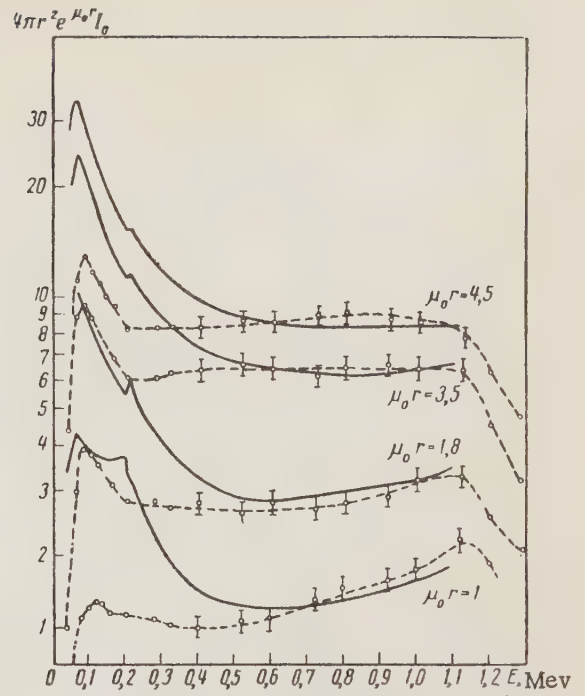


Fig. 6. Energy distribution in water for a  $\text{Co}^{60}$ . The experimental data (o-o-o) are normalized to the calculated data (solid lines) for  $E = 0.6$  Mev and  $\mu_0 r = 4.5$ .

curves do not differ by more than 40% for the lines at 265 and 365 keV and 20% for the line at 750 keV.

The angular distribution  $I_\theta$ , defined by

$$I_\theta = 2\pi \sin \theta d\theta \int N(r, \theta, E) E dE,$$

is shown in Fig. 5. The angular distributions are exponential to within 7-10% from 5-10 to 90°.

In [11] the integrated angular distribution has been measured in water with a  $\text{Co}^{60}$  source:

$$I_\theta^\alpha = 2\pi \int_\alpha^\pi \sin \theta d\theta \int N(r, \theta, E) \sigma(E) E dE,$$

where  $\sigma(E)$  is the absorption factor for  $\gamma$  radiation in air. The quantity  $I_\theta^\alpha$  is an exponential function of the angle  $\alpha$ . The exponential factor is included with the data given in the table.

The energy spectra for the scattered  $\gamma$  radiation

$$I_0 = 2\pi \int \sin \theta N(r, \theta, E) E d\theta$$

are shown in Fig. 6. The quantity  $I_0$  is found by graphical interpolation of the measured  $N(r, \theta, E)$  distributions. For purposes of comparison the calculated data obtained in [1] are shown by solid lines.

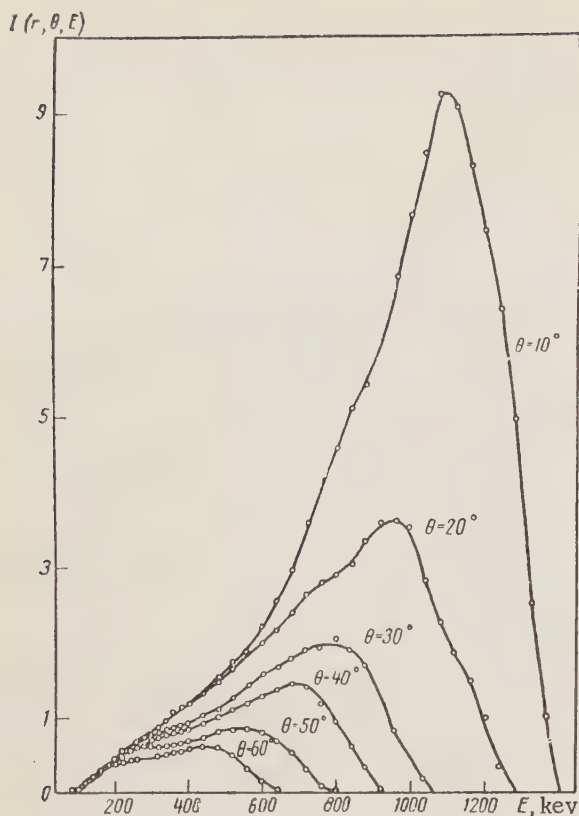


Fig. 7. Angular distributions in iron for a  $\text{Co}^{60}$  source ( $\mu_0 r = 5.9$ ).

In Fig. 7 we show the angle-energy distributions for  $\gamma$  radiation scattered in iron. A comparison of the angle-energy distributions for iron and water obtained in the present work with the data for concrete [4] shows that in the low-energy (100-400 keV) the contribution of the radiation scattered in concrete is one and one-half or two times greater than for water, and even more for iron. The discrepancy lies outside the limits of error of the

measurements and is probably due to the fact that in analyzing the results of the measurements the author of [4] has not taken account of the line shape of the Compton spectrometer.

The energy spectrum  $I_0$  in iron, obtained by graphical interpolation of the results of the measurements, is shown in Fig. 8. The solid line shows the spectrum calculated in [1].

The angular distribution  $I_\theta$  is shown in Fig. 9.

#### Discussion of the Results of the Measurements

The angle-energy distributions for the scattered  $\gamma$  radiation have a more or less sharp maximum near the energy corresponding to single scattering at the angle  $\Theta$ . In Fig. 10 we show the energy distributions for various materials for  $\Theta$  equal to  $10^\circ$  and to  $40^\circ$  (the source of the primary  $\gamma$  radiation is  $\text{Co}^{60}$ ). A similar maximum is observed when the energy of the primary  $\gamma$  radiation is approximately 0.5 Mev [6, 8].

It has been shown in [7] that for a primary  $\gamma$ -radiation energy of approximately 3 Mev (plane unidirectional source) the angle-energy distributions have a maximum whose position coincides with the maximum in the energy-distribution computed for the single-scattering approximation. Thus, the maximum in the angular distributions close to the energy of single scattering at an angle  $\Theta$  is a general characteristic of the energy distribution. This result indicates the great importance of scattering at small angles and can be used in various kinds of approximation calculations.

The angular distribution at a primary  $\gamma$  radiation energy of 1 Mev can be given analytically in the range  $5-90^\circ$  with an accuracy which lies within the experimental errors, by the following expression,

$$I_\theta = k e^{-\Theta/\Theta_0}, \quad (4)$$

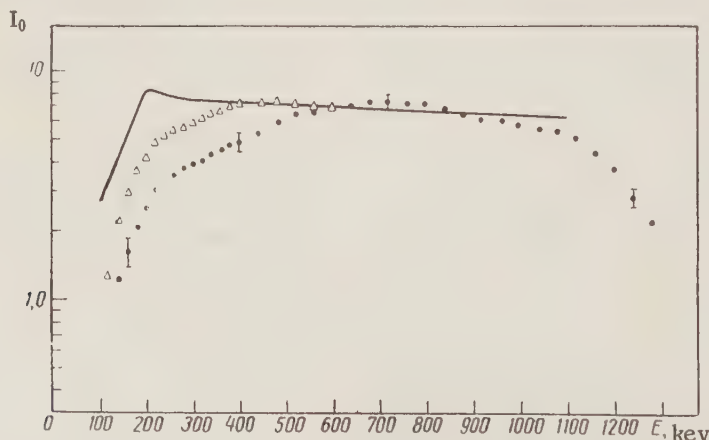


Fig. 8. Energy distribution in iron  $\text{Co}^{60}$  source. The experimental data (dots) are normalized to the calculated data at ( $E = 0.8$  Mev). The triangles show the energy distribution taking account of the scattered radiation from  $60$  to  $90^\circ$  found by extrapolation.

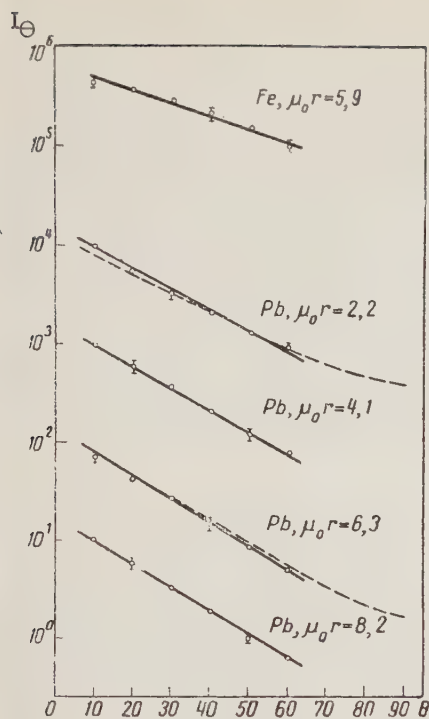


Fig. 9. Angular distributions in iron and lead for a  $\text{Co}^{60}$  source. The --- show the calculated distributions computed for single scattering and normalized to the experimental data for  $\Theta = 10^\circ$ .

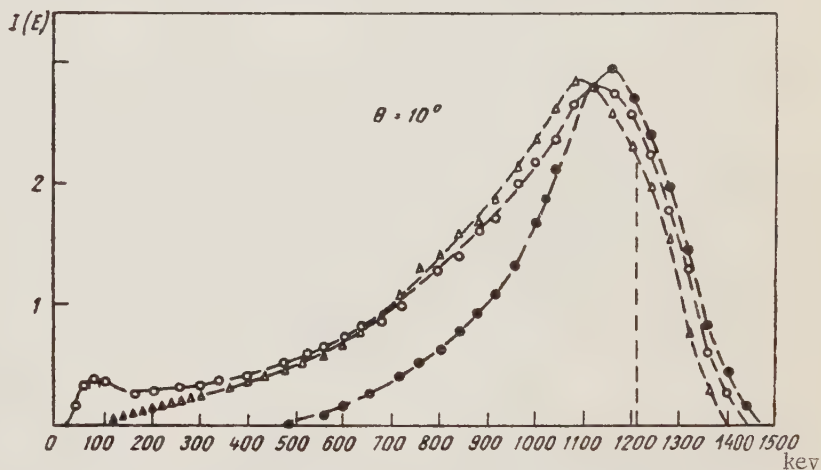
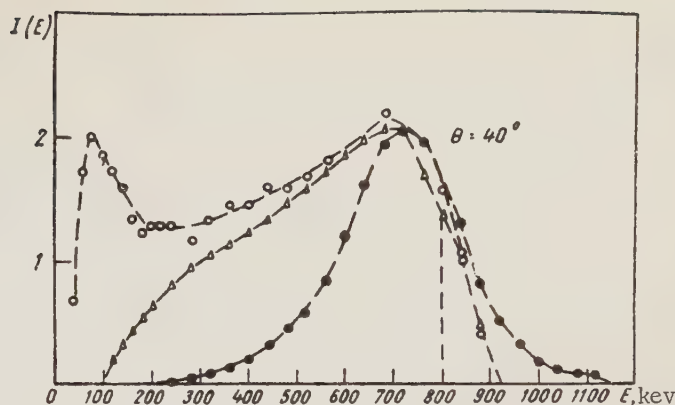


Fig. 10. The energy distributions for angles  $\Theta$  of 10 and  $40^\circ$  for a  $\text{Co}^{60}$  source in water ( $\circ-\circ-\circ$ ), iron ( $\Delta-\Delta-\Delta$ ), and lead ( $\bullet-\bullet-\bullet$ ). The distributions are normalized for  $E = 1.14$  Mev ( $\Theta = 10^\circ$ ) and  $E = 0.72$  Mev ( $\Theta = 40^\circ$ ). The vertical dashed lines indicate the energy for single scattering of  $\gamma$  radiation at angles of 10 and  $40^\circ$ .

Experimentally determined values of  $\Theta_0$  for various materials and ranges

Lead		Iron		Water	
$\mu_0 r$	$\Theta_0$	$\mu_0 r$	$\Theta_0$	$\mu_0 r$	$\Theta_0$
2,2	$21 \pm 0,7$	5,9	$33 \pm 2$	1,0	$36 \pm 1$
4,1	$19,5 \pm 0,3$	—	—	1,8	$38 \pm 2$
6,3	$18,7 \pm 0,3$	—	—	3,5	$42 \pm 1$
8,2	$18,5 \pm 0,3$	—	—	4,5	$38 \pm 1$

where  $\Theta_0$  is the exponential factor for the angular distribution and  $k$  is a coefficient of proportionality.

If we assume that Eq. (4) applies for values of  $\Theta$  from 0 to  $90^\circ$ , the proportionality coefficient  $k$  can be given in the form

$$k = \frac{I_0^0 (B_{1/2} - 1)}{\Theta_0 (1 - e^{-\pi/2 \Theta_0})}, \quad (5)$$

where  $I_0^0$  is the intensity of the primary  $\gamma$  radiation at point  $\underline{r}$  and  $B_{1/2}$  is the energy build-up factor associated with the point  $\underline{r}$  for a semiinfinite geometry.

Although the representation of the angular distribution in Eq. (4) is not verified experimentally for small angles ( $\Theta < 5^\circ$ ) the error in the determination of  $I_\Theta$  is not greater than 5–10% because the contribution of radiation for  $\Theta$  between 0 and  $5^\circ$  is insignificant.

The experimentally determined values of  $\Theta_0$  for various materials and ranges for the case when the primary  $\gamma$  radiation source is  $\text{Co}^{60}$  are shown in the table.

The exponential factor for the angular distribution falls off linearly as the value of  $Z$  of the medium increases. For  $\mu_0 r \approx 5$ , we find  $\Theta_0 \approx 39 - (Z/4)$ .

For purposes of comparison, calculations were made of the angular distributions taking account only of single scattering for lead ( $\mu_0 r = 2.2$  and  $\mu_0 r = 6.3$ ) with a primary  $\gamma$ -radiation source with an energy of 1.25 Mev. The calculated curves are shown in Fig. 9; the shapes of these curves are in good agreement with the experimental data.<sup>†</sup> For water, the results of similar calculations show a marked discrepancy with the experimental values (cf. Fig. 5).

<sup>†</sup> The data are taken from [6].

If we assume that the exponential nature of the angular distributions also obtains at angles  $\Theta > (\pi/2)$ , we can estimate the ratio of the energy build-up factor for infinite and semiinfinite geometries. Integrating Eq. (4) with respect to  $\Theta$  from 0 to  $90^\circ$ , we find

$$\frac{(B_{1/2} - 1)}{(B_\infty - 1)} = \frac{(1 - e^{-\pi/2\Theta_0})}{(1 - e^{-\pi/\Theta_0})}. \quad (6)$$

The ratio calculated from Eq. (6) can be compared with similar calculations for the case of a plane unidirectional source [12].<sup>‡</sup> For lead the agreement lies within 1.5% and for iron the agreement is 5%. For water, discrepancies up to 20% are observed. Apparently the assumption that Eq. (4) holds for  $\Theta > 90^\circ$  is justified only when  $Z > 20$ .

For a primary radiation energy of 1 Mev and a  $\text{Au}^{198}\gamma$  source in iron [6] the dependence of the angular distributions on the angle  $\theta$  becomes weaker. In this case for  $\Theta > 20^\circ$ , we find  $I_\Theta \approx e^{-\Theta/50^\circ}$ . It is reasonable to expect that because of the increase in anisotropy of Compton scattering with an increase in energy of the primary  $\gamma$  radiation, the angle  $\Theta_0$  will be reduced. However, the function  $I_\Theta(\Theta)$ , plotted from the data of [7] (a plane unidirectional source of electron bremsstrahlung with electron energies of 10 Mev and a lead barrier 152.4 mm thick) for  $\Theta > 20^\circ$  is proportional to  $e^{-\Theta/18^\circ}$ ; that is to say it coincides with the  $I_\Theta$  curve in lead for a  $\text{Co}^{60}$  source.

Energy spectra of scattered radiation. The energy spectra  $I_0$  plotted from the results of other measurements of the angle-energy distributions measured under conditions of semiinfinite geometry were compared with the calculations [1] which were carried out by the method of moments for a medium of infinite extent (cf. Figs. 6 and 8 and [5, 6]). When the  $\text{Co}^{60}$  is used as a radiation source agreement within 5–10% is generally obtained with the calculations for energies greater than 0.4–0.5 Mev. As a rule, for energies below 0.4 Mev the experimental data lie below the calculated data; this finding is explained by the difference in geometries in the calculations and the experiments.

It is of great interest to compare the experimental and calculated energy spectra for higher primary  $\gamma$  radiation energies. In [7] a comparison has been made of the energy spectra for scattered bremsstrahlung  $\gamma$  radiation,

using the calculations in [1]. The discrepancy of about 25% is attributed by the authors to the difference in geometry and the fact that no account has been taken of the bremsstrahlung due to secondary electrons in the calculations. It should be noted that the discrepancy is actually more significant since the authors of [7] have compared the energy spectrum of  $\gamma$  radiation which intersects a fixed unit area in all directions (flux) with calculations [1] of the spectrum for scattered  $\gamma$  radiation which intersects a sphere of unit radius in all directions.

In conclusion the author wishes to thank I. I. Bondarenko and V. I. Kukhtevich and S. G. Tsypin for discussion of the present work; the author is also indebted to A. N. Voloshin and V. I. Popov for help in carrying out the experiments.

#### LITERATURE CITED

1. H. Goldstein and J. Wilkins, Calculation of the Penetration of Gamma Rays (New York, 1956, NYO-3075).
2. L. Spenser and F. Stinson, Phys. Rev. 85, 662 (1952).
3. M. Berger, J. Appl. Phys. 26, 1504 (1955).
4. G. Whyte, Canad. J. Phys. 33, 96 (1955).
5. Yu. A. Kazanskii and S. P. Belov, Physics and Heat Technology of Reactors. Suppl. No. 1 of Atomnaya Energiya, p. 123.\*\*
6. Yu. A. Kazanskii, S. P. Belov, and E. S. Matusevich, Atomnaya Energiya 5, 2, 457 (1958).\* \*
7. J. Hubbell, E. Hayward, and W. Titus, Phys. Rev. 108, 1361 (1957).
8. W. Dixon, Canad. J. Phys. 36, 419 (1958).
9. Yu. A. Kazanskii, Pribor. i Tekh. Éksp. 4, 32 (1959).
10. M. Weiss and M. Bernstein, Phys. Rev. 92, 1264 (1953).
11. V. I. Kukhtevich, S. E. Tsypin, and B. P. Shemenenko, Atomnaya Energiya 5, 6, 638 (1948).
12. M. Berger and J. Doggett, J. Res. Nat. Bur. Standards, 56, 89 (1956).

<sup>‡</sup>A comparison of the ratio of the energy build-up for different geometries is possible because of the small difference in the accumulation factors under conditions of infinite geometry for a point source and a plane unidirectional source with small values of  $\mu_0 r$  [1].

\*\*Original Russian pagination. See C. B. translation.

# UNIVERSAL APPARATUS WITH A $\text{Co}^{60}$ $\gamma$ -RAY SOURCE WITH AN ACTIVITY OF 60,000 g-eq OF Ra FOR SIMULATING RADIATION-CHEMICAL APPARATUS, AND INVESTIGATIONS (THE "K-60,000")

A. Kh. Breger, V. B. Osipov, and V. A. Gol'din

Translated from *Atomnaya Énergiya*, Vol. 8, No. 5, pp. 441-445,

May, 1960

Original article submitted August 20, 1959

The article describes a universal apparatus for radiation-chemical investigations with a  $\text{Co}^{60}$   $\gamma$ -ray source possessing an activity of about 60,000 g-eq of Ra. The design of the apparatus makes it possible to simulate radiation-chemical apparatus with powerful isotopic  $\gamma$ -ray sources of various configurations and dimensions: a cylindrical radiating element, a radiating element in the form of two plates, a radiating element in the form of a "heat exchanger," and a radiating element in the form of one or more rods. The dosage rate (without taking into account the attenuation in the protective vessels) varies from  $\sim 250$  r/sec in a volume of 36 liters to  $\sim 3000$  r/sec in a volume of 0.1 liter. The apparatus is designed for carrying out radiation-chemical investigations under practically any physicochemical parameters; it ensures the possibility of remote control and observations both of the experimental conditions and the processes taking place in the investigated systems during irradiation.

As a result of the development of radiation-chemical investigations [1, 2] and the imminent change-over from laboratory work to processes on an enlarged scale it has become necessary to develop new apparatus which meet both ordinary requirements (for isotopic apparatus) [3] and a number of new requirements.

On the one hand, the apparatus must meet requirements associated with the necessity of irradiating large volumes of substances (liters, tens of liters) at high dosage rates ( $10^2$ - $10^3$  r/sec) and adequate uniformity of the dosage field.\* On the other hand, the necessity arises of carrying out investigations of radiation processes in flowing and circulating systems. In the latter case, uniform distribution of the dosage field in a large volume is not obligatory and it is more important to have high dosage rates. Moreover, with the development of radiation-chemical investigations the physicochemical conditions under which the experiments are carried out become more complicated. Finally, for a change-over from laboratory experiments to industrial processes, experimental simulation of radiation-chemical apparatus with powerful radiating elements of various shapes and sizes is necessary. Reliable scientifically-based methods of calculating pilot-plant and industrial apparatus can evidently only be developed by means of such experiments. This includes calculations of dosage fields of energy [4-6] that is absorbed by the irradiated system,† the efficiency of the radiating element and the apparatus as a whole [7, 8], the choice of the optimum shape and size of the radiating element, the heat conditions, etc.

When the K-60,000 apparatus‡ was developed, together with ordinary requirements previously formulated [3, 9] and included in the design of the apparatus described in [10, 11], the above-listed requirements were also taken into account.

It should be noted that in a number of works published after the construction of series K apparatus, during the development of apparatus for radiation-chemical investigations, the authors took as their basis considerations and requirements similar or closely similar to ours. This applies particularly to those works whose authors made efforts to analyze literature data and approach the development of a new apparatus from the aspect of a scientifically-based problem of general significance [12, 13], not a particular constructional problem applicable only to the given conditions.

The K-60,000 apparatus was also developed on the basis of such considerations.

Principal parameters and design of the K-60,000 apparatus. The K-60,000 apparatus is designed for:

1) The simulation of radiation-chemical apparatus with powerful  $\gamma$ -ray sources of various configurations, that is,

\* The latter is important mainly during irradiation of objects in the solid phase.

† The calculations of the absorbed energy in irradiated systems were made by A. Kh. Breger, B. I. Vainshtein, L. S. Gusei, N. P. Syrkus, and Yu. S. Ryabukhin.

‡ The development was commenced in July, 1957.

a) with a radiating element in the form of a hollow cylinder of height 32 cm, and an internal diameter of 2-38 cm; in this case, a mean dosage rate\*\* of  $\sim 3000$  r/sec (in a volume of 0.1 liter) to  $\sim 250$  r/sec (in a volume of 36 liters) is ensured;

b) with a radiating element in the form of two plates of height 32 cm and length up to 32 cm, the distance between the plates being from 5 cm (in a volume of 4 liters the mean dosage rate\*\* was  $\sim 1300$  r/sec) to 25 cm

(in a volume of about 26 liters the mean dosage rate\*\* was  $\sim 450$  r/sec);

c) with a radiating element of the "heat exchanger" type with different arrangements of the sources in the irradiated medium;

d) with a radiating element in the form of one or more rods.

It is possible to vary (other conditions being equal) the activity of the radiating element from 3000 to 60,000 g-eq of Ra.

2) For carrying out radiation-chemical processes in various apparatus with the use of the radiating elements indicated in section 1, and in practice under any physico-chemical conditions.

The K-60,000 apparatus is located on two stages of a specially equipped room. The labyrinth (Fig. 1) and the working chamber (Fig. 2), in which irradiation is carried out, are located on the lower stage. The working chamber and the labyrinth are separated from the neighboring rooms by concrete ceilings and walls (specific density of the concrete  $2.3 \text{ t/m}^3$ ), which protect the personnel when the cassettes with the  $\gamma$ -ray sources are in the working position.

The following principal units of the apparatus are located in the working chamber.

1) The  $\gamma$ -ray source, consisting of 20 articulated four-membered cassettes (Fig. 3). Each cassette contains four standard  $\text{Co}^{60}$  preparations, each having an activity of 700-750 g-eq of Ra (in its sheath, a preparation has a length of 81 mm and a diameter of 11 mm).

2) The store of the  $\gamma$ -ray source, consisting of 20 isolated, specially curved, tube-channels, the area between which is filled with iron shot of diameter 2-3 mm (bulk density  $4.5 \text{ g/cm}^3$ ).<sup>††</sup> During the intervals between irradiation of the objects the cassettes with the  $\text{Co}^{60}$  preparations are kept in the lower parts of the channels of the store. The layer of iron shot, of height 1.6 m, and the curved channels attenuate the  $\gamma$  radiation to the permissible norm.

3) The radiating element of the apparatus, consisting of 20 individual tubes connected to the corresponding channels of the store by means of flexible metal sleeves.<sup>‡‡</sup>

4) The working table of the apparatus, on which the objects to be irradiated are arranged, and which is used

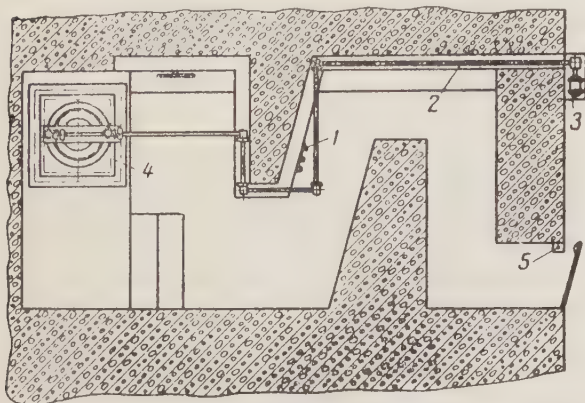


Fig. 1. Horizontal section of the K-60,000 apparatus: 1) transducers of the USID-1 dosimetry apparatus; 2) transmission; 3) electrical drive; 4) working table; 5) solenoid shutter.

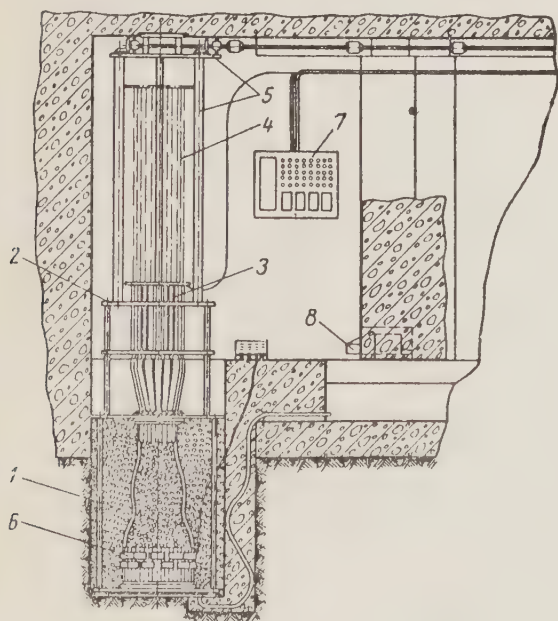


Fig. 2. Vertical section of the K-60,000 apparatus: 1) store; 2) working table; 3) radiating element tubes; 4) ropes for raising the cassettes with  $\text{Co}^{60}$ ; 5) mechanism for moving the sources; 6) induction transducers; 7) switchboard connecting the electric cables with the instruments of the physicochemical control-board; 8) transmitting camera of the television system.

\*\* The dosage rate is calculated without taking into account the attenuation of irradiation in the materials of the cassette, the tubes of the radiating element, etc. Such data on the calculation of the dosage fields and their experimental investigation will be published later

†† The K-60,000 apparatus is made without the use of lead.

‡‡ The channels of the store, the cassettes and the radiating element tubes are made of mark Kh18N9T stainless steel.

to support the tubes of the radiating element, the configuration of which is determined by the experimental conditions (Figs. 2 and 4).

5) The ropes with electromagnets fixed on the ends by means of which the required number of cassettes (from 1 to 20) is lifted to the radiating element of the apparatus.

6) The mechanism for moving the source, with transmission gear and electric drive.

In addition to these components the working chamber contains the outlets of the gas and liquid pipelines, the switchboard for connecting the electric cables to the secondary instruments on the control desk and for observing the physicochemical conditions of the experiments: remote control and adjustment of the temperature, pH, pressure, electrical resistance, dosage rate, etc. A television system is installed in the working chamber for visual observations on the irradiated objects. The control desk of the apparatus has a light-signalling system for indicating the position of the individual irradiation sources.

Working principle of the apparatus. Before the commencement of irradiation all the cassettes with the  $\text{Co}^{60}$  preparations are located in the lower part of the channel; this is signalled by the induction transducers installed in the channels of the store. The induction transducers

consist of double coils\*\*\* with an ac feed. As a result of the presence of cores, which in the given system are formed by the  $\text{Co}^{60}$  preparations, an emf is induced in the secondary winding of each coil; this actuates a relay which operates in the signal and locking circuit of the inlet door of the labyrinth. Thus, entry into the labyrinth. Thus, entry into the labyrinth and working chamber is only possible when all the cassettes with the  $\text{Co}^{60}$  preparations are located in lower part of the channels†††.

To prepare the apparatus for radiation-chemical experiments the operator installs and fixes both the tubes of the irradiating element and the ropes with fitted electromagnets according to the selected configuration of the radiating element‡‡‡. When the objects to be irradiated have been placed in the guard vessel, the cables can be fed through the central tube<sup>1</sup>. The apparatus having been made ready for work in this way, the operator in the working chamber switches on the locking device as a result of which the core of the solenoid shutter of the door<sup>2</sup> is attracted and held for 20 sec. This period is sufficient for the operator to leave the chamber and close the door. The power supply of the electromagnets<sup>3</sup> is switched on to raise the required number of cassettes with  $\text{Co}^{60}$  preparations, by means of the toggle switches on the control desk.

After the power supply has been switched on, the cassettes are drawn toward the electromagnets by a plug-yoke and are raised to the working position by means of the displacement mechanism. The signal lamps serve as

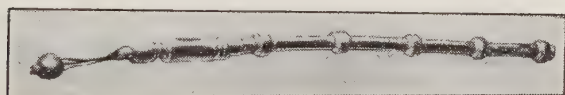


Fig. 3. Cassette with  $\text{Co}^{60}$   $\gamma$ -ray source and electromagnet.

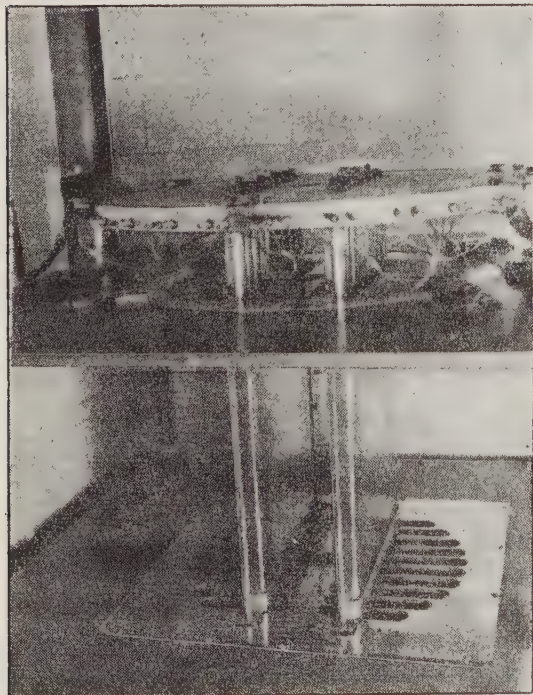


Fig. 4. Working table of the K-60,000 apparatus, with radiating element in the form of two plates.

\*\*\* The winding of the coils is made of mark PETKSO-0.35 wire, resistant to the action of  $\gamma$  rays, impregnated with organosilicon lacquer.

††† In addition to the locking device by means of the induction transducers, the USID-1 dosimetry device operates in the locking circuit of the inlet door. When the door is opened the electromagnets are automatically disconnected by the key, and if cassettes with  $\text{Co}^{60}$  are present in the radiating element they fall into the store via the channels. In this way additional locking is obtained during functioning of the apparatus.

‡‡‡ The change-over from one variant of radiating element to another is carried out under safe conditions in 30 min.

<sup>1</sup>For any variants of the radiating element the objects to be irradiated can be placed on the ends of the working table and on the floor of the working chamber.

<sup>2</sup>When the core of the solenoid shutter is lowered the door to the labyrinth can only be closed if the time relay (the button of which is located in the chamber of the apparatus) is switched on; this eliminates the possibility of the presence of personnel in the chamber when the source is raised.

<sup>3</sup>The supply for the electromagnets is obtained from an ordinary buffer circuit with a VSA-6 rectifier and a 384 x 2 amp/hr storage battery.

a means for indicating when each cassette has been lifted into the tube of the radiating element.

When the experiment has been completed all the operations are carried out in the reverse order; the irradiated objects can be removed from the chamber for further investigation and the apparatus prepared for the next experiment.

Method of assembling the powerful  $\gamma$ -ray source of the K-60,000 apparatus. The  $\gamma$ -ray source, consisting of 80 standard  $\text{Co}^{60}$  preparations, is assembled by means of a special transport container, similar to that developed by us previously [8], by the method described in [10, 11]. The container is installed on a plate located in the room above the working chamber of the apparatus. From the center of the plate a pipeline is passed through the concrete ceiling; this pipeline is first connected in the working chamber to one of the channels of the store containing the empty cassette. Four  $\text{Co}^{60}$  preparations are passed in succession into each cassette via the pipeline; the plug-yoke is then screwed into the cassette by means of an electromagnetic screw driver. When the plug is screwed up (or unscrewed) each cassette is held securely in a hexagonal jack in the lower part of the channel.

The authors wish to express their thanks to V. I. Vainshtein, M. A. Dembrovskii, and N. P. Syrkus, who took part in the discussion of individual problems of the design of the apparatus, and also to A. I. Dombrovskii, V. M. Kasatkin, A. V. Tatov, D. V. Yasinskii, I. A. Gromov, V. G. Ivanov, M. N. Demichev, V. V. Serebryakobaya, N. V. Troinov, and others, who took part in the construction and assembly of the apparatus.

#### LITERATURE CITED

1. S. S. Medvedev, Proc. All-Union Scientific-Technical Conference on the Use of Radioactive and Stable Isotopes and Radiations in the National Economy and Science (April 4-12, 1957). Isotopes and Radiations in Chemistry [in Russian] (Izd. AN SSSR, Moscow, 1958) p. 85.
2. A. I. Topchiev, I. G. Alad'ev, and P. S. Savitskii, *Atomnaya Énergiya* 5, 3, 321 (1958).<sup>4</sup>
3. A. Kh. Breger, *Problemy Fiz. Khim.*, 1, 61 (1958).
4. Yu. S. Ryabukhin and A. Kh. Breger, "Simulation of isotopic radiation sources of possible industrial radiation-chemical apparatuses," Proc. First All-Union Conference on Radiation Chemistry [in Russian] (Izd. AN SSSR, Moscow, 1958) p. 318.
5. A. Kh. Breger et al., *Problemy Fiz. Khim.* No. 2, 132 (1959).
6. A. V. Bibergal', M. M. Korotkov, and T. G. Ratner, *Atomnaya Énergiya* 7, 3, 244 (1959).<sup>4</sup>
7. B. I. Vainshtein, A. Kh. Breger, and N. P. Syrkus, *Zhur. Khim. Prom-ti*, 7, 6 (1959).
8. N. P. Syrkus, A. Kh. Breger, and B. I. Vainshtein, *Zhur. Khim. Prom-ti*, 8, 1 (1959).
9. A. Kh. Breger et al. in: Symp. The Action of Ionizing Radiations on Inorganic and Organic Systems. Ed. by S. Ya. Pshezhetskii [in Russian] (Izd. AN SSSR, Moscow, 1958) p. 379.
10. A. Kh. Breger et al., Proc. All-Union Conference on the Use of Radioactive and Stable Isotopes and Radiations in the National Economy and Science (April 4-12, 1957). The Preparation of Isotopes. Powerful  $\gamma$  Ray Apparatus. Radiometry and Dosimetry [in Russian] (Izd. AN SSSR, Moscow 1958) p. 182.
11. A. Kh. Breger et al., Report No. 29, UNESCO International Conference on the Use of Radioisotopes in Scientific Investigations (Paris, September, 1957).
12. G. S. Murray, R. Roberts, and D. Dove, Report No. 19, UNESCO International Conference on the Use of Radioisotopes in Scientific Investigations (Paris, September, 1957).
13. O. Joklik, *Atompraxis* 10, 10, 355 (1958).

<sup>4</sup>Original Russian pagination. See C. B. translation.

# INVESTIGATION OF THE SPENT FUEL ELEMENT OF THE FIRST ATOMIC POWER STATION\*

A. P. Smirnov-Averin, V. I. Galkov, Yu. G. Sevast'yanov, N. N. Krot, V. I. Ivanov, I. G. Sheinker, L. A. Stabenova, B. S. Kir'yanov, and A. G. Kozlov

Translated from *Atomnaya Énergiya*, Vol. 8, No. 5, pp. 446-447, May, 1960

Original article submitted January 28, 1960

In designing new nuclear reactors for power stations and in developing new operating parts, it is necessary to study the changes occurring in fuel elements (FE) during their operation. Thorough investigations of spent FE make it possible to design power station reactors where the nuclear fuel is utilized with maximum efficiency. One of the stages in studying spent FE is the investigation of the nuclear fuel isotope composition after operation in the reactor, the burn-up variation along the FE length, and the state of the outside and inside FE jackets.

We investigated the fuel element of the First Atomic Power Station [1], which was in operation over an effective period of 104 days† and then stored over a period of 1160 days after the end of the run. It was transferred from the storeroom of the First Atomic Power Station to the unloading room of the "hot" laboratory and then placed into a protection cell by means of the remote-handling unloading mechanism.

The fuel element was observed by means of special binoculars through the lead glass of the cell. A thin oxide film was detected on the outside jacket. This jacket was not damaged. In measuring the outside diameter at different spots along the FE length by means of a remote-measurement micrometer, it was found that the jacket was deformed. As a result of irradiation the average diameter along the FE length increased from  $14.11 \pm 0.02$  to  $14.20 \pm 0.02$  mm.

In the course of further investigations, six specimens 1 cm long were cut from different spots along the FE length.

An inspection of the specimen inside tube on the side where it was in contact with the coolant (water) revealed a brown deposit. By means of an MIM-6 metal microscope, it was established that the deposit had a thickness of  $1 \mu$ . The metal structure at the metal-deposit interface was not disturbed, which indicated that the layer consisted of scale and that it was not a product of stainless steel corrosion.

The burn-up was determined with respect to the activity of  $\text{Cs}^{137}$ , which evolved from the specimen. Cesium is the most suitable fragment for this purpose, since its yield is well known [2] and its half life is long, due to which the corrections used in calculating the burn-up are small. The chromatographic method was used for separating cesium. The purity in chemically separating  $\text{Cs}^{137}$  was controlled by means of a scintillation  $\gamma$  spectrometer as well as by measuring the  $\beta$  spectrum according to the absorption method. The absolute  $\beta$  activity of  $\text{Cs}^{137}$  was measured by means of a  $4\pi$  counter.

In burn-up calculations we took into account the  $\text{Cs}^{137}$  activity due to  $\text{Pu}^{239}$  fission as well as the reduction in  $\text{U}^{235}$  nuclei due to the radiation capture of neutrons. Data on the burn-up at different FE spots are shown in Fig. 1. The average burn-up is equal to 12.5%.

For the specimen taken from a spot 95 cm from the lower FE end, the burn-up was determined by means of a mass spectrometer. The uranium content in this speci-

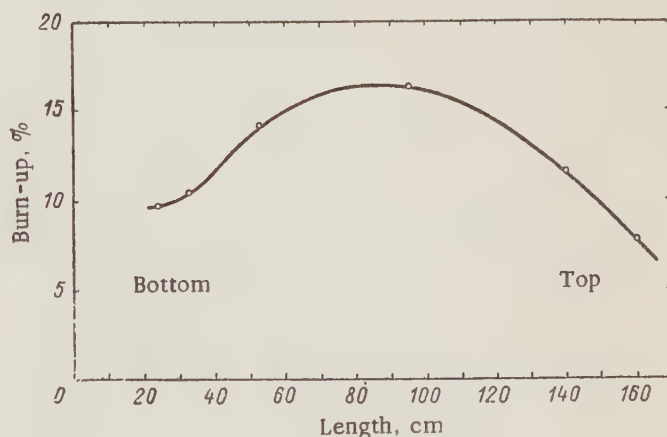


Fig. 1. Burn-up along the FE length.

\* First communication.

† The investigation of elements with deeper burn-up is in progress.

Data	Pu <sup>238</sup>	Pu <sup>239</sup>	Pu <sup>240</sup>	Pu <sup>241</sup>	Am <sup>241</sup>
Experimental	$2,54 \cdot 10^{-4}$	1,20	0,102	$1,27 \cdot 10^{-2}$	$1,86 \cdot 10^{-3}$
Theoretical	—	1,17	0,100	$1,36 \cdot 10^{-2}$	—

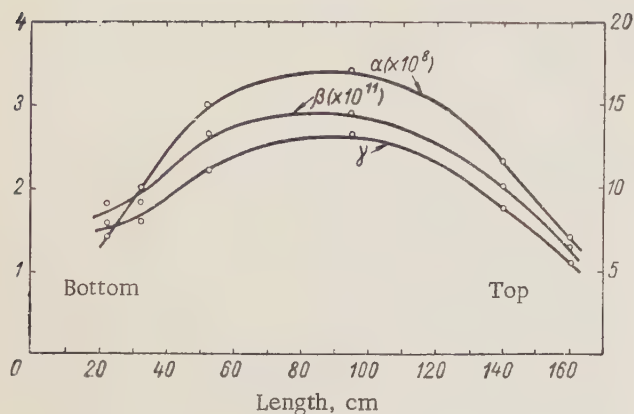


Fig. 2. Variation of over-all  $\alpha$ ,  $\beta$ , and  $\gamma$  activities along the FE length.

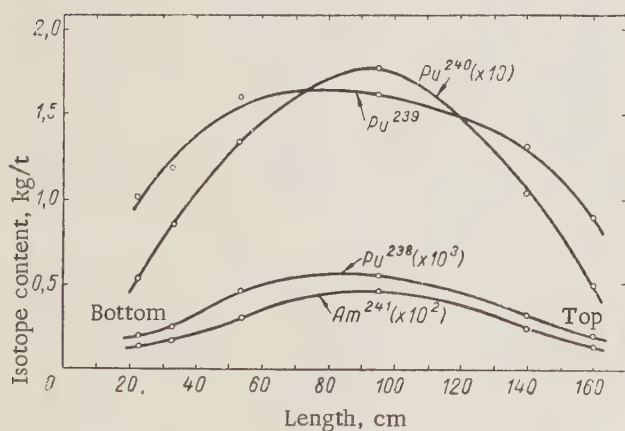


Fig. 3. Distribution of the content transuranic element isotopes along the FE length.

men was 4.32%, which corresponded to a burn-up of 16.1%. This value was in good agreement with the value obtained with respect to the Cs<sup>137</sup> yield.

The over-all  $\alpha$  activity was measured by means of a standard Da-49 device, and the over-all  $\beta$  activity was measured by means of a  $4\pi$  counter. The  $\gamma$ -radiation activity was measured by means of an ionization chamber, which was calibrated with respect to the  $\gamma$  activity of a radium standard. The measurement results are shown in Fig. 2. As was to be expected, the shape of the relative

family of the over-all  $\beta$ - and  $\gamma$ -activity curves was similar to the shape of the burn-up curve.

The content of transuranic element isotopes was determined with respect to  $\alpha$ -radiation spectra and with respect to the number of spontaneous fission events. The spectra were obtained by means of an ionization  $\alpha$  spectrometer, which consisted of an ionization chamber with a small collecting electrode (a ball 1.5 cm in diameter), an amplifier, a discriminator, a second amplifier, a stabilized rectifier, and a 50-channel pulse analyzer. The  $\alpha$ -spectrometer resolving power was 2%.

Complete data on the content of transuranic element isotopes cannot be obtained directly from the spectrum of the specimen  $\alpha$  radiation, since the spectral peaks of Pu<sup>239</sup> and Pu<sup>240</sup>, as well as Pu<sup>238</sup> and Am<sup>241</sup>, coincide with each other.

After we measured the  $\alpha$ -radiation spectrum of plutonium that evolved from the specimen, we succeeded in separately determining the Pu<sup>238</sup> and Am<sup>241</sup> content. The Pu<sup>240</sup> content was determined with respect to the number of spontaneous fission events produced by the layers prepared from the evolved plutonium.

Figure 3 provides data on the content of transuranic element isotopes (in kilograms per 1 ton of uranium) at different spots on the FE. The Pu<sup>241</sup> content was determined theoretically by using data obtained from Am<sup>241</sup>.

On the basis of experimental data, we determined the amounts of various isotopes (in kilograms per 1 ton of uranium), which were averaged with respect to the FE length. The theoretical and experimental results obtained in measuring the FE isotope composition are shown in the table. A comparison of these results indicates that the theoretical and experimental data are in good agreement.

The authors extend their thanks to G. M. Kukavadze and R. N. Ivanov, who performed the mass-spectrometer analysis of irradiated uranium, and also to V. N. Sharapov who calculated the FE isotope composition.

#### LITERATURE CITED

1. D. I. Blokhintsev, N. A. Dollezhal', and A. K. Krasin, *Atomnaya Energiya*, 1, 10 (1956).‡
2. S. Katcoff, *Nucleonics* 16, 4, 78 (1958).

‡Original Russian pagination. See C. B. translation.

# ON IMPROVING THE EFFICIENCY OF POWER STATION REACTORS WITH GASEOUS COOLANTS

T. Kh. Margulova and L. S. Sterman

Translated from *Atomnaya Énergiya*, Vol. 8, No. 5, pp. 448-451,

May, 1960

Original article submitted September 3, 1959

An increase in the gaseous coolant temperature  $t_{c,1}$  at the reactor downstream end always leads to an increase in the reactor efficiency. However, the choice of the maximum temperature depends on the material of which the fuel-element jacket is made. If the material cost is high and is not justified by an increase in the cycle efficiency, it is advisable to use lower coolant temperatures.

The gas temperature  $t_{c,2}$  at the reactor upstream end cannot be determined without a careful analysis of the power station thermodynamic layout. The power station efficiency is usually the highest for a large gas temperature drop between the reactor upstream and downstream ends (of the order of 150 to 200°C and over). If a two-pressure operating cycle instead of a single-pressure cycle is used in the power station layout, the resulting complications and the higher cost are entirely justified by the advantages offered by an increase in efficiency. The use of a three-pressure operating cycle is hardly advisable, since in this, the efficiency is very little improved in comparison with the case of the two-pressure cycle, and the power station layout becomes much more complicated.

Figure 1 shows the dependences of the efficiency ( $\eta_e$ ) on the vapor pressure  $P_{hp}$  in the high-pressure loop for a power station with a two-pressure operating cycle. The curves were plotted for the case without regenerative

preheating of the feed water, when the gas temperature at the reactor downstream end was equal to 375°C. Each value of  $t_{c,2}$  corresponds to a  $P_{hp}$  value that secures the optimum efficiency. The initial points of these curves correspond to the  $\eta_e$  value for the single-pressure operating cycle.

In reactors with gaseous coolants, for constant  $t_{c,1}$  and  $t_{c,2}$  and a chosen value of  $P_{hp}$ , the vapor pressure in the low-pressure loop drops with an increase in the feed water temperature  $t_{fw}$ , and the quantity of this vapor, reduced to the same quantity of high-pressure vapor, increases. This negatively affects the power station efficiency. Therefore, regeneration exerts a positive influence only in a certain definite feed water temperature interval, which depends on the number of preheaters; the optimum  $t_{fw}$  value is lower than that for ordinary power stations.

Figure 2 shows the efficiency vs. feed water temperature curves for different numbers of regenerative preheaters for single-pressure (a) and two-pressure (b) cycles.

Figure 3 shows the dependences of the maximum efficiency value on the coolant temperature  $t_{c,2}$  for single-pressure (curves 1 and 3) and two-pressure cycles (curves 2 and 4) in the presence ( $\eta_{e,n}^{\max}$  solid curves) and absence ( $\eta_e^{\max}$ , dotted curves) of regenerative preheating. It can be seen that regenerative preheating for the single-pressure operating cycle is beneficial only if the  $t_{c,2}$  value in the reactor exceeds ~170°C; for the two-pressure cycle, regenerative preheating leads to an increase in efficiency even for lower  $t_{c,2}$  values. Obviously, in deciding on the power station layout, it is necessary to determine to what extent the advantages resulting from the use of regeneration with a given number of preheaters exceed the additional costs involved.

For higher  $t_{c,2}$  values, the efficiency as well as the coolant circulation losses increase. The efficiency calculated by taking into account these losses is determined by the equation

$$\eta_e = \frac{N_e - K N_e}{Q_r} = \frac{N_e - K N_e}{Q_{vap} - K \eta_{bl} \text{ mot } \eta_{bl} \text{ mech } N_e}, \quad (1)$$

where  $Q_r$  is the reactor heat output,  $N_e$  is the reactor electrical output,  $K$  is the portion of the electrical energy

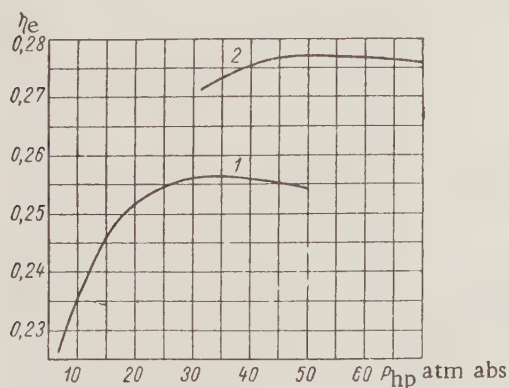


Fig. 1. Variation of  $\eta_e$  in dependence on the vapor pressure  $P_{hp}$  for the following temperatures  $t_{c,2}$  (°C): 1) 140; 2) 200;

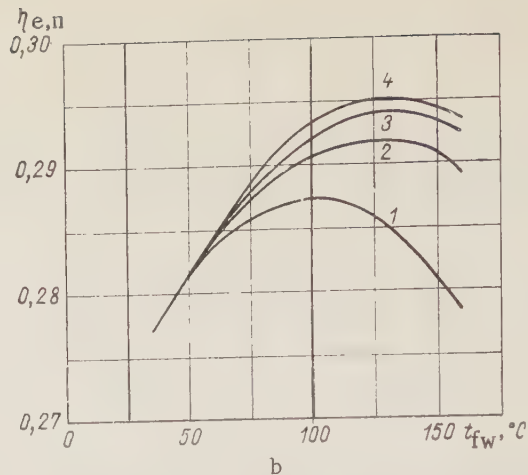
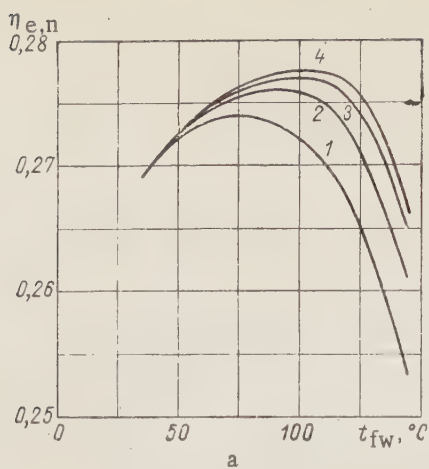


Fig. 2. Variation of  $\eta_{e,n}$  in dependence of the feed water temperature  $t_{fw}$  and the number of regenerative preheaters  $z$  (mixing-type preheaters): 1)  $z=1$ ; 2)  $z=3$ ; 3)  $z=5$ ; 4)  $z=10$ ;  $t_{c,1}=375^\circ\text{C}$ ;  $t_{c,2}=200^\circ\text{C}$ .

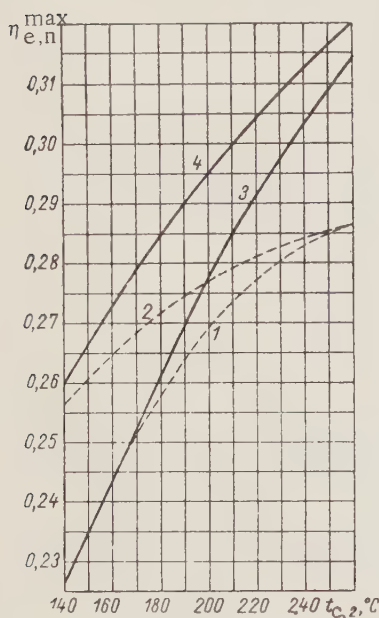


Fig. 3. Dependence of the maximum values  $\eta_e^{\max}$  and  $\eta_{e,n}^{\max}$  on the coolant temperature  $t_{c,2}$  for the constant value of  $t_{c,1} = 375^\circ\text{C}$ .

$N_e$  expended on coolant circulation,  $Q_{vap}$  is the heat transferred to the vapor generator,  $\eta_{bl\ mech}$  is the blower mechanical efficiency, and  $\eta_{bl\ mot}$  is the blower motor efficiency.

Equation (1) can be reduced to the following form:

$$\eta_e^H = \frac{(1-K)\eta_e}{1-K\eta_e\eta_{bl\ mot}\eta_{bl\ mech}} \quad (2)$$

The maximum efficiency values,  $(\eta_{e,n}^H)$ , calculated by taking into account circulation losses in the presence

of feed water regenerative preheating for a single-pressure (a) and a two-pressure cycles, are given in Fig. 4. The variation of  $\eta_{e,n}^H$  in dependence on  $t_{c,2}$  for constant loop hydrodynamic characteristics and for a constant reactor heat output is shown by dotted lines. Under these conditions, the following relation holds:

$$\frac{K'}{K''} = \left( \frac{t_{c,1} - t_{c,2}''}{t_{c,1} - t_{c,2}'} \right)^3 \left( \frac{\gamma_2}{\gamma_1} \right)^2 \left( \frac{C_{p,2}}{C_{p,1}} \right)^3 \frac{\eta_{e,n}''}{\eta_{e,n}'}, \quad (3)$$

where  $K'$  is the fraction power expended on coolant circulation,  $\gamma_1$  is the average coolant specific weight,  $C_{p,1}$  is the average coolant specific heat, and  $\eta_{e,n}'$  is the electrical efficiency without taking into account the piping losses for  $t_{c,2}'$ ;  $K''$ ,  $\gamma_2$ ,  $C_{p,2}$ , and  $\eta_{e,n}''$  are the values of the same quantities for  $t_{c,2}''$ .

If we know the fraction power  $K'$  for the given operating conditions, we can determine its value  $K''$  for the same reactor output, but for a different value of  $t_{c,2}$ .

As can be seen from Fig. 4, there are optimum  $t_{c,2}$  values which correspond to the maximum efficiency value where coolant circulation losses are taken into account.

An increase in the coolant temperature at the reactor upstream end initially leads to such an increase in efficiency that  $\eta_{e,n}^H$  also increases (regardless of higher circulation losses). Subsequently, increasing circulation losses lead to the fact that  $\eta_{e,n}^H$  begins to decrease with an increase in  $t_{c,2}$ . It is obvious from Fig. 4 that the optimum  $\eta_{e,n}^H$  values for the single-pressure operating cycle correspond to  $t_{c,2}$  values higher than the  $t_{c,2}$  value for the two-pressure cycle. The fraction power expended on coolant circulation in the single-pressure cycle is also higher than that in the two-pressure cycle under conditions securing the optimum efficiency, and the efficiency value where circulation losses are taken into account is always lower.

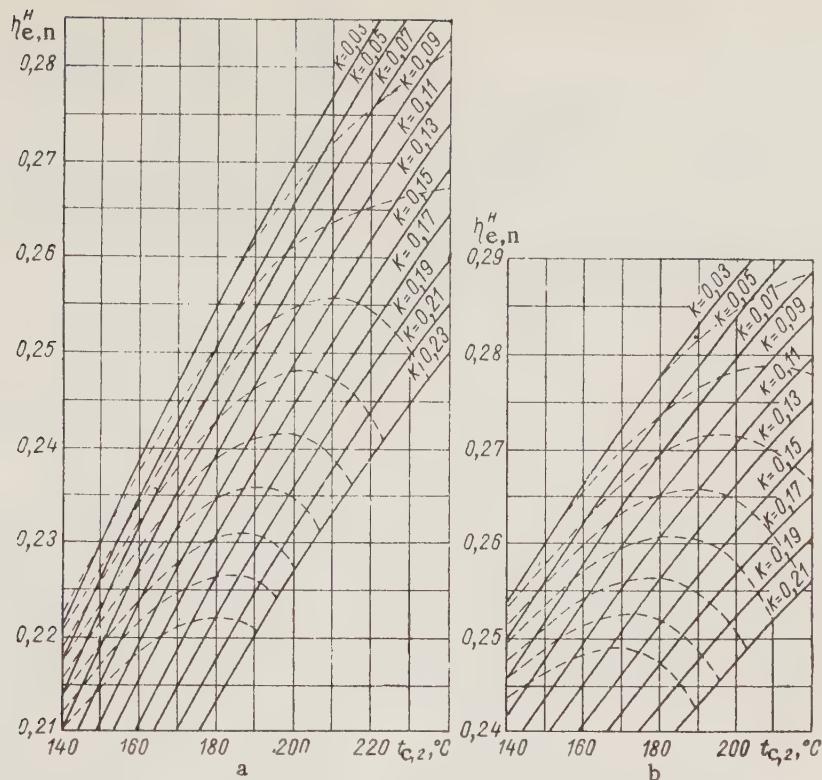


Fig. 4. Dependence of  $\eta_{e,n}^H$  on the coolant temperature for various values of the fraction power expended on coolant circulation ( $t_{c,1}=375^\circ\text{C}$ ).

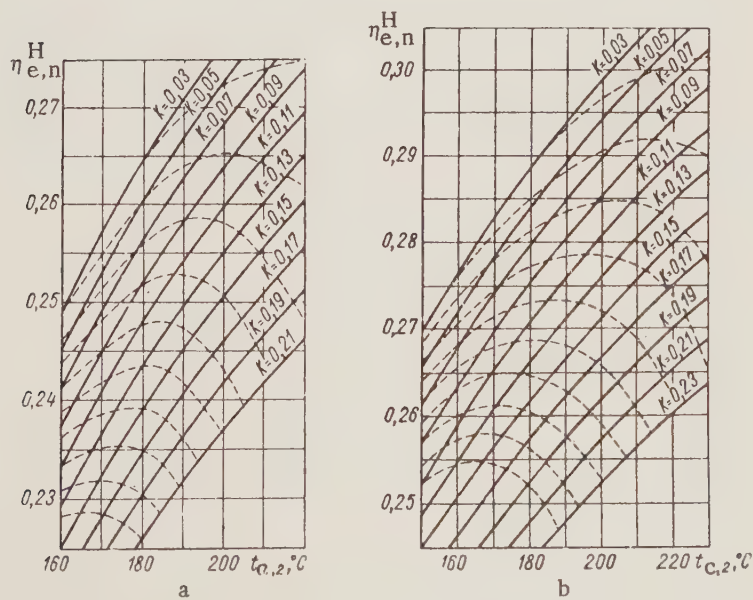


Fig. 5. Dependence of  $\eta_{e,n}^H$  on the coolant temperature  $t_{c,2}$  for various relative values of the fraction power expended on coolant circulation (two-pressure cycle): a)  $t_{c,1}=340^\circ\text{C}$ , b)  $t_{c,1}=400^\circ\text{C}$ .

The above analysis pertains to conditions where  $t_{C,1} = 375^\circ\text{C}$ . In order to determine the effect of  $t_{C,1}$  values on the power station efficiency, we also performed calculations for different  $t_{C,1}$  values.

Figure 5 shows the  $\eta_{e,n}^H$  vs.  $t_{C,2}$  curves. From Figs. 4b, 5a, and 5b, it is obvious that, for equal relative circulation losses,  $\eta_{e,n}^H$  increases with an increase in the gas temperature at the reactor downstream end, and the maximum efficiency values are obtained for higher  $t_{C,2}$  values.

We are justified in increasing the reactor heat output if the increase in the fuel cost in producing electrical

energy due to a lower power station efficiency is compensated by lower capital expenditures. For a given reactor heat output, it is necessary to strive for the maximum power station efficiency while taking into account circulation losses. It is necessary to bear in mind that the maximum efficiency value decreases with an increase in the heat output of a given reactor, i.e., as can be seen from Figs. 4 and 5, the lower dotted curves correspond to large reactor heat output values.

# MEASUREMENT OF THE FAST NEUTRON FLUX DISTRIBUTION IN THE CORE OF THE VVR-S REACTOR WITH RESPECT TO CHANGES IN THE ELECTRICAL CONDUCTIVITY OF GERMANIUM SPECIMENS

E. Aleksandrovich and M. Bartenbakh

Institute of Nuclear Research, Polish Academy of Sciences, Warsaw

Translated from *Atomnaya Énergiya*, Vol. 8, No. 5, pp. 451-452,

May, 1960

Original article submitted December 28, 1959

In connection with the investigations of the behavior of semiconductors under neutron irradiation that are in progress at the Institute of Nuclear Research in Warsaw, it was necessary to determine the fast neutron flux distribution in the reactor core.

Under the action of fast-neutron irradiation, the electrical conductivity of a germanium monocrystal of the  $n$  type gradually decreases, and, in the final stage, the germanium monocrystal is converted to the  $p$  type [1-7]. The typical curve representing the variation of germanium electrical conductivity in time during irradiation by fast neutrons is shown in Fig. 1. The initial portion of this curve can be considered as linear, which is noticeable only in the case where the neutron energy exceeds  $\sim 300$  ev.

Nine germanium specimens cut from the monocrystal were used for measurements. The specimens were in the shape of parallelepipeds whose dimensions were  $1.5 \times 1.5 \times 10$  mm. They were selected in such a manner that their electrical conductivity was at the maximum.

In order to eliminate the influence of thermal neutrons, each specimen was enclosed in a cadmium shell

0.25 mm thick. The specimens were placed at equal distances from each other in a special aluminum probe and then introduced into the core of the VVR-S reactor between the fuel elements. Thus, seven specimens were distributed along the reactor core height and two specimens were placed outside the core: one was above and the other below it.

The electrical conductivity of the specimens in the reactor was measured during irradiation with respect to the current intensity through the specimens; the current was supplied by a dc voltage source. The current intensity was such that the specimens were not heated during measurements. The reactor power, equal to 1.5 kw, was kept constant.

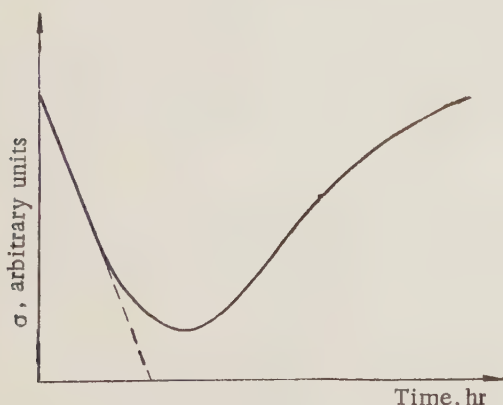


Fig. 1. Variation of the electrical conductivity ( $\sigma$ ) of a germanium specimen (monocrystal) in time during irradiation by fast neutrons.

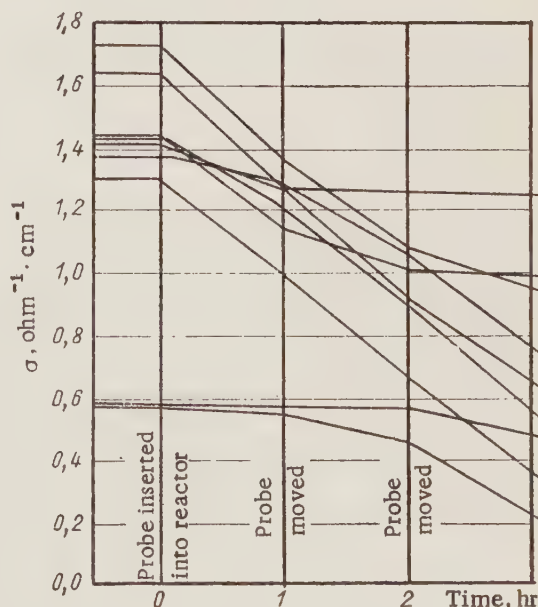


Fig. 2. Variation of the electrical conductivity ( $\sigma$ ) of germanium specimens lowered to various depths into the core of the VVR-S reactor during irradiation by fast neutrons.

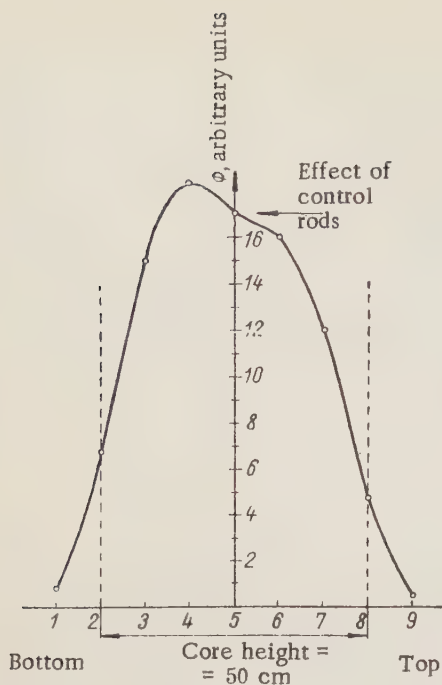


Fig. 3. Fast-neutron flux distribution along the VVR-S reactor core axis.

The variation of the electrical conductivities of all specimens during irradiation is shown in Fig. 2. A sharp change in the magnitude of  $d\sigma/dt$  at the points  $t=1$  hr and  $t=2$  hr was caused by changing the probe position in the reactor.

The slope of the  $\sigma(t)$  curve is the measure of the intensity of the fast neutron flux at the point where the specimen is located. Figure 3 shows the fast neutron flux distribution along the core axis. In plotting this curve, we used the time interval enclosed between the points  $t=1$  hr and  $t=2$  hr in Fig. 2.

This method can also be used for absolute measurements.

#### LITERATURE CITED

1. R. Davis et al., Phys. Rev. 74, 1255 (1948).
2. W. Johnson and K. Lark-Horovitz, Phys. Rev. 76, 442 (1949).
3. J. Crawford, jr., K. Lark-Horovitz, Phys. Rev. 78, 815 (1950); Phys. Rev. 79, 889 (1950).
4. J. Cleland et al. Phys. Rev. 83, 312 (1951). Phys. Rev. 84, 861 (1951).
5. H. James and K. Lark-Horovitz, Z. phys. Chem. 198, 107 (1951).
6. J. Cleland, J. Crawford and J. Pigg, Phys. Rev. 98, 1742 (1955).
7. B. Buras et al., Report No. 101/I-B, Institute of Nuclear Research, (Warsaw, 1959).

# CALCULATION OF THERMAL SHOCKS IN REACTOR STRUCTURAL PARTS

Yu. E. Bagdasarov

Translated from *Atomnaya Énergiya*, Vol. 8, No. 5, pp. 452-454,

May, 1960

Original article submitted July 13, 1959

Thermal shocks in the walls of reactor structural parts arise due to a sudden drop in the coolant temperature at the core downstream end after reactor emergency shutdown. Since sharp temperature changes lower the strength of such important and irreplaceable parts as tanks, collectors, and pipes, it is necessary to know how to calculate the thermal shock in reactor structural parts if power station devices are to be designed correctly. The thermal shock effect has been studied by a number of investigators [1-3].

An effective method for protecting the walls of important reactor structural parts from thermal shock is the provision of a thermal screen between the wall and the coolant.

The wall thickness of tanks, collectors, and pipes used in reactor loops is considerably smaller than their diameters. From the point of view of changes in temperature fields and thermal stresses, these walls can be considered to be flat. Therefore, we shall hereafter consider only the two-dimensional geometry. For technical reasons, in the majority of practical cases, the carrying walls and the thermal screen are made of the same material. This makes it possible to obtain analytical equations for the calculation of thermal stresses if we assume that ideal thermal contact exists between the thermal screen layers and between the thermal screen and the carrying wall and that liquid layers are absent. The neglect of the thermal resistance and the heat capacity of the coolant layers lead to somewhat higher thermal stress values in the carrying wall, which provides a safety margin in calculations.

The temperature changes in the plane of the wall cross section are found from the following system of equations [4]\*:

$$\left. \begin{aligned} a \frac{\partial^2 t}{\partial x^2} &= \frac{\partial t}{\partial \tau}; \\ t|_{\tau=0} &= \theta_0 = \text{const}; \\ \frac{\partial t}{\partial x} \Big|_{x=0} &= 0; \\ -\lambda \frac{\partial t}{\partial x} \Big|_{x=\delta} &= a [t|_{x=\delta} - \theta(\tau)]. \end{aligned} \right\}$$

The solution of this system is given by the equation

$$t(x, \tau) = \theta(\tau) + \sum_{n=1}^{\infty} A_n(\tau) \cos \left( \epsilon_n \frac{x}{\delta} \right),$$

where

$$A_n(\tau) = -B_n e^{-b\epsilon_n^2 \tau} \int_0^{\tau} \frac{\partial \theta}{\partial \tau} e^{b\epsilon_n^2 \tau} d\tau;$$

$$B_n = \frac{4 \sin \epsilon_n}{2\epsilon_n + \sin 2\epsilon_n}.$$

The proper values of  $\epsilon_n$  are found from the transcendental equation  $\text{tg } \epsilon_n = \text{Bi}/\epsilon_n$ , and, for  $\text{Bi} \geq 50$  we can assume that  $\epsilon_n = (2n-1)(\pi/2)$ , where  $n=1, 2, \dots$ . The thermal stress on the outside surface of the  $k$ th layer is determined from the relations [5]

$$\sigma_{c_k}(\tau) = \frac{\alpha_w E_w}{1-\nu} [\bar{t}_k(\tau) - t(c_k, \tau)];$$

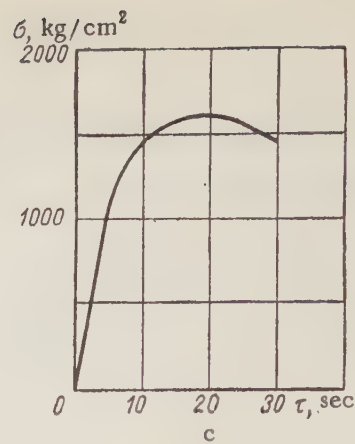
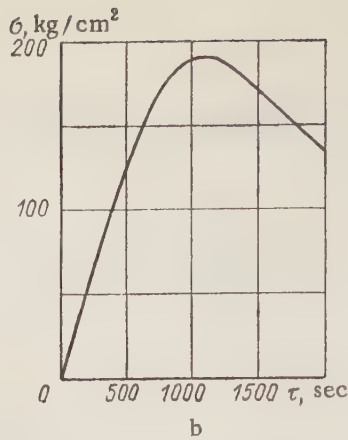
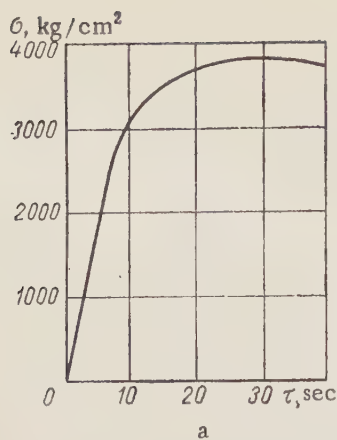
$$\bar{t}_k(\tau) = \frac{1}{c_k - \gamma_k} \int_{\gamma_k}^{c_k} t(x, \tau) dx.$$

Each form of the  $\theta(\tau)$  function yields a separate form of the expression for  $\sigma_{c_k}(\tau)$ . The table provides the final formulas for the cases of linear and exponential changes in  $\theta(\tau)$ . As an example, the figure shows the results obtained in calculating thermal shocks in the carrying wall and the thermal screen of a fast reactor vessel with sodium cooling [6].

The following initial data were used in calculations: the material was Steel 1Kh18N9T;  $\theta(\tau) = \theta_{\infty} + \Delta \theta_0 e^{-m\tau}$ ;  $\Delta \theta_0 = 140^\circ\text{C}$ ;  $m = 0.1 \text{ sec}^{-1}$ ;  $\delta = 0.2 \text{ m}$ ;  $\gamma_1 = 0$ ;  $c_1 = 0.05 \text{ m}$ ;  $\gamma_N = 0.19 \text{ m}$ ;  $c_N = \delta = 0.2 \text{ m}$ .

The following notation was used in these calculations:  $t(x, \tau)$  is the carrying wall and the thermal screen temperature ( $^\circ\text{C}$ );  $\theta_0$ ,  $\theta(\tau)$ , and  $\theta_{\infty}$  are the coolant temperatures at the initial instant of time, at the time  $\tau$ , and the asymptotic value, respectively.

\* The notation used is explained at the end of the article.



Thermal shock calculation. a) Carrying wall without thermal screen; b) carrying wall with thermal screen; c) end layer (in contact with sodium) of the 10-mm thermal screen.

#### Calculation Formulas for Determining Thermal Stresses

Coolant temperature	Equation for calculating thermal stresses
<p>For exponential changes</p> $\theta(\tau) = \theta_{\infty} + \Delta\theta_0 e^{-m\tau}$	$\sigma_{c_k}(\tau) = A\Delta\theta_0 \sum_{n=1}^{\infty} \frac{B_n m}{b\epsilon_n^2 - m} \times$ $\times \left[ \frac{\sin\left(\epsilon_n \frac{c_k}{\delta}\right) - \sin\left(\epsilon_n \frac{\gamma_k}{\delta}\right)}{\frac{c_k - \gamma_k}{\delta} \epsilon_n} - \cos\left(\epsilon_n \frac{c_k}{\delta}\right) \right] [e^{-m\tau} - e^{-b\epsilon_n^2 \tau}]$
<p>For linear changes*</p> $\theta(\tau) = \theta_0 - p\tau$	$\sigma_{c_k}(\tau) = A \frac{p}{b} \sum_{n=1}^{\infty} \frac{B_n}{\epsilon_n^2} \left[ \frac{\sin\left(\epsilon_n \frac{c_k}{\delta}\right) - \sin\left(\epsilon_n \frac{\gamma_k}{\delta}\right)}{\frac{c_k - \gamma_k}{\delta} \epsilon_n} - \cos\left(\epsilon_n \frac{c_k}{\delta}\right) \right] [1 - e^{-b\epsilon_n^2 \tau}]$ <p style="text-align: center;">for <math>\tau \leq \tau_0</math>:</p> $\sigma_{c_k}(\tau) = A \frac{p}{b} \sum_{n=1}^{\infty} \frac{B_n}{\epsilon_n^2} \times$ $\times \left[ \frac{\sin\left(\epsilon_n \frac{c_k}{\delta}\right) - \sin\left(\epsilon_n \frac{\gamma_k}{\delta}\right)}{\frac{c_k - \gamma_k}{\delta} \epsilon_n} - \cos\left(\epsilon_n \frac{c_k}{\delta}\right) \right] [e^{\epsilon_n^2 b \tau_0} - 1] e^{-b\epsilon_n^2 \tau}$ <p style="text-align: center;">for <math>\tau \geq \tau_0</math></p>

\* Linear temperature changes occur during the time  $\tau_0$ , when  $\theta = \theta_{\infty}$ .

otic value of the coolant temperature for  $\tau \rightarrow \infty$  ( $^{\circ}\text{C}$ ), respectively;  $\Delta\theta_0 = \theta_0 - \theta_{\infty}$  is the maximum change in the coolant temperature ( $^{\circ}\text{C}$ );  $\bar{\tau}_k(\tau)$  is the average temperature of the  $k$ th layer ( $^{\circ}\text{C}$ );  $\tau$  is the time (sec);  $\tau_0$  is the time during which the coolant temperature drops linearly (sec);  $x$  is the coordinate measured from the ves-

sel outside surface toward the interior (m);  $\delta$  is the overall thickness of the carrying wall and of the thermal screen sheets (m);  $c_k$  is the coordinate of the  $k$ th layer outside surface (m);  $\gamma_k$  is the coordinate of the  $k$ th layer inside surface (m). Here, the carrying wall represents the first layer.

The structural material parameters are the following:  $\underline{a}$  is the diffusivity coefficient ( $\text{m}^2/\text{sec}$ );  $\lambda$  is the thermal conductivity coefficient ( $\text{kcal}/\text{m} \times \text{sec} \times ^\circ\text{C}$ );  $\alpha_w$  is the linear thermal expansion coefficient ( $1/^\circ\text{C}$ );  $E_w$  is the elasticity modulus ( $\text{kg}/\text{cm}^2$ );  $\nu$  is the Poisson coefficient;  $\alpha$  is the coefficient of heat transfer from the wall to the coolant ( $\text{kcal}/\text{m}^2 \times \text{sec} \times ^\circ\text{C}$ );  $b = a/\delta^2$ ;  $Bi = a\delta/\lambda$ ;  $A = \alpha_w E_w / (1 - \nu)$ ;  $\sigma_{ck}(\tau)$  is the thermal stress at the  $k$ th layer outside surface ( $\text{kg}/\text{cm}^2$ );  $p$  is a parameter ( $\text{deg}/\text{sec}$ );  $\underline{m}$  is a parameter ( $\text{sec}^{-1}$ ).

#### LITERATURE CITED

1. R. Tidball and M. Shrut, Transactions of the ASME 76, 4, 639 (1954).

2. A. A. Klypin, Teploenergetika, 1, 33 (1957).
3. M. Heisler, J. Appl. Mech. 20, 2, 261 (1953).
4. A. V. Lykov, Theory of Thermal Conductivity [in Russian] (Gostekhizdat, Moscow, 1952).
5. S. P. Timoshenko, Strength of Materials [in Russian] (Gostekhizdat, Moscow, 1946) Vol. 2.
6. A. I. Leipunskii, et al., Transactions of the Second International Conference on the Peaceful Uses of Atomic Energy (Geneva, 1958). Reports by Soviet scientists: Nuclear Reactors and Nuclear Power Engineering [in Russian] (Atomizdat, Moscow, 1959) Vol. 4, p. 212.

# 600-kev PROTON INJECTOR FOR A LINEAR ACCELERATOR

Yu. N. Antonov, L. P. Zinov'ev, and V. P. Rashevskii

Translated from *Atomnaya Énergiya*, Vol. 8, No. 5, pp. 454-457,

May, 1960

Original article submitted December 10, 1958

The necessity for increasing the injection current at the 10-Bev proton synchrotron at the Joint Institute for Nuclear Studies prompted the authors of the present paper to undertake the following problem: using an ion source capable of furnishing a large proton current, extract and focus this current for acceleration to an energy of 600 kev. In doing this it is necessary that the geometric dimensions and angular convergence of the beam at the output of the accelerator tube satisfy the injection conditions in the linear accelerator.

**Ion source.** This is a gas discharge with a doubly contracted pinch [1] in which electron oscillations are used. The source was developed in NII-5 and then modified by the authors and V. M. Blagoveshchenskii, T. I. Gutkin, and Yu. V. Kursanov of the High-Energy Laboratory of the Joint Institute for Nuclear Studies. A schematic diagram of the source is shown in Fig. 1. In this source we used cathode 1 of a TGI-90/8 thyatron. The cathode leads 2 are cooled by circulating water and isolated from the cathode flange 5 by porcelain insulators 4. The hydrogen is introduced into the discharge chamber through a palladium filter and tube 3.

The internal cavity of the intermediate anode 6 forms the cathode region of the discharge; the presence in the intermediate anode of the channel 15, 9 mm in diameter and 10 mm long, causes the formation of a double layer of hemispherical shape. The spherical part points toward the cathode and serves to contract the pinch. The intermediate anode is also cooled by water which flows in the cavity 7. Directly on the intermediate anode there is a coil 8 that produces an axial magnetic field that contracts the plasma in the space between the channel 15 and the emission aperture 17. The intermediate anode 6, the wall of the source, 16 and the output flange 12 form an open magnetic conductor. The copper anode 10 has an aperture 9 mm in diameter which is concentric with the channel 15 and the emission aperture; the electron oscillation takes place in the space between these two electrodes. The output flange of the source (anticathode) has an insert 13 made from nonmagnetic material (tungsten or stainless steel) with an emission aperture 2 mm in diameter and approximately 0.5 mm long.\* Since the source is at a potential of 600 kv with respect to ground the entire power supply circuit, which is mounted on porcelain insulators 2.6 m in height, has its own

generator (220 v, 50 cps, 3.5 kw) and a GSM-1 generator (220 v, 500 cps, 0.6 kw). The drive that connects the generator and the motor, which is at ground potential, is a shaft made from  $\delta$  wood which is approximately 2 m in length.

The power supply for the source is shown in Fig. 2. The filament supply for the cathode of the source comes from transformer  $Tr_1$ . The filament requires 7.8 v at 6.4 amp. The hydrogen pressure in the discharge chamber is maintained at about  $1.5 \cdot 10^{-2}$  mm Hg; the hydrogen is admitted through the palladium filter Pa and the flow rate is controlled by heating the filter.

The magnetic field in the source is produced by a coil with 320 turns. The magnetic induction in the space between the intermediate anode and the anticathode is 1000 gauss for a coil current of approximately 2 amp.

When the artificial line is discharged through the thyatron a negative pulse approximately 500  $\mu$ sec long appears at the cathode; the amplitude of this pulse is controlled by the voltage from the power supply  $B_2$  which is used to charge the line. The thyatron is fired by a pulse

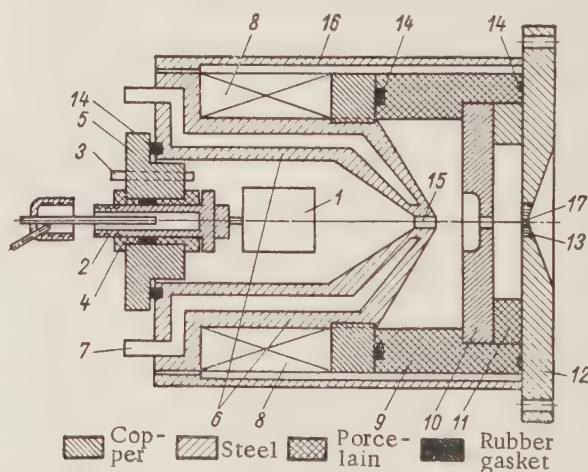


Fig. 1. Schematic diagram of the source: a) copper, b) steel, c) porcelain, d) rubber gasket.

\*If the emission aperture is a channel the loss of ion current to the wall increases appreciably; hence, the condition  $l \ll d$  must be satisfied for the aperture.

which is obtained from a photomultiplier which is mounted on an insulator; this tube is triggered by the flash from an MN-3 neon lamp which is located at the base of the insulator.

The pulse from the line (amplitude of 400–500 v) is applied to the cathode of the source and ignites an arc between the cathode and the intermediate anode. The arc current produces a potential difference across the resistance  $R_1=200$  ohm; this potential difference causes the ignition of an arc in the channel in the intermediate anode. Any disturbance of the uniformity of the discharge gap in the channel causes electron drift in the region of the anode plasma; the hemispherical double layer accelerates and focuses the electrons, providing the required electron current density in the region of the anode plasma. The potential jump in the double layer automatically reaches a level such that the generation of ions in the region of the anode plasma is sufficient for satisfactory stability of the space-charge limited bipolar current:

$$\frac{I_p}{I_e} = \left( \frac{m_e}{m_p} \right)^{1/2},$$

where  $I_p$  is the directed current of positive ions;  $I_e$  is the directed electron current;  $m_e$  and  $m_p$  are the mass of the electron and positive ion, respectively.

The strong inhomogeneous magnetic field in the region of the anode plasma causes a still greater contraction of the discharge, leading to an additional increase in the density of carriers. The double contraction of the discharge and the use of electron oscillation in the space between the intermediate anode and the anticathode causes an appreciable degree of ionization in the anode region of the discharge. The current extracted from the source can reach values of 270 ma. Knowing the mass spectrum of the beam and the gas consumption in the source (source parameters are given below) we can show that the ionization percentage in the discharge is close

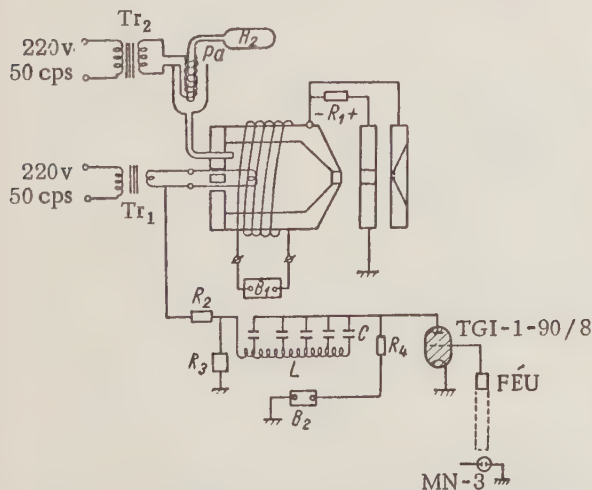


Fig. 2. Power supply for the source ( $R_1=200$  ohm;  $R_2=$   
 $=R_3=12$  ohm;  $R_4=5 \cdot 10^3$  ohm;  $C=10$   $\mu$ f;  $L=25$ mh).

to 100%. Under the effect of the electric field the ions generated in the anode plasma are directed toward the emission aperture of the source and extracted by the extraction system.

The geometry of the discharge chamber of the source is chosen experimentally for optimum conditions for igniting the pulsed arc. The opening angle of the cone of the intermediate anode in the working version is  $120^\circ$ . If this angle is varied the current extracted from the source falls off sharply since the axial magnetic field has a strong effect on the electron kinetics and parameters of a low-pressure plasma [2].

When the diameter of the emission aperture is increased from 0.8 to 2.0 mm the current increases approximately as the square of the diameter (Fig. 3). However, when the diameter of the emission aperture is increased to 3.0 mm it is difficult to ignite the arc in the source because the field of the extraction electrode "drops" in the discharge chamber. A very important factor is the presence of the nonmagnetic insert 13 (cf. Fig. 1). The absence of this insert causes a noticeable reduction in the extracted current and deteriorates the focusing. In the working model the diameter of the insert is 10 mm. Some increase in current is achieved if the diameter of the insert is increased to 20 mm.

The current at the output of the injector, as a function of discharge current, is shown in Fig. 4. For any magnetic field configuration the contraction falls off as the discharge current is increased, i.e. with an increase in charge concentration. (In a discussion of the relaxation length of a Maxwellian distribution, I. Langmuir [3]

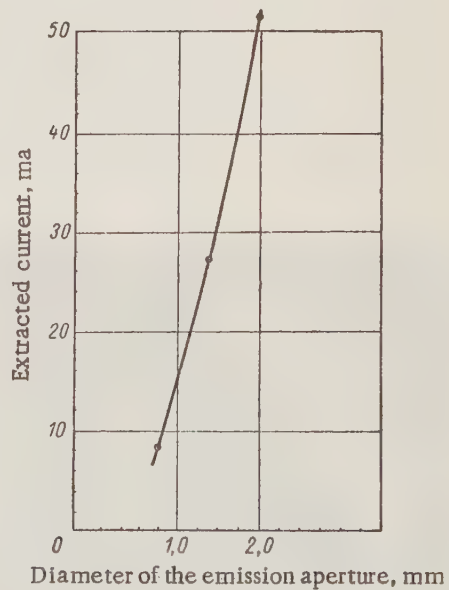


Fig. 3. The current extracted from the source as a function of the diameter of the emission aperture.

has shown that with an increase in electron concentration causes a reduction in mean free path. Since the magnetic field is effective over the mean free path length, the effect of the field is reduced as the concentration is increased.) In Fig. 5 we show the source mounted on the accelerator.

The parameters which characterize the operation of the source are as follows:

Filament voltage, v	7.8
Filament voltage, amp	6.4
Arc voltage, v	90-120
Arc current, amp	30
Magnetic field in the gap, gauss	1000
Gas pressure in the discharge chamber, mm Hg	$1.5 \cdot 10^{-2}$
Gas consumption	150
Proton component of the extracted current, percent.	75

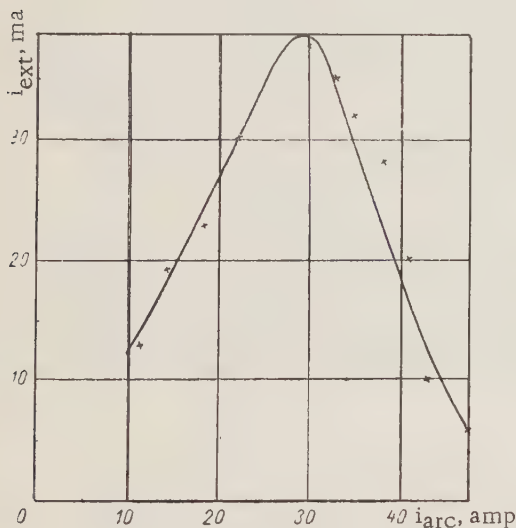


Fig. 4. The extracted current as a function of arc current. ( $P_{H_2} = 1.2 \cdot 10^{-5}$  mm Hg;  $U_{ext} = 45$  kv;  $i_{mag} = 1.1$  amp).

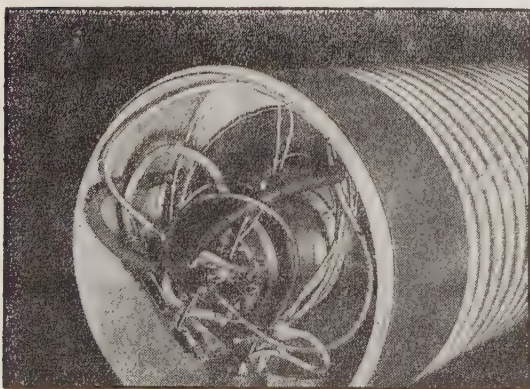


Fig. 5. The source mounted on the accelerator tube.

The percentage proton composition of the beam which passes through the linear accelerator in the absence of resonator excitation is measured by means of a sector magnet (deflection angle,  $75^\circ$ ).

#### Accelerator, extraction and focusing of the beam.

The useful diameter of the 600-kv accelerator is 350 mm while the length is 1670 mm. The tube has 70 irises and every other iris has an anticorona ring which is connected to an appropriate tap on a voltage divider. The divider is a vinyl plastic tube 8 mm in diameter with uniformly distributed taps, along which distilled water flows (this water is also used for cooling the source).

The source is mounted directly on the input flange of the accelerator. The extraction and focusing electrodes are located inside the accelerator tube and the power supply leads are introduced through the first anticorona rings.

The arrangement of the extraction and focusing electrodes in the source and accelerator and the power supply system are shown on Fig. 6. A TRVV pulse transformer is used to apply a pulse to the accelerator tube. The amplitude of this pulse is 600 kv and its length is approximately 300  $\mu$ sec. A special system is used to maintain the voltage of the flat part of the pulse with an accuracy of better than 0.5%. The transformer load is the divider D ( $R = 430$  kilohm) part of which is used to derive the 50-kv extraction voltage. The resistance of the accelerator tube divider is approximately  $5 \cdot 10^6$  ohm. The voltage to the focusing electrode is taken from a high-voltage power supply PF which is located on the source insulating column. In order to focus the beam, at the output of the tube (1 m from the output iris) we apply a focusing voltage of 3 kv with respect to the source. This voltage determines the energy spread of the beam at the output due to ion generation in the extraction region. The energy spread in the beam at the output is less than 0.5%.

The beam is monitored visually at the output of the tube by means of the radiation from a quartz shield. The

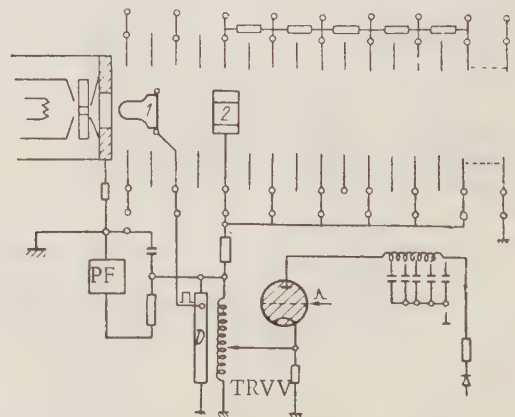


Fig. 6. Diagram showing the arrangement and power supplies for the extraction electrode (1) and the focusing electrode (2).

ion current is measured with a Faraday cylinder; a coil which provides a field of approximately 500 oe at the axis of the cylinder is mounted on the Faraday cylinder in order to protect it from secondary electrons.

The angular divergence of the beam at the input to the linear accelerator is estimated to be  $3 \cdot 10^{-3}$ . The diameter of the spot at the input to the linear accelerator (a distance of approximately 6 m from the output of the tube) is 8–10 mm. With a beam focused, at a distance of approximately 1 m from the output of the tube the spot diameter is approximately 2 mm.

In conclusion the authors wish to take this opportunity to thank M. S. Vasil'ev and V. V. Slesarev for taking part in this work.

#### LITERATURE CITED

1. M. von Ardenne, Tabellen der Elektronen-physik, Ionenphysik und Übermikroskopie. Deutscher Verlag der Wissenschaften (1957).
2. O. N. Repkova and G. V. Spivak, Scientific Records: of a Plasma in a Magnetic Field, Moscow State University, (Izd. MGU, Moscow, 1945).
3. I. Langmuir, Proc. Nat. Acad. Sci. USA, 14, 627 (1928).

# MEAN NUMBER OF PROMPT NEUTRONS EMITTED IN PHOTOFISSION OF $\text{Th}^{232}$ AND $\text{U}^{238}$ $\gamma$ RAYS PRODUCED IN THE $\text{F}^{19}(\text{p}, \alpha\gamma)\text{O}^{16}$ REACTION

L. I. Prokhorova and G. N. Smirenkin

Translated from *Atomnaya Énergiya*, Vol. 8, No. 5, pp. 457-459,

May, 1960

Original article submitted January 3, 1960

In [1] attention has been directed to the fact that the data available in the literature concerning the mean number of neutrons  $\bar{\nu}$  in spontaneous fission of  $\text{U}^{238}$  ( $2.1 \pm 0.1$  [1],  $2.26 \pm 0.16$  [2]) and for photofission of  $\text{U}^{238}$  by  $\gamma$  rays from bremsstrahlung with a maximum energy  $E_{\text{max}} = 5.5$  Mev ( $1.65 \pm 0.5$  [3]) are not in agreement with a linear dependence of  $\bar{\nu}$  on the excitation energy of the fissioning nucleus  $E_x$  [4]. The values given for  $\bar{\nu}$  in photofission of  $\text{U}^{238}$  indicate that all neutrons are released in one fission event:

$$n = \bar{\nu} + \frac{\sigma(\gamma, n)}{\sigma(\gamma, f)} + 2 \frac{\sigma(\gamma, 2n)}{\sigma(\gamma, f)} + \dots \quad (1)$$

since the energy  $E_{\text{max}} = 5.5$  Mev is smaller than the reaction threshold for  $\text{U}^{238}(\gamma, n)$ . A similar value of  $\bar{\nu}$  for  $\text{Th}^{232}$ ,  $3.15 \pm 0.5$  ( $E_{\text{max}} = 6.8$  Mev), can be obtained from [3]. Other information on the number of prompt neutrons in photofission is not available in the published literature.

In the present note we report on measurements of the mean number of prompt neutrons  $\bar{\nu}$ , emitted in one photofission event  $\text{U}^{238}$  and  $\text{Th}^{232}$  by  $\gamma$  rays from the reaction  $\text{F}^{19}(\text{p}, \alpha\gamma)\text{O}^{16}$ . The reaction is realized by irradiating a  $\text{CaF}_2$  crystal with 2.6-Mev protons. The  $\gamma$ -ray

spectrum for the  $\text{F}^{19}(\text{p}, \alpha\gamma)\text{O}^{16}$  reaction [5] consists of three lines: 6.13, 6.9, and 7.1 Mev. The proton energy for the last two lines is 3.2 times greater than the component at 6.13 Mev. The admixture of  $\gamma$  rays with an energy of 12 Mev for the  $\text{F}^{19}(\text{p}, \gamma)\text{Ne}^{20}$  reaction is less than 0.2%. The mean energy of the  $\gamma$  rays causing fission of  $\text{U}^{238}$  and  $\text{Th}^{232}$  is approximately 6.7 Mev. The measurements were carried out with a van de Graaff generator.

The accelerator target and the fission chamber are surrounded by 12  $\text{B}^{10}\text{F}_3$  counters in paraffin which serve as neutron detectors. The pulses due to fission neutrons selected by means of a coincidence circuit with a resolution time of  $\tau \approx 2 \cdot 10^{-4}$  sec. The method of making these measurements is well known and has been described in detail in [6]. Accidental coincidences, which amount to approximately 70% of the recorded coincidences, are eliminated by measurement of the resolution time  $\tau$ . The spread  $\tau$  is less than 1% for the entire measurement time.

The number of neutrons recorded for one photofission event in  $\text{U}^{238}$  and  $\text{Th}^{232}$  is compared with the corresponding quantity for spontaneous fission of  $\text{Pu}^{240}$  for which the value of  $\bar{\nu}_0$  (accuracy of 2%) is  $2.26 \pm 0.05$  [7]. Thus the

Values of  $\bar{\nu}$  in photofission of  $\text{U}^{238}$  and  $\text{Th}^{232}$

Ref.	$E_{\text{max}}$ , Mev	$E_x$ , Mev	$\text{U}^{238}$			$\text{Th}^{232}$		
			$n$	$\frac{\sigma(\gamma, n)^*}{\sigma(\gamma, f)}$	$\nu$	$n$	$\frac{\sigma(\gamma, n)^{**}}{\sigma(\gamma, f)}$	$\bar{\nu}$
[3]	5.5	5.3	$1.65 \pm 0.5$	0	$1.65 \pm 0.5$	—	—	—
	6.8	5.9	$4.3 \pm 0.5$	1.15	$3.15 \pm 0.7$	$3.15 \pm 0.5$	0	$3.15 \pm 0.5$
	8.6	6.6	—	—	—	$4.5 \pm 0.5$	3.65	$0.85 \pm 1.0$
	10.3	7.7	$5.3 \pm 0.5$	3.8	$1.50 \pm 1.6$	$8.0 \pm 0.5$	6.25	$1.75 \pm 1.6$
[9]	8	6.3	7.07	1.8	$5.3 \pm 0.75$	4.65	2.00	$2.65 \pm 0.5$
	9	6.8	6.92	2.5	$4.4 \pm 1.0$	6.35	4.35	$2.0 \pm 1.1$
	10	7.5	7.25	3.25	$4.0 \pm 1.3$	8.65	5.7	$2.95 \pm 1.4$
	11	8.2	7.47	4	$3.5 \pm 1.6$	11.4	7.0	$4.4 \pm 1.8$
* Error			$\pm 40\%$ .					
** Error			$\pm 25\%$ .					

ratio  $\bar{\nu}/\bar{\nu}_0$  is measured directly in the experiment. The measured results are modified by certain corrections ( $\lesssim 2\%$ ) for variation in detection efficiency for prompt neutrons in fission of the materials being studied and neutrons from spontaneous fission of  $\text{Pu}^{240}$ . This difference arises as a consequence of the angular anisotropy of the fragments in photofission and the correlation between the prompt neutrons and the fragments. After corrections are introduced, the experimental values of the ratio  $\bar{\nu}/\bar{\nu}_0$  are  $1.86 \pm 0.09$  for uranium and  $1.42 \pm 0.09$  for thorium. Using the value of  $\bar{\nu}_0$  given above we find  $\bar{\nu}_{\text{U}} = 4.2 \pm 0.2$  and  $\bar{\nu}_{\text{Th}} = 3.2 \pm 0.2$ .

Starting with the data on  $\bar{\nu}$  for fission in the neighboring nuclei  $\text{U}^{239}$  and  $\text{Th}^{233}$ , produced with the same excitation energy in neutron irradiation, and the small variation in  $\bar{\nu}$  in going from one isotope to another [8], one would expect substantially smaller values of  $\bar{\nu}$  and approximately 2.7 for  $\text{U}^{238}$  and approximately 2.2 for  $\text{Th}^{232}$ . Large values are obtained for  $\bar{\nu}$  if we exclude the fraction of  $(\gamma, n)$  neutrons from the total neutron yield measured in [9]. The earlier data reported in [3] are not in agreement with the results reported in [9]. In the table we show values of  $\bar{\nu}$  computed from the neutron yield  $n$  [3, 9] and the energy dependence  $\sigma(\gamma, n)/\sigma(\gamma, f)$  [10], according to Eq. (1) (for  $E_{\text{max}} < 11$  Mev, only the reactions  $(\gamma, f)$  and  $(\gamma, n)$  are possible.)

The excitation energy of the fragments and the number of neutrons emitted in fission are determined by the deformation of the fissioning nucleus at rupture. From the results of the present note and the data of [9] it would appear that in photofission of  $\text{Th}^{232}$  and  $\text{U}^{238}$  the fragment deformation is greater than in neutron-induced fission.

The authors wish to thank A. I. Leipunskii and I. I. Bondarenko for their interest in this work, L. S. Kutsaev for help in setting up the experiment, N. E. Tokmantsev

and Yu. I. Baranov for help in the measurements, and V. A. Romanov for helpful cooperation.

#### LITERATURE CITED

1. B. D. Kuzminov, L. S. Kutsaeva, V. G. Nesterov, L. I. Prokhorova, and G. N. Smirenkin, *Zhur. Éksp. i Teoret. Fiz.* **37**, 406 (1959).
2. K. Geiger and D. Rose, *Canad. J. Phys.* **32**, 498 (1954).
3. L. E. Lazareva, et al. Proceedings of the Academy of Sciences USSR on the Peaceful Use of Atomic Energy (Sessions of the Division of Physicomathematical Science) [in Russian] (Izd. AN SSR, 1955) p. 306.
4. R. Leachman, *Phys. Rev.*, **101**, 1005 (1956).
5. W. Hornyak et al. *Rev. Mod. Phys.*, **22**, 291 (1950).
6. V. I. Kalashnikova, et al., Proceedings of the Academy of Sciences USSR on the Peaceful Use of Atomic Energy (Sessions of the Division of Physicomathematical Science) [in Russian] (Izd. AN SSSR, Moscow, 1955) p. 156.
7. R. Leachman, Proc. of the Second International Conference on the Peaceful Uses of Atomic Energy (Geneva, 1958), Selected Reports of Foreign Sciences, Neutron Physics [Russian translation] (Atomizdat, Moscow, 1959) Vol. II p. 342.
8. I. I. Bondarenko, B. D. Kuzminov, L. S. Kutsaeva, L. I. Prokhorova, and G. N. Smirenkin, Proc. of Second International Conference on the Peaceful Uses of Atomic Energy (Geneva, 1958) Reports of Soviet Scientists, [in Russian] (Atomizdat, Moscow, 1959) Vol. I, p. 438.
9. L. Katz, A. Baerg, and F. Brown, Report No. 200 (Canada), Second International Conference on the Peaceful Uses of Atomic Energy (Geneva, 1958).
10. J. Gindler and J. Huizenga, *Phys. Rev.* **104**, 425 (1956).

# ELECTRON ACCELERATION IN A TRAVELING-WAVE CYCLICAL WAVEGUIDE ACCELERATOR

A. A. Vorob'ev, A. N. Didenko, and E. S. Kovalenko

Translated from *Atomnaya Energiya*, Vol. 8, No. 5, pp. 459-461,

May, 1960

Original article submitted March 9, 1959

In [1] a proposal has been made that a closed curved waveguide, inside of which electromagnetic waves of the appropriate type are excited, be used as a cyclical accelerator. In the figure we show such a waveguide; an electric field with a nonzero  $\varphi$  component propagates inside the waveguide. The waveguide is loaded in such a way that close to the mean radius the phase velocity  $v_{ph} = c$ .

Because the field configuration can be controlled it is of interest to explore the possibility of controlling the trajectory of particles by the field produced by the wave itself.

The propagation of a wave in a curved waveguide which is infinite in the axial direction has been studied in [2]. At the present time there is available an approximate dispersion equation for synchronous waves of the  $LE_{mn}$  type for a waveguide which is bounded in the  $z$  direction:

$$\operatorname{ctg} \alpha_1 d - \frac{\alpha_1}{\alpha} \operatorname{tg} \alpha (b-d) = \frac{1}{2\alpha_1 r_0}, \quad (1)$$

where

$$\alpha_1 = \sqrt{k^2 - \frac{m^2 \pi^2}{a^2}}; \quad \alpha = \sqrt{k^2 - \frac{k_\varphi^2}{r_0^2} - \frac{m^2 \pi^2}{a^2}};$$

$k$  is the wave number;  $m$  is the number of field periods along the  $z$  direction;  $k_\varphi$  is the azimuthal propagation constant.

Equation (1) applies when  $|\alpha r_0| \gg 1$  and when the curvature of the waveguide is small. From the analogous equation for an straight waveguide [3] we see that Eq. (1) differs by the presence of the second term in the right-hand side, which determines the effect of the bend on the dispersion properties of the system.

Equation (1) indicates that:

- 1) The bend in the waveguide reduces the phase velocity of synchronous waves;
- 2) The effect of a bend on the dispersion properties of a bounded system for  $v_{ph}=c$  is very much greater than for a waveguide which is infinite in the  $z$  direction. This last result follows from the fact that there is a change in the field structure in the radial direction in the bounded waveguide. Actually, the point  $\alpha \approx 0$  in a bounded waveguide, as far as the field distribution along  $r$  is concerned, is equivalent to the mode  $v_{ph}=c$  in an unbounded wave-

guide. Calculations show that the effect of curvature is the same at these points in both waveguides.

Equation (1) establishes a relation for the waveguide dimensions but does not allow us to determine these dimensions uniquely. The final choice of waveguide dimensions is carried out on the basis of eliminating spurious modes; this choice involves the calculation of the cut-off frequencies for these modes. The greatest difficulty is found for the calculation of the TM mode, which cannot be carried out in the zeroth approximation. This eliminates the possibility of calculations for these modes when there are small bends. However, for small curvature we can use the results for a straight waveguide. The following formula applies for the critical wavelength for the  $TM_{m(2n+1)}$  mode [3]:

$$\lambda_{cr}^{m,n} = \frac{2a(b-d)}{\sqrt{m^2(b-d)^2 + \frac{y_n^2}{\pi^2} a^2}}, \quad (2)$$

$$m = 0, 1, 2, \dots$$

where  $y_n$  is the  $n$ th root of the equation

$$\operatorname{ctg} y = \frac{0.220s}{(b-d)} y. \quad (3)$$

Equations (2) and (3) are obtained taking account of all spatial harmonics. In addition to Eq. (1), when  $v_{ph}=c$ , the condition  $\lambda > \lambda_{cr}^{0,1}$  imposes a second limitation on the dimensions of the waveguide.

The optimum coupling impedance gives the third condition for choosing the waveguide dimensions. Calculations show that the coupling impedance depends strongly on  $b-d$ ; as  $b-d$  increases, the coupling impedance is reduced from thousands of ohms to tens of ohms.

It has been shown that for waveguide dimensions used in practice we can obtain propagation of the fundamental mode with  $v_{ph}=c$  in the region of the mean radius with no spurious modes and with a coupling impedance of several hundred ohms.

In contrast with the usual synchrotron, the high-frequency field of a waveguide accelerator is highly inhomogeneous in the radial and axial directions and has components which depend in complicated fashion on  $r$  and  $z$ . The appearance of additional wave components

leads to an oscillation frequency which obeys the condition:

$$\omega_r^2 + \omega_z^2 + \omega_\phi^2 = \text{const.} \quad (4)$$

Thus, there is only a redistribution of the oscillation frequencies. The changes in  $\omega_r$  and  $\omega_z$  are usually small. Furthermore, any variations of the high-frequency fields do not lead to a change in any of the oscillation damping factors. This result verifies the conclusion [4] that the sum of damping factors is a constant; this result can be understood on the basis of the following simple considerations. If we neglect the increase in energy and radiation, in the coordinate system which rotates with the angular velocity of the wave the particle Hamiltonian is independent of time. It thus follows that the characteristic equation does not contain odd powers of the characteristic number [5]; thus, no damping is introduced by the wave field. This conclusion is not changed if one takes account of the radiation and increase in electron energy.

It then follows that the motion of particles in a waveguide cyclical accelerator is similar to that of particles in a synchrotron, and that the complicated field configuration does not interfere with the normal operation of the accelerator.

We may note that in the analysis of particle dynamics in accelerators with a resonator, the resonator field is "spread" over the entire azimuthal range; this is equivalent to replacing the accelerating slit by a traveling wave. It is assumed that the high-frequency field has only an  $E_\phi$  component and that this component falls off in the radial direction as  $1/r$ . Whence it follows that these results are valid for synchrotrons in which the high-frequency field depends on  $r$  and  $z$  in arbitrary fashion.

In order to avoid shielding of the guiding field, the waveguide must be fabricated from separate sections which are coupled to each other only at high frequencies.

For this purpose the thickness of the walls of the sections must be kept at a minimum. The mechanical strength can be increased if each section is placed in a dielectric shell.

In [6] a proposal has been made for acceleration with control of particle trajectories in a bent waveguide in a traveling-wave field. In this case the condition of stability reduces to the following inequalities:

$$\left. \begin{aligned} n < 0; \quad n > -1; \quad n_1 > 0; \\ (1+n)^2 > 4n_1, \end{aligned} \right\} \quad (5)$$

where

$$n = \frac{\frac{\partial^2}{\partial z^2} \left( r \frac{\partial \Pi}{\partial r} + r \psi \right)}{\frac{\partial^2 \Pi}{\partial z^2} - \frac{\partial \psi}{\partial r}}; \quad n_1 = \frac{\frac{1}{r^2} \frac{\partial^2}{\partial \phi^2} \left( r \frac{\partial \Pi}{\partial r} + r \psi \right)}{\frac{\partial^2 \Pi}{\partial z^2} - \frac{\partial \psi}{\partial r}};$$

$\Pi$  is the  $z$  component of the magnetic Hertz vector,  $\psi$  is the scalar potential of the field. The inequalities  $n < 0$  and  $n_1 > 0$  are satisfied simultaneously if  $k_z^2 < 0$ . This means that the stability conditions are met only for an iris-loaded waveguide with irises in the plane  $z = \text{const}$ .

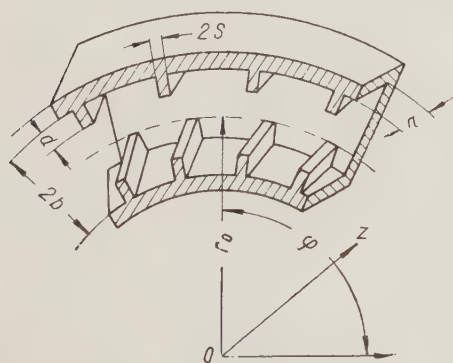
We may note that in a bent waveguide the transition to a coordinate system which moves with the wave means transition to a noninertial coordinate system; the field in this system is static but it cannot be described by Laplace's equation. Hence, Earnshaw's theorem, which describes instability in a straight waveguide, does not apply to a bent waveguide and it is possible to satisfy all the relations in (5).

The use of bent waveguides in cyclical accelerators is of interest first from the point of view of solving a number of technical difficulties which arise in the design of high-energy cyclical electronic accelerators, and second from the point of view of building cyclical accelerators in which the waveguide field performs the guiding and accelerating functions simultaneously.

#### LITERATURE CITED

1. A. A. Vorob'ev, *Izv. Vyssh. Ucheb. Zavedenii Elektromekhanika* No. 5, 106 (1958).
2. A. N. Didenko, Dissertation, Moscow State University [in Russian] (1958).
3. E. S. Kovalenko and V. I. Shimanskii, *Izv. Vyssh. Ucheb. Zavedenii. Elektromekhanika* No. 2 (1960).
4. A. A. Kolomenskii and A. N. Lebedev, *Atomnaya Energiya* 5, 5, 554 (1958).\*
5. A. M. Lyapunov, *Selected Works* [in Russian] (Izd. AN SSSR, Moscow-Leningrad 1956) Vol. 2, p. 78.
6. A. A. Vorob'ev, *Charged Particle Accelerators* [in Russian] (Gosenergoizdat, Moscow, 1949) p. 220.

\*Original Russian pagination. See C. B. translation.



Section of a cyclical waveguide.

# USE OF SCINTILLATION COUNTERS IN GAMMASCOPY

V. E. Nesterov

Translated from *Atomnaya Énergiya*, Vol. 8, No. 5, pp. 461-463,

May, 1960

Original article submitted February 13, 1959

The gammascopic method for field measurements of soil and ground densities is of great interest for construction and geology engineering, for reclamation and soil research, because it makes possible the immediate obtainment of the results, and the taking of several measurements in the same place without a disturbance of the medium.

The law of attenuation of a parallel beam of  $\gamma$  rays lies at the basis of the gammascopic method:

$$I = I_0 e^{-\mu \rho x},$$

where  $I_0$  and  $I$  are the  $\gamma$ -radiation intensities without and with absorber, respectively;  $\rho$  is the density of the medium;  $x$  is the thickness of the layer crossed by the beam;  $\mu$  is the mass attenuation coefficient for  $\gamma$  rays.

The mass coefficients for grounds and soils of various types coincide with each other rather precisely when  $\text{Co}^{60}$  and  $\text{Cs}^{137}$  are used, because soils and grounds consist mainly of light chemical elements. The only exception is water, whose mass coefficient is 11% higher than that of soils and grounds, due to the presence of hydrogen.

Knowing  $\mu$ ,  $x$ , and measurements  $I_0$  and  $I$ , it is possible to determine the absolute value of the medium density:

$$\rho = \frac{\ln I_0 - \ln I}{\mu x}.$$

The most important measurements of soil and ground densities are those made in the field. Under these conditions the customary procedure consists in boring two parallel holes; one receives a  $\gamma$ -ray source at a certain depth, whereas the other receives at the same depth the detector, and then the radiation intensity is measured. However, in this case, there arise some difficulties due to the fact that it is impossible to obtain precise geometrical conditions since in the practice of soil research holes of a small diameter are used, and it is impossible to avoid the recording of scattered radiation by collimating and diaphragming the beam. In this case, it is impossible to use the theoretical values of the mass attenuation coefficient. The scattered radiation is usually taken into account by introducing an effective attenuation coefficient,

whose value depends upon the actual conditions of gammascopy: thickness and depth of the irradiated layer, medium density, sizes of the counters, etc. Therefore, the effective attenuation coefficient must be determined experimentally by means of a preliminary calibration [1-3]. However, the need for such a calibration reduces the value of the method, because the possibility for the conditions not to be the same upon calibration and actual measurements introduces a serious cause of error.\*

The difficulty mentioned above can be overcome if a scintillation counter is used for the detection of  $\gamma$  quanta, with an amplitude discriminator in series to it. Since multiply scattered  $\gamma$  quanta have an energy appreciably lower than that of nonscattered  $\gamma$  quanta, one can find such a discrimination threshold that the scattered radiation will not be recorded. This method for suppressing the effect of scattered radiation on gammascopic measurements was tested experimentally, taking the attenuation curves of  $\text{Co}^{60}$  radiation in water with various discrimination thresholds. As the discrimination threshold increased, the value of the effective attenuation coefficient changed from  $0.038 \text{ cm}^{-1}$  to  $0.063 \text{ cm}^{-1}$ , i. e., approached gradually the theoretical value. Recording of  $\gamma$  radiation in the same conditions by means of a Geiger counter gave an effective attenuation coefficient equal to  $0.039 \text{ cm}^{-1}$ .

After this testing of the method, an experimental field-scintillation-counter was constructed: in it a photomultiplier FEU-35 with an NaI (Tl) monocrystal was mounted in a case having a diameter of 44 mm together with a divider and an emitter-repeater using the transistor P11. The conversion block of the TPRP radiometer [4] was used as a numerator, with some modifications in

\*It must be noted that the measurement of the density of a pulp or of a liquid in pipe is a much simpler problem since, first, the geometry does not change during the process of measurement, second, the calibration can be carried out in the same geometric conditions as the measurements, third, compensation schemes can be used, and, consequently, one can use devices operating according to the principle of pulse integration.

# Field tests of the gammascopic method of ground measurement.

Depth, cm	Density, g/cm <sup>3</sup>			
	Intermediate argillaceous soil		Lower peat	
	Cutting cylinders	Gamma-scscopy	Cutting cylinders	Gamma-scscopy
2	—	—	1,34±0,05	1,34±0,04
10	1,63±0,04	1,41±0,02	—	—
12	—	—	1,23±0,01	1,42±0,02
20	1,76±0,04	1,74±0,01	—	—
22	—	—	1,07±0,01	1,08±0,03
30	1,87±0,01	1,86±0,01	—	—
32	—	—	1,07±0,01	1,11±0,03
40	1,87±0,01	1,89±0,02	—	—
42	—	—	1,11±0,01	1,09±0,04
50	1,87±0,01	1,90±0,04	—	—
52	—	—	1,15±0,02	1,19±0,01
60	1,88±0,01	1,95±0,03	—	—
62	—	—	1,26±0,02	1,29±0,02

Note. On sandy ballast, the density measured by cutting cylinders at a depth of 10 cm, was equal to  $1.95 \pm 0.01$  g/cm<sup>3</sup>, that measured by the gammascopic method was  $1.97 \pm 0.01$  g/cm<sup>3</sup>.

the circuit. A crystal diode was used as an integral discriminator. Field tests of the scintillation apparatus for the measurement of ground density (Fig. 1) were carried out on various soils and grounds and gave satisfactory results (table, Fig. 2).

The best agreement was obtained from aluminous brown earth, where gammascopy was carried out on ten lines, and in the determination of the density with a Kachinskii perforator of the volume of 200 cm<sup>3</sup> 34 separate measurements were made. With other soils and grounds the number of repeated determinations was significantly lower.

It was not possible to measure the density of argillaceous brown earth by cutting sylinders at a depth of more than 65 cm, due to the high density of the soil. The disagreements between the values of the density of argillaceous soil at a depth of 10 cm and the density of the peat at a depth of 12 cm was due to the presence of fractures in the first case and of rocks in the second, and this led to an increase of the density of the argillaceous soil and to a decrease of the density of peat when measured with cutting cylinders. The calibration of the apparatus consisted in finding the correspondence between the discrimination level for a given voltage on the photomultiplier and the effective attenuation coefficient.

In calculating the densities the difference between the attenuation coefficients of soil and water was not taken into account. It can be shown that such a simplification leads to an increase of the density by 1/10 of the volume moisture, which is 1.5% for a density of 2.0 g/cm<sup>2</sup> and a moisture of 30%. In accurate density measurements one must take into account the water content of the soil. One must know the amount of moisture also

in order to determine the weight by volume of the solid phase. However, when gammascopy is combined with a thermostatic-weight method, of moisture measurements, one of the advantages of gammascopy is lost, namely its operativeness. The combination of gammascopy with a mesurement of the volume moisture by the neutron method, using the same holes, looks more promising.

Thus, the use of scintillation counters permits us to carry out absolute measurements of soil and ground densities in field conditions, and may be useful for other applications of the gammascopic method.

The author is grateful to V. A. Emel'yanov for his discussion of the results, to E. G. Petrov for his valuable advice, and to V. L. Volodarskii for his help in the construction of the apparatus and in the measurements.

Note added in proof. In 1959, when this letter had already been submitted for publication, a communication

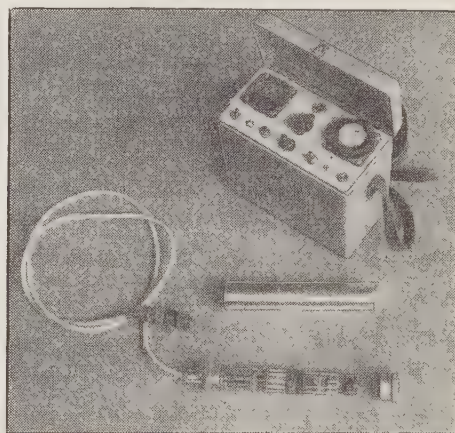


Fig. 1. Field scintillation counting apparatus on transistors.

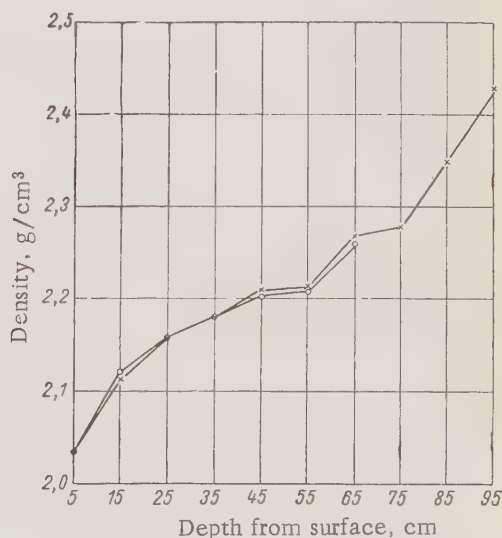


Fig. 2. Density of argillaceous brown earth. Method of measurement: X gammascopic method; O, cutting cylinders.

concerning a similar investigation carried out in the USA (C. Van Bavel, Soil Sci. 87, 50 [1959]) was published; however, this communication does not include data regarding comparisons of the gammascopic method with any other method.

#### LITERATURE CITED

1. Vomochil, Proc. of the International Conference on the Peaceful Uses of Atomic Energy (Geneva, 1955) [in Russian] (Sel'kozgiz, Moscow, 1958) Vol. 12, p. 266.
2. V. A. Durante, et al., Materials of the IV International Congress of the Mechanics of Grounds and Foundation Laying [in Russian] (Izd. AN SSSR, Moscow) 1957.
3. A. A. Tatarnikov, Razvedka i okhrana nedr No. 4, 17 (1957).
4. G. R. Gol'bek and A. N. Vil'shin, Transactions of Scientific-Technical Conference on the Applications of Radioactive and Stable Isotopes and Radiations to the National Economy. Radiometry and Dosimetry [in Russian] (Izd. AN SSSR, Moscow, 1958) p. 220.

## ATOMIC ENERGY AT THE SOVIET EXPOSITION IN HAVANA

L. Kimel' and V. Tsutkov

The National Museum of Fine Arts in Havana, Cuba was host in February 1960 to the Soviet Exposition on Science, Culture, and Industry.

On the behest of the Soviet Government, the First Vice-Chairman of the USSR Council of Ministers, A. I. Mikoyan, was on hand to inaugurate the exposition.

Residents of the Cuban capital manifested a tremendous interest in the Soviet Exposition, 40-50 thousand persons showing up as visitors each day.

There was always a large number of visitors grouped around the stands and exhibits of the "Atomic Energy for Peace" section.

Particularly great success and favor was enjoyed by a model of the atomic icebreaker "Lenin", a model of the world's first functioning atomic electric power generating station, a model of a heavy water research reactor, stands on which various reactor types designed for atomic electric power stations now in construction in the USSR were displayed, and a model of the ALPHA thermonuclear experimental facility.

Devices illustrating the applications of isotopes in industry (radioactive counter-monitor, wall-thickness

meter, a meter for measuring the thickness of lead jacketing, a rolling-thickness gauge) were also exhibited in the atomic section; the model illustrated the principle behind the use of isotopes in oil-well borehole logging, while other exhibits dealt with blast-furnace applications, gamma-ray nondestructive testing, etc.

Also demonstrated at the Exposition were: a model of the 10-Bev proton synchrotron, one of a cyclotron, and another of an electrostatic generator.

All the Cuban visitors to the Exposition reached the unanimous conclusion that atomic energy should be solely in the service of the cause of peace. From the example set by the Soviet Union, they see that the peaceful uses of atomic energy will bring great benefits to mankind. Cubans expressed this opinion in conversations, in innumerable remarks left in the guest ledger, and in their newspapers. All of the newspapers gave a glowing account of the Soviet Exposition.

The Exposition of Science, Culture, and Industry aided in getting the Cuban people to know the Soviet Union better.



At the Soviet Exposition in Havana



At the Soviet Exposition in Havana



At the Soviet Exposition in Havana

\* \* \*

## ATOMIC ENERGY AT THE ALL-CHINA EXPOSITION ON INDUSTRY AND MEANS OF COMMUNICATION

Sheng Ch'ung-p'ao

At the All-China Exposition on Industry and Means of Communication held in Peking, work accomplished in the Chinese Peoples Republic on uses of atomic energy was given wide publicity. The four principal trends in atomic industry were represented, viz.: reactor design, accelerators, applications of radioactive isotopes, and instrumentation.

The first area of activity was represented by a plastic lighted model of a heavy water research reactor with laboratory caves and accessory units. This reactor was built in the (Chinese) Institute of Atomic Energy with the assistance of the USSR. The reactor was started up in July, 1958. At the present time, Chinese specialists are using this reactor for a broad variety of experiments. Many radioactive isotopes, e.g.,  $\text{Co}^{60}$ ,  $\text{I}^{131}$ ,  $\text{Fe}^{59}$ , are being produced in the reactor.

Accelerator engineering was represented by several mockups of accelerator machines: the first Chinese cyclotron, now in operation here in Peking, built with the aid of the Soviet Union and commissioned in July 1958; models of an electrostatic generator, an electron induction accelerator, and a high-voltage generator model.

Applications of radioactive isotopes to the Chinese national economy was the best represented field of activity at the Exposition. Significant successes have been registered in recent years in this field. Radioisotopes,  $\text{Co}^{60}$   $\gamma$ -emitting sources in particular, began to find applications in many projects in industry, agriculture, and medicine. Many industrial outfits are using isotopes for flaw detection and inspection, determination of wear on blast-furnace hearths and walls, as well as in the lumber and mining industries. It was shown that grains

exposed to gamma-irradiation or immersed in solutions of some radioactive isotopes show improvement and faster growth, with greater crop yield. Methods for preservation and storage of agricultural and food products by radiation treatment to kill harmful pests and bacteria were also described.

China's doctors are putting isotopes to widespread use. A cobalt gun used in cancer therapy, and designed in China, was demonstrated in one exhibit, and an account was given of work on applications of the  $I^{131}$  isotope in the diagnosis and treatment of hypertonicity, and of the isotope  $P^{32}$  in the diagnosis of breast cancer and therapy of skin ailments.

Nucleonics instrumentation were given good publicity. Production of many nuclear instruments has been in full swing for several years in China. On exhibit were a good representation of counters and radiation detectors used in industry, agriculture, medicine, and geology, as well as various instruments for quality control of production processes (liquid-level indicators, neutron soil-moisture meters, devices for counting bottles and cans, etc.).

The Exposition showed that the Chinese Peoples Republic, in its ten years since liberation, has achieved great successes in the peaceful utilization of atomic energy.

\* \* \*

## MEASUREMENT OF MAGNETIC MOMENT OF $Li^8$

The capture of polarized thermal neutrons by nuclei leads in some cases to the polarization of the nuclei involved in capturing the neutrons. If these nuclei then decay to emit  $\beta$  particles, the latter emerge asymmetrically with respect to the direction of polarization of the nuclei [1, 2]. By depolarizing the resulting  $\beta$ -active nuclei via the nuclear magnetic resonance method and observing the disappearance of  $\beta$ -radiation asymmetry, the nuclear g-factors may be measured. This technique also makes it possible to measure the magnetic moments of several short-lived nuclides.

The first report to appear on the use of some such technique turned up recently [3]. The experimental

arrangement may be seen from the accompanying diagram. A beam of polarized neutrons is allowed to strike the  $Li^7F$  crystal. The  $Li^8$  forming in response to neutron capture emits beta particles with half life 0.8 sec. These particles are recorded by two plastic scintillation counters. Due to the asymmetry of  $\beta$  decay, counter No. 2 picked up 10% more  $\beta$  particles than counter No. 1.

A static magnetic field of intensity  $H_0 = 5418 \pm 1$  oe was impressed on the crystal. A coil was used to superpose a pulsed magnetic field  $2H_1$  with frequency varied over a wide range, at right angles to the field  $H_0$ .

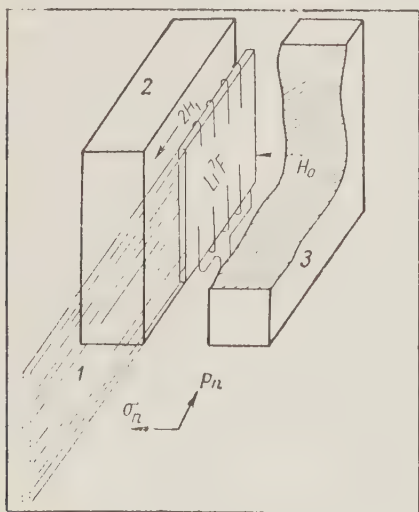
When the field frequency coincides with the Larmor precessional frequency of the magnetic moments of the  $Li^8$  nuclei in the  $H_0$  field, these nuclei become depolarized, and the asymmetry of  $\beta$  decay disappears. It is interesting to note that, under the conditions of this experiment, only 20,000  $Li^8$  nuclei are present in the crystal at any given instant.

The Larmor frequency of precession was  $3413 \pm 1$  kc, from which we find the g-factor for  $Li^8$  to be  $0.8265 \pm 0.0004 \mu_0/h$  (where  $\mu_0$  is the nuclear magneton). Since the spin of  $Li^8$  is 2 (cf. [4]), the magnetic moment will be  $1.653 \pm 0.008 \mu_0$ .

The empirically measured value is found to be in agreement with the intermediate-coupling model [5].

### LITERATURE CITED

1. M. Burgy, et al., Bull. Am. Phys. Soc. 2, 206 (1957).
2. F. L. Shapiro, Uspekhi Fiz. Nauk 65, 1, 133 (1958).
3. D. Connor, Phys. Rev. Letters 3, 9, 429 (1959).
4. F. Ajzenberg-Selove and T. Lauritsen, Nucl. Phys. 11, 1 (1959).
5. D. Kurath, Phys. Rev. Letters 3, 9, 431 (1959).



Experimental arrangement:  $\sigma_n$  direction of polarization of the neutrons;  $P_n$  direction of flight of neutrons; 1) beam of polarized neutrons; 2) beta counter No. 1; 3) beta counter No. 2.

## NEW LITERATURE

## THEY BUILT THE ATOMIC ICEBREAKER

The world's first atomic-powered icebreaker, the Soviet ship "Lenin," was recently put into service. Anyone interested in reading a detailed account of the designers and builders of the nuclear-propelled ship, and of the tests it underwent, may avail himself of the brief popular-style book ["How the Atomic Icebreaker 'Lenin' Was Built"]\*.

The value of the book is that it is "hot news" dealing with the process of building the vessel, fresh from those participating in the venture.

The authors tell about the reason behind the Soviet Union's decision to build the nuclear icebreaker, the purposes it is to serve, and compare it with the conventional icebreaker.

The nuclear ship has a virtually unlimited sailing range. In a single run, it can cover from the Arctic to the shores of Antarctica.

The workers at the Admiralty plant in Leningrad, where the ship was built and launched, had quite a bit of experience behind them in the building of ships of different types. However, the job of building an icebreaker with nuclear propulsion units entailed the solution of complicated engineering problems, and required improved technology and new labor techniques. The authors of the book describe the difficulties confronting the shipbuilders, and point out how those bugs were ironed out.

The layout of the ship's hull involved the use of the new photooptical method. For the first time in the practice of Soviet shipbuilding, a spherical wooden turntable was used to launch the icebreaker hull, resulting in savings of over a million rubles.

The authors of the brochure tell of the ship's superstructure, the arrangement of the crew compartments and living quarters, the performance and design of the nuclear propulsion unit.

However, the lion's share of the attention in the booklet is given to the people involved, the ones who built the ship. The enthusiasm of the shipbuilding workers is described, an account is given of the life of the work-force engaged in constructing the prototype of the Soviet nuclear-powered icebreaker fleet, of the contribution which was made to the task of building the ship by some work team or some individual specialist.

L. D. Chernous'ko

V. Fedorov, *Fifteen Days at Geneva*. Moscow, Atomizdat, 1960. 80 pages, 1 ruble, 15 kopeks.

This brochure, written by a participant at the Second International Conference on the Peaceful Uses of Atomic Energy, and intended for a broad reader audience, tells of the principal questions discussed at the Conference, on the paths pursued by the USSR and by the USA in striving to harness thermonuclear energy, the nuclear electric power generating stations which have sprung up in the three years following the world's first such station in the USSR, on the exhibits viewed by the participants at the Conference. The booklet is illustrated with photographs and diagrams.

M. M. Konstantinov (deceased) and E. Ya. Kulikova, *Uranium Provinces*. Moscow, Atomizdat, 1960. 306 pages, 15 rubles, 20 kopeks.

This item provides a systematic review of uranium provinces and uranium deposits in foreign countries. The principal features of geologic structure and metallogeny, uranium deposits, and extent of uraniferous rocks in the various countries of North America, South America, Africa, Europe, and Asia are discussed. Data are given on the state of the theory explaining the formation of uranium deposits, the main patterns of uranium distribution throughout the earth's crust, uraniferous provinces, criteria for prospecting, and the state of the raw-materials base in foreign countries.

The book is recommended for scientific, engineering, and technical workers and economists. It may prove useful to teachers and students in the related disciplines. A. I. Burnazyan and A. V. Lebedinskii (editors), *Handbook for Doctors and Students -- Radiation Medicine*. Moscow, Atomizdat, 1960. 314 pages, 11 rubles, 60 kopeks.

The book contains a systematized account of the fundamentals of radiobiology and radiation medicine. The action mechanisms of radiation effects on living organisms, the pathogenesis, clinical treatment, and diagnosis and therapy of various forms of radiation sickness in humans and animals are discussed. Radiation injuries resulting from the ingestion of radioactive matter by the organism are also discussed. A special chapter is devoted to problems of physics and dosimetry.

The material is presented in clear and understandable language, and may be of service not only as a manual for doctors and student doctors, but also as a reference book for engineers and technicians engaged in work requiring some knowledge of radiation shielding.

\*Sudpromgiz, 1959. Leningrad. 64 pages. 1 ruble, 25 kopeks.

S. A. Prechistenskii, Centrifugation of Aerosols in a Centrifugal Rotating Dust Separator. Moscow, Atomizdat, 1960, 144 pages, 4 rubles, 20 kopeks.

The book outlines the theoretical fundamentals of the centrifugation of aerosols in a new type of centrifuging equipment, the centrifugal rotating dust separator. Problems concerning design are elucidated, empirical data are given for various technological processes. The book is intended for engineers and designers, research workers engaged in the field of aerosol separation. A. A. Gusev, Contemporary Foreign Literature on Physics, Mechanics, and Applied Mathematics. Moscow, Atomizdat, 1959, 72 pages, 2 rubles, 30 kopeks.

A critical evaluation is given in this booklet of foreign books on physics, mechanics, and applied mathematics appearing during 1952-1958.

Among the books discussed are monographs on nuclear and reactor physics, nuclear engineering, and popular editions, bilingual, and encyclopedic works on those branches of science and engineering.

#### Articles from the periodical literature\*

I. REACTOR POWER PHYSICS. Neutron and reactor physics. Physics of hot plasmas and controlled thermonuclear reactions. Physics of acceleration of charged particles.

Doklady Akad. Nauk SSSR 130, No. 2 (1960)

Yu. A. Tserkovnikov, pp. 295-298. The problem of plasma convective instability.

Zhur. Tekh. Fiz. 30, No. 1 (1960)

S. G. Denisov et al., pp. 31-36. Study of electron distribution in a betatron donut.

G. F. Mikheeva, N. N. Chernov, pp. 37-40. Stabilization of gamma radiation intensity in betatrons and synchrotrons.

L. I. Pivovarov et al., p. 74-81. A compact 1.5 Mev electrostatic accelerator.

G. M. Voskoboinikov, pp. 90-95. On the problem of the accuracy of and the range of applicability of the diffusion approximation to the solution of gamma-ray propagation problems.

Zhur. Éksp. i Teoret. Fiz. 38, No. 1 (1960)

O. G. Zagorodnov et al., pp. 7-9. On the reflection of electromagnetic waves from a plasma moving down slow-wave waveguides.

Ya. M. Fogel' et al., pp. 26-32. Electron trapping and losses in collisions between fast He, B, and F atoms and gas molecules.

G. N. Flerov et al., pp. 82-94. Experiments on producing element 102.

V. M. Strutinskii, pp. 122-133. Excitation of vibrational levels and coulombic excitation in alpha decay.

F. M. Nekrasov, pp. 233-238. Contribution to the nonlinear theory of stationary processes in an electron plasma.

N. I. Tarantin, pp. 250-252. Competition between the processes of neutron evaporation and fission in interactions of multiply charged ions and heavy nuclei.

K. N. Stepanov, pp. 265-267. On cyclotron absorption of electromagnetic waves in a plasma.

A. I. Obukhov, pp. 271-274. On the asymmetry in the fission of uranium nuclei at high proton energies.

N. A. Vlasov, et al., pp. 280-282. The (d, t) reaction on intermediate and heavy nuclei.

O. I. Leipunskii, pp. 302-304. On the possible magnetic effect in high-altitude explosions of atomic bombs.

Uchenye Zapiski Tartus. Univ. No. 74 (1959)

Yu. Ya. Lembra, pp. 96-99. On the choice of parameters for a sector cyclotron.

Yu. Ya. Lembra, pp. 100-111. Derivation of an approximate formula for the Q in a sector cyclotron.

Elektrichestvo No. 1 (1960)

M. A. Gashev et al., pp. 6-10. Supply system for the electromagnet of the proton synchrotron at the Joint Institute for Nuclear Studies (Dubna).

Am. J. Phys. 27, No. 9 (1960)

M. Livingston, pp. 626-629. Development of charged-particle accelerators.

Energia Nucleare 7, No. 1 (1960)

A. Fasana, pp. 1-10. Method for measuring longitudinal polarization of beta particles, and the circular polarization of gamma radiation.

G. Bacchella, pp. 11-22. The present state of the art and the perspectives of development of neutron diffraction.

G. Felcher et al., pp. 31-38. Absolute calibration of the (Ra-Be)-neutron source.

Helv. Phys. Acta 32, No. 6-7 (1959)

D. Chauvy, J. Rossel, pp. 481-485. The luminescence spectrum of CsI.

Industries Atomiques 3, No. 11-12 (1959)

G. Béné, pp. 37-51. Determination of nuclear moments.

Kerntechnik 2, No. 1 (1960)

D. Kamke, pp. 15-19. A cascade accelerator. II. Ion sources.

Nucl. Energy 14, No. 141 (1960)

J. Wilkins, A. Egginton, pp. 57-61. NIMROD, the British 7 Bev proton synchrotron.

Nucl. Sci. and Engng. 6, No. 5 (1960)

S. Gunst, pp. 376-378. Reactivity of  $\text{Np}^{239}$  in the irradiated dioxide of natural uranium.

\*The list of foreign journals used in the Bibliography section is published in the January issue. For Soviet journals, see the "Letopis' zhurnal'nykh statei" of the All-Union Book House.

C. Bigham, pp. 379-385. Temperature dependence of fission cross sections of  $\text{Pu}^{239}$ ,  $\text{U}^{235}$ , and  $\text{U}^{233}$ .

G. Safford, et al., pp. 433-440. Accurate determination of the total cross section of uranium-235 in the energy range from 0.000818 to 0.0818 ev.

W. Arnold, pp. 456-457. Neutron age in  $\text{D}_2\text{O}$ - $\text{H}_2\text{O}$  mixtures.

R. Hansen et al., pp. 458-460. Some problems in research on mixtures of water and uranium oxides.

II. NUCLEAR POWER ENGINEERING. Theory and design of nuclear reactors. Performance of nuclear reactors and nuclear electric power stations. Reactor design.

Izvest. Akad. Nauk SSSR. Otdel Tekhn. Nauk. Énergetika i Avtomatika, No. 6 (1959)

—pp. 196-197. N. A. Dollezhal', Corresponding Member of the USSR Academy of Sciences (Specialist in the field of nuclear power. On his 60th birthday)

Inzhener.-Fiz. Zhur. 2, No. 12 (1959)

I. S. Kochenov, pp. 64-67. Contribution to thermal calculations of a nuclear reactor fuel channel.

L. N. Muchnik, pp. 105-109. Simplified method for thermal calculations for a PWR.

Priroda, No. 12 (1959)

Yu. I. Klimov, pp. 35-40. The atomic icebreaker.

Atomkernenergie 5, No. 1 (1960)

W. Balz, R. Schwarzwälder, pp. 1-6. Calculation of coolant flow in a boiling-water reactor. II.

M. Angelopoulos, pp. 7-9. Determination of the critical state of a cylindrical heterogeneous bare reactor, using multigroup diffusion theory.

W. Kattwinkel, pp. 9-13. Computation of flux of fast and thermal neutrons appearing at the surface of cylindrical pressure vessels, owing to induced  $\text{N}^{17}$  radioactivity in the water.

T. Jaeger, pp. 15-18. Power reactor shielding.

H. Bühler, F. Schmidt, pp. 18-22. Heat transfer from heated solids by fluids, with steam formation, and with flow conditions taken into account.

Atompraxis 6, No. 1 (1960)

H. Smets, pp. 1-3. Transfer function for beryllium-moderated reactors.

H. Schludi, pp. 3-7. Investigation of a heavy-water-moderated and heavy-water-cooled reactor, and of a heavy-water reactor using  $\text{CO}_2$  coolant.

Atomwirtschaft 5, No. 1 (1960)

W. Hepburn, D. Specht, pp. 9-13. Comparative evaluation of four reactor types from the viewpoint of their possible service aboard ships.

H. Hardung-Hardung, pp. 14-16. Problems in the handling of fuel in seagoing nuclear reactors.

W. Ende, pp. 17-21. Planning and building of research reactors.

G. Kourim, pp. 22-27. Effect of temperature on reactor dynamics. II

Energia Nucl. 7, No. 1 (1960)

C. Lo Surdo, pp. 39-52. Utilization of the method of spherical harmonics in the group study of the transport equation.

Industries Atomiques 3, No. 11-12 (1959)

V. Lasareff, pp. 75-78. Requirements on siting of nuclear electric power stations.

P. Sevette, pp. 79-85. The role of nuclear power in the energy balance of the future.

pp. 88-91. The Haldén nuclear reactor.

Jaderná Energie 6, No. 2 (1960)

R. Servit, pp. 37-45. High-pressure reactor vessels of prestressed concrete.

J. Vorlicek, V. Seifert, pp. 46-49. Corrosion strength of metals in organic coolants.

J. Elemark, M. Panýr, pp. 50-52. Heavy and hydrated concretes. Composition and applications.

Kernenergie 3, No. 1 (1960)

K. Meyer, E. Griepentrog, pp. 1-13. Outline of burn-up calculations in a hard-spectrum thermal reactor. III.

T. Margulowa, pp. 23-37. Heat-power engineering techniques in the rational organization of the water technology of nuclear electric power generating stations.

Nucl. Energy 14, No. 141 (1960)

—pp. 62-64. Improved water-reactor systems. II.

A. Bowden, J. Drumm, pp. 69-73. Design of large gas piping.

P. Lottes, et al., pp. 74-77. Experimental study of natural water circulation in a boiling-water reactor.

Nucl. Engng. 5, No. 45 (1960)

K. Campbell, pp. 53-57. Experience in the operation of an organic-moderated reactor.

O. Wyatt, pp. 64-66. Fuel elements for organic-moderated reactors.

E. Weisner, pp. 68-71. Design of the organic-moderated reactor at Piqua.

R. Berman, pp. 72-74. Economics of large organic-moderated reactors.

Nucl. Power 5, No. 46 (1959)

G. Lockett, R. Huddle, pp. 112-117. Development and design of the gas-cooled DRAGON high-temperature reactor.

Nucl. Power 5, No. 46 (1960)

M. Hillier, pp. 128-130. Thermal stresses in reactor components, caused by  $\gamma$  radiation.

K. Spinney, pp. 134-137. Nuclear reactor shielding design.

Nucl. Sci. and Engng. 6, No. 5 (1959)

R. Schechter, E. Wissler, pp. 371-375. Heat transfer to plastics in laminar flow through annular tubes, with an internal heat source.

R. George, pp. 409-413. Simplified simulation of a power plant with a nuclear reactor.

C. Velez, pp. 414-419. Autocorrelation functions of counting rate in nuclear reactors.

E. Wigner, pp. 420-432. New ideas for reactor design.

R. Stoughton et al., pp. 441-447. Effective cadmium cutoff energy.

M. Moore, pp. 448-452. Transfer function for power oscillations in a reactor.

E. Gelbard, J. Pearson, pp. 453-455. Separation of spatial and energy variations in the flux of thermal neutrons through a diffusion medium.

S. Hasnain, R. Murray, pp. 455-456. Feasibility of the  $\beta$  method for analysis of fuel cycles.

C. Bigham, R. Pearce, pp. 457-458. Slowing-down of neutrons in a heterogeneous reactor.

Nucl. Sci. and Engng. 6, No. 6 (1959)

H. Corben, pp. 461-465. Transfer of zero-power reactors.

R. Stone, R. Slovacek, pp. 466-474. Neutron spectrum measurements.

W. Kofink, pp. 475-486. Complete solution of the Boltzmann equation in cylindrical geometry by the method of spherical harmonics for the case of neutron flow through a homogeneous medium.

G. Gardner, pp. 487-492. Fission fragment impact trapping by thorium dioxide slurry particles.

A. Foderaro, pp. 514-524. Use of iterated approximations for determination of group Laplacians in the multigroup solution of the kinetic equation.

R. Uhrig, pp. 530-532. Measurements of material buckling in a subcritical facility.

F. Holzer, M. Crouch, pp. 545-553. Experiments on determination of mean lifetime of thermal neutrons.

Nucleonics 18, No. 2 (1960)

W. Ergen, pp. 60, 62-63. Breeding—how soon a necessity?

E. Zebroski, pp. 61-66, 87. Economic prerequisites for breeding.

D. Dickey, J. Mc Ewen, pp. 88, 90, 92-95. Slide rule simplifies xenon computations.

H. Ruhl, p. 96. Hot reloading of in-pile tests.

Nukleonik 2, No. 1 (1960)

W. Matthes, pp. 21-30. Determination of neutron Fermi age and fractional leakage for a heterogeneous water reactor, using the Monte Carlo approach.

G. Blässer, pp. 31-36. Resonance capture of neutrons when fuel elements are arranged in complex arrays.

K. Hecht, pp. 37-38. Nuclear reactor experiments on xenon poisoning models.

H. Dušek, pp. 38-39. A criterion for the determination of reactor regions with positive and negative void coefficients.

III. NUCLEAR FUEL AND MATERIALS. Nuclear geology and primary ore technology. Nuclear metallurgy and secondary technology. Chemistry of nuclear materials.

Geol. Rusn. Mestorozhdenii No. 6 (1959)

A. G. Betekhtin, pp. 5-26. On exogenic processes in the formation of uranium deposits.

V. I. Danchev et al., pp. 27-38. On uranium mineralization in carbonate sedimentary rocks.

G. A. Pelymskii, pp. 39-51. On the effects of intrusive rock formations on ore deposition processes in hydrothermal uranium deposits.

Doklady Akad. Nauk SSSR 129, No. 5 (1959)

I. E. Starik, et al., pp. 1142-1145. Distribution of the radioelements in Black Sea sediments.

Zhur. Neorg. Khim. 4, No. 12 (1959)

A. D. Gel'man, L. M. Zaitsev, pp. 2688-2696. Simple and complex plutonium (IV) carbonates.

A. E. Klygin et al., pp. 2766-2771. Solubility of EDTA in ammonia and hydrochloric acid, and interaction between EDTA and uranium (IV) and plutonium (IV).

A. S. Solovkin et al., pp. 2826-2827. Tri-n-butyl phosphate extraction of plutonium (IV) perchlorate.

Zhur. Obshch. Khim. 29, No. 12 (1959)

Zh. Gershkovich et al., pp. 4097-4099. A new method for producing radioactive standards for  $C^{14}$ .

Zapiski Vsesoyuz. Mineralogich. Obshch. 88, No. 6 (1959)

V. I. Lebedev, pp. 667-671. On the causes of oxidation of uranium in uraninites.

Izvest. Akad. Nauk Kirgiz. SSR. Seriya Estestv. i Tekh. Nauk 2, No. 1 (1960)

A. G. Zhil'tsov, P. I. Chalov, pp. 109-116. Distribution of uranium and thorium in the rocks on the Kenkol' pluton.

Izvest. Akad. Nauk SSSR, Seriya Geofiz. No. 12 (1959)

A. N. Timofeev, pp. 1873-1875. Contribution to gamma prospecting theory.

Priroda No. 12 (1959)

Yu. V. Sharkov, pp. 13-21. Prospecting for nuclear raw materials deposits.

Radiokhimiya 1, No. 6 (1959)

E. A. Ippolitova et al., pp. 660-664. Investigations in the field of the chemistry of uranates of some divalent elements.

V. G. Knyaginina, O. G. Nemkova, pp. 665-667. A study of uranium compounds not readily soluble in low-valency acids of phosphorus.

Fizika Metallov i Metalloved. 8, No. 6 (1959)

S. Ya. Zalivadnyi, B. M. Mikhailovskii, pp. 904-907. Effect of thermal cycling on uranium bicrystals.

Atompraxis 6, No. 1 (1960)

W. Crane, pp. 12-15. The future of the actinides.

Canad. J. Chem. 38, No. 1 (1960)

R. Woods, J. Spinks, pp. 77-93. Radiolysis of several organic halide derivatives in aqueous solution.

Chem. and Process Engng. 41, No. 1 (1960)

B. Eriksson, pp. 5-7. The Swedish process for heavy water production, based on dual-temperature isotope exchange between hydrogen sulfide and water.

Chem. and Process Engng. 41, No. 2 (1960)

F. Paulsen, pp. 49-52. Ceramics and cermets for nuclear fuel.

B. Eriksson, pp. 53-57. The Swedish heavy-water production process. 2.

Energia Nucl. 7, No. 1 (1960)

E. Cerrai, C. Testa, pp. 53-54. Calorimetric determination of hafnium and zirconium in their mixtures.

Industr. Chemist 36, No. 420 (1960)

-- pp. 80-82. Processing of uranium ore concentrates, and recovery of wastes at the Springfield plant.

J. Appl. Phys. 30, No. 12 (1959)

L. Hunter, pp. 1969-1975. Effect of fission recoil fragments on the thermal conductivity of graphite.

J. Nucl. Materials 1, No. 4 (1959)

G. Greenwood et al., pp. 305-324. The role of vacancies and of dislocations in the formation of embryos and in the growth of gas bubbles in irradiated fissionable material.

D. Calais, et al., pp. 325-344. Effect of the deformation mechanism on recrystallization of uranium monocystals placed in tension.

M. Smith, R. Honeycombe, pp. 345-355. Effect of oxygen, carbon, and nitrogen on the properties of sintered thorium.

G. Cabane, G. Donze, pp. 364-373. Stabilization of  $\gamma$  phase in ternary alloys based on the uranium-molybdenum system.

C. Britton, N. Wilkins, pp. 374-476. Local penetrating corrosion of an alloy of sintered aluminum powder (SAP) in high-temperature vapor.

Kerntechnik 2, No. 1 (1960)

K. Zander, pp. 28-29. A control device used in the vaporization of radioactive liquids on targets.

Nucl. Energy 14, No. 141 (1960)

-- pp. 65-68. Investigation and production of new metals.

Nucl. Engng. 5, No. 45 (1960)

-- pp. 49-52. Uranium; its reserves, production, and markets.

-- pp. 59-60. Radiolytic analysis of various organic liquids.

J. Scrivins, pp. 61-63. Use of terphenyl as moderator and coolant in nuclear reactors.

S. Baxter, J. Churchill, p. 67. Use of polyphenyls as moderators and coolants for nuclear reactors in Great Britain.

D. Collins, J. Woods, pp. 75-76. The Dounreay hot laboratory.

Nucl. Power 5, No. 46 (1960)

V. Thayer, pp. 108-111. Heavy water production in the USA.

A. Cottrell, pp. 130-131. Radiation damage in materials.

-- pp. 140-141. Development of the technology of the rare metals for industrial use.

Nucl. Sci. and Engng. 6, No. 5 (1959)

E. Byron et al., pp. 361-370. Clad titanium-base dispersions containing boron.

C. Smith, pp. 391-395. Properties of uranium monocarbide.

H. Hungerford et al., pp. 396-408. New shielding materials for high-temperature applications.

Nucl. Sci. and Engng. 6, No. 6 (1959)

L. Burris et al., pp. 493-495. Melt refining of uranium. Applications to the EBR-II fast reactor. Introduction.

G. Bernstein et al., pp. 496-500. Melt refining of spent uranium. II. Experimental furnaces.

D. Hampson et al., pp. 501-502. Melt refining of spent uranium. III. Preparation of alloys for experiments.

C. Rosen et al., pp. 504-510. Melt refining of spent uranium. IV. Interaction of uranium and alloys with refractory oxides.

G. Bennett, pp. 511-513. Melt refining of spent uranium. V. Yield of fissionable material upon pouring.

F. Dodge et al., pp. 533-536. Low-decontamination reprocessing of uranium-thorium alloys by induction drip melting.

J. Chernick, S. Moore, pp. 537-544. Nuclear fuel breeding in thermal reactors.

Nucleonics 18, No. 2 (1960)

W. Rice, D. Kirk, pp. 67-71. Radiation-resistant fluids and lubricants.

C. Stevenson, pp. 72-73. How AEC plans to process power reactor fuels.

Phys. Rev. Letters 3, No. 12 (1959)

J. Adam, B. Cox, pp. 543-544. Effect of neutrons and fission fragments on the structure of zirconium.

IV. NUCLEAR RADIATION SHIELDING. Radiobiology and radiation hygiene. Theory and practice of shielding for nuclear facilities. Instrumentation.

Biokhimiya 24, No. 6 (1959)

O. Ya. Tereshchenko, pp. 1113-1115. Conference on the problem of the biochemical effects caused by ionizing radiations.

Gigiena Truda i Prof. Zabolevaniya No. 1 (1960)

V. S. Kushneva, pp. 22-28. Combined effect of quartz dust and radon in an experiment.

G. V. Bokova, pp. 49-50. Study of the behavior of metallic thorium and some of the compounds it forms in different media.

Kristallografiya 4, No. 6 (1959)

G. S. Belikova, L. M. Belyaev, pp. 929-930. Mixed organic crystals for scintillation counters.

Med. Radiologiya 5, No. 1 (1960)

A. V. Bykhovskii, pp. 60-67. Basic problems of labor safety practices in handling and mining radioactive minerals.

A. L. Agre, V. I. Korogodin, pp. 67-73. On the distribution of radioactive impurities in a nonflowing water reservoir.

Trudy Nauchno-Issled. Inst. Betona i Zhelezobetona Akad. Stroit i Arkhit. SSSR No. 11 (1959)

A. E. Desov, V. I. Nadol'skii, pp. 69-108. Physical and engineering properties of heavy concretes intended for shielding against radioactive effects.

Energia Nucl. 7, No. 1 (1960)

L. Gatti et al., pp. 23-30. Measurement of the effect of passivation on G-M counters filled with organics.

Industries Atomiques 3, No. 9-10 (1959)

A. Gruget, pp. 116-118. Protection of the respiratory tract.

Jaderna Energie 6, No. 2 (1960)

F. Behounek, pp. 53-61. Problems of disposal of radioactive wastes on a world scale.

Kerntechnik 2, No. 1 (1960)

M. Oberhofer, P. Kienle, pp. 20-27. Radiation shielding in working with reactors and in nuclear enterprises.

Nucl. Power 5, No. 46 (1960)

F. Wells, pp. 123-127. Electronic instruments for radiation detection. IV. Multichannel analyzers.

Nucl. Sci. and Engng. 6, No. 6 (1959)

C. Horton, pp. 525-529. Helical-duct shielding.

Nucleonics 18, No. 2 (1960)

S. Friedland, J. Mayer, pp. 54-59. Tiny semiconductor is fast linear detector.

C. Murphy, J. Hill, pp. 78-80. Detection of irradiation effects by differential thermal analysis.

J. Gaskill, O. Meadors, p. 82. Transistorized voice amplifier for use with respiratory masks.

R. Steinberg, p. 85. Semiconductor fission probe for flux mapping.

Sewage and Industr. Wastes 31, No. 12 (1959)

R. Foster, pp. 1409-1415. The need for biological monitoring of surface waters contaminated by radioactive wastes.

V. RADIOACTIVE AND STABLE ISOTOPES. Labeled atoms. Use of radioactive radiations. Direct conversion.

Vestnik mashinostroeniya No. 1 (1960)

E. P. Nadeinskaya, pp. 62-67. Studies of resistance to wear of end milling cutters, using the radioactive isotope technique.

V. V. Kondashevskii et al., pp. 67-70. Active quality control of parts on grinding machines, by means of radioactive sensors.

Zavod. laboratoriya 25, No. 12 (1959)

K. N. Magarik, S. S. Nikol'skii, pp. 1512-1515. Automatic scintillation counter facility for studying wear on mechanisms.

Izvest. Akad. Nauk SSSR, Otdel. Tekh. Nauk. Metallurgiya i Toplivo No. 6 (1959)

A. M. Samarin, M. S. Fomichev, pp. 121-126. Perspectives in applications of radioactive isotopes and nuclear radiations in metallurgy and the other technical sciences.

Izvest. Vyssh. Ucheb. Zaved. Mashinostroenie No. 5 (1959)

A. A. Vorob'ev et al., pp. 195-202. Flaw detection of parts of large thickness using betatrons.

Izvestiya Timiryazevsk. Sel'sko-Khoz. Akad. No. 6 (1959)

V. V. Rachinskii, F. P. Platonov, pp. 239-250. The radioisotopes laboratory at the Timiryazev Academy.

Inzhener-Fiz. Zhur. 2, No. 12 (1959)

E. A. Zhikharev, pp. 112-115. The international conference on the use of high-level radiation sources in industry.

Konservnaya i Ovoshchesushil'naya Prom. No. 1 (1960)

L. V. Metlitskii, pp. 29-33. The use of atomic energy for year-round storage of potatoes.

Narodnoe Khozyaistvo Uzbekistana No. 12 (1959)

S. Yakubdzhanov, pp. 56-58. They are harnessing the atom.

Sbornik Rabot Nauchno-Issled. Inst. Chernoi Metallurgii 2, (1959)

P. L. Gurzin et al., pp. 8-10. On the use of radioactive isotopes in blast-furnace work.

Tekhnika v Sel'skom Khozyaistve No. 1 (1960)

R. Srapenyants, pp. 65-70. Radioactive isotopes and scientific research in the field of mechanization.

Atompraxis 6, No. 1 (1960)

S. Clark, pp. 8-11. Radioactive isotopes as heat sources.

Industr. Chemist 36, No. 419 (1960)

G. Hall, pp. 25-26, 37. The use of high-level radiation sources in industry, Part 2.

Industr. Chemist 36, No. 420 (1960)

G. Hall, pp. 65-68. The use of high-level radiation sources in industry, Part 3.

J. Appl. Phys. 30, No. 12 (1959)

G. Grover et al., pp. 1861-1865. Characteristics of a plasma thermocouple.

F. Jablonski, et al., pp. 2017-2018. Space charge neutralization by fission fragments in the direct conversion plasma diode.

Kerntechnik 2, No. 1 (1960)

I. Wendt, pp. 1-9. Radioisotope applications in practical geology.

Nucl. Power 5, No. 46 (1960)

J. Lakey, pp. 131-132. Studies of radioactivity of materials, using the paper chromatography technique.

— pp. 139-140. Radiation sources for industry and scientific research.

Nucleonics 18, No. 2 (1960)

R. Ellis, pp. 98-99. Russian gamma sources.

J. Tunstall, pp. 100-104. British pilot plant for radiation processing of packaged goods at Wantage.

S. Eaton, pp. 105-107. Radiation seeks commercial use.

